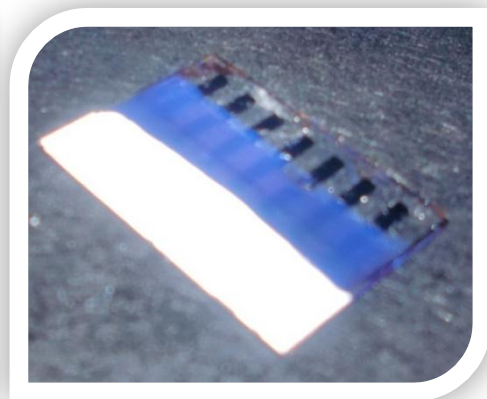
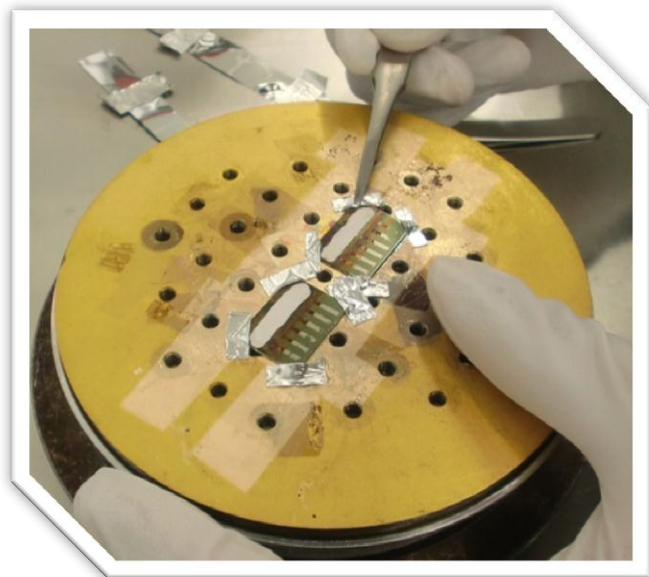


# Prolonged lifetime of organic solar cells through encapsulation processing



Bachelor thesis by  
Mathias Hausladen

Supervisor: Morten Madsen

Hand-in date: 01.06.2012  
Examination date: 21.06.2012

In corporation with MCI SDU Sønderborg and NanoSYD



## Preface

This project completes my Bachelor of Science degree in mechatronics at SDU in Sønderborg. This work has been carried out at the Mads Clausen Institute at SDU in Sønderborg, at the NanoSYD group.

The goal of this project is to establish an encapsulation procedure that provides increased performance stability for organic solar cells. The project involves the fabrication of inverted bulk-heterojunction solar cells from P3HT:PCBM and the characterizing of the produced cells by I-V measurements to determine their efficiency. Furthermore the cells are encapsulated and variations in the performances over time for different encapsulation materials are investigated.

At this point I would like to thank my supervisor Morten Madsen (Assistant Professor, MCI, SDU) for his guidance concerning the theory and development of the project. Also I would like to thank Roana Melina de Oliveira Hansen (Post Doc, MCI SDU) for her technical assistance concerning the production and characterization processes of the organic solar cells throughout the entire project. I want to stress the point, that both Morten and Roana are highly dedicated teachers and that I am thankful for the opportunity to learn from them during the work on this project.

Furthermore I want to thank professor Horst-Günter Rubahn, Luciana Tavares (Researcher, MCI SDU) for technical guidance concerning the  $\text{SiO}_x$  deposition procedure, Yinghui Liu [Master student, MCI SDU] for helping me with the ellipsometer measurements and Helge Jürgensen [Sales engineer at DELO adhesives] for providing free samples and information of one of their companies' products.

Sønderborg d.01. juni 2012

---

Mathias Hausladen

## Contents

<b>Preface .....</b>	<b>2</b>
<b>1. Project formulation.....</b>	<b>5</b>
1.1. Project background.....	5
1.2. Problem Formulation.....	6
1.3. Problem Delimitation .....	6
<b>2. Types of solar cells.....</b>	<b>7</b>
2.1. Mono and polycrystalline cells (1 <sup>st</sup> generation) .....	7
2.2. Thin film cells (2 <sup>nd</sup> generation) .....	7
2.3. Emerging photovoltaic technologies (3 <sup>rd</sup> generation).....	8
<b>3. Theory.....</b>	<b>10</b>
3.1. Inorganic solar cells working principles.....	10
3.2. Organic solar cells .....	11
3.2.1. Organic semiconductor theory .....	11
3.2.2. Materials and processes .....	12
3.2.3. Photo conversion in organic solar cells .....	13
3.2.4. Cell Architecture .....	15
3.3. Challenges .....	17
3.3.1. Power conversion efficiencies.....	17
3.3.2. Stability .....	17
3.3.3. Encapsulation .....	19
3.4. Characterization.....	20
3.5. Lifetime measurements .....	24
3.5.1. Standardized measurements .....	24
<b>4. Fabrication &amp; characterization of inverted ITO free BHJ organic solar cells .....</b>	<b>27</b>
4.1. Production of the OSC substrate with metal bottom electrodes .....	27
4.2. Cleaning of “OSC substrates with bottom electrodes” .....	28
4.3. Active material and PEDOT solution preparation.....	28
4.3.1. Active layer material (P3HT/PCBM) preparation.....	28
4.3.2. PEDOT solution preparation .....	29
4.4. OSC manufacturing in glove box .....	29
4.5. Characterization of organic solar cells .....	31
4.5.1. Electrical characterization .....	32
<b>5. Lifetime measurement of non-encapsulated cell.....</b>	<b>33</b>
5.1. Development of a standardized measuring procedure.....	33

5.2.	Minor device structure change .....	37
5.3.	Reproducibility experiments .....	39
<b>6.</b>	<b>Encapsulations.....</b>	<b>41</b>
6.1.	Requirements .....	41
6.2.	Initial encapsulations.....	41
6.2.1.	Glass plate encapsulation.....	41
6.2.2.	Glass plate / PMMA encapsulation .....	42
6.2.3.	Glass plate with epoxy encapsulation .....	43
6.2.4.	Wire bonding experiments.....	43
6.3.	PMMA/SiO <sub>x</sub> encapsulation .....	44
6.3.1.	Materials and encapsulation concept .....	44
6.3.2.	Initial experiments.....	45
6.3.3.	Encapsulation procedure.....	46
6.3.4.	Lifetime measurement results .....	49
6.4.	Epoxy encapsulation.....	57
6.4.1.	Encapsulation procedure.....	57
6.4.2.	Lifetime measurement results .....	60
<b>7.</b>	<b>Comparison.....</b>	<b>66</b>
7.1.	Advantages and disadvantages .....	66
<b>8.</b>	<b>Future projects .....</b>	<b>67</b>
<b>9.</b>	<b>Conclusion and outlook.....</b>	<b>68</b>
	<b>Bibliography .....</b>	<b>69</b>
	<b>Abbreviations.....</b>	<b>72</b>

## 1. Project formulation

### 1.1. Project background

The energy demand of the world is increasing (see figure 1) and renewable energy sources have to be developed and funded. A projection of the U.S. “Energy Information Administration” states that renewables are the fastest growing source of world energy. This is due to the concern about the environmental impact of fossil fuels, climbing oil prices and strong government support opportunities for increasing the use of renewable energies in many different countries around the world. [1] The yearly energy from the sun which is absorbed by the earth’s atmosphere, oceans and land masses is about 3.850.000 EJ<sup>1</sup>. [2] The total world electricity consumption in 2006 was about 58.9 EJ. [3]

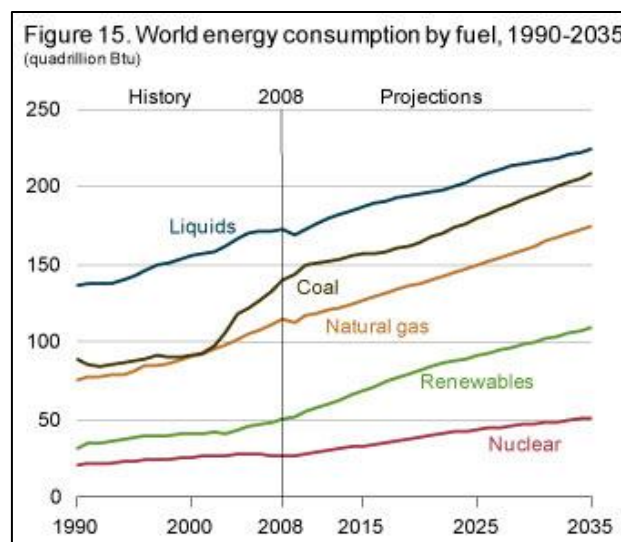


Figure1 U.S. Energy Information Administration. International Energy Outlook 2011. (18.04.2012) <http://www.eia.gov/forecasts/ieo/world.cfm>.

In the past years the interest in organic solar cells as a future renewable energy source has increased. These new types of solar cells are flexible, light weight and can be produced at lower costs compared to their inorganic counterparts. Efficiencies of around 10 %<sup>2</sup> are achieved today for polymer and small molecule cells, but to make a commercialization possible the issue of degradation, which drastically reduces the lifetime of the cells, needs to be solved first.

In this project encapsulation materials and the performance development of P3HT:PCBM inverted bulk-heterojunction solar cells will be investigated. The project is done in corporation with the nanotechnology center “NanoSYD” at the “Syddansk Universitet” in Sønderborg.

<sup>1</sup> Exajoule = 10<sup>18</sup> J

<sup>2</sup> Figure 7 - National Center for Photovoltaics – Latest cell efficiency records NREL p.8

## 1.2. Problem Formulation

The core problem of this project is the degradation of the organic solar cells which results in a short lifetime. The ultimate objective of this project is to investigate encapsulation of inverted bulk-heterojunction solar cells in order to find materials that consider following requirements: a high barrier to water and oxygen, optical transparency, mechanical flexibility and low cost with the aim to establish an encapsulation procedure that prolongs the lifetime of the organic solar cell.

This project will include both theoretical and experimental aspects of organic solar cells and their lifetime.

The specific tasks in this project are:

- Fabricate inverted bulk-heterojunction solar cells from P3HT:PCBM in the SDU Sønderborg laboratories using a pre-established procedure
- Characterize the produced cells by I-V measurements under standard conditions in order to determine their efficiency
- Investigate and find qualified materials for encapsulations based on the listed requirements
- Encapsulate P3HT:PCBM inverted bulk-heterojunction solar cells
- Investigate the variation in performances over time for different encapsulation materials
- Establish an encapsulation procedure that provides increased performance stability for the investigated solar cells

The project has a timeframe of 4 months and is handed in on the 01.06.2012. Equipment and material will be available from NanoSYD and SDU Sønderborg.

## 1.3. Problem Delimitation

Due to the short time frame the material requirements for the encapsulation are split up in two groups with different priorities:

Must have requirements (essential to be fulfilled):

- high barrier to water and oxygen
- optical transparency

Could have requirements (can be excluded)

- mechanical flexibility
- low cost

The focus of this project will be on **performance stability** of the organic solar cells.

## 2. Types of solar cells

For clarity of the topic I will briefly introduce some of the important types of solar cell technologies.

### 2.1. Mono and polycrystalline cells (1<sup>st</sup> generation)

The most common solar cell devices are single PN-junction mono and polycrystalline cells. These cells have a world market share of about 80-90%. [4] Compared to other solar technologies they have higher production costs due to the need of a relative thick layer of doped semiconductor material like silicon, in order to achieve reasonable photon capturing rates. In 2008 the price for 1 kg of contracted silicon was US \$165. [5] **Mono crystalline cells** have a dark blue to blackish coloring (see figure 2).

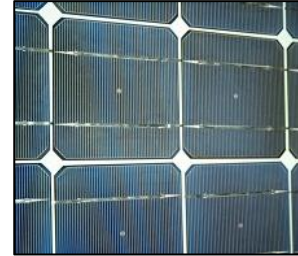


Figure 2 Mono crystalline cell [7]

They are produced from single crystalline silicon and can achieve efficiencies of about 23% (see figure 7 p.8). The theoretical maximum of a single p-n junction solar cell was calculated by Shockley and Queissier to be 33.7% at a band gap of 1.1 eV. [6]

**Polycrystalline cells** also have a bluish color but not as dark as mono crystalline cells. This cell type is made from polycrystalline silicon, which gives it the characteristic crystalline surface structure (see figure 3). This cell type is cheaper to manufacture compared to mono crystalline cells and the cell efficiencies are at 20.4% (see figure 7 p.8).



Figure 3 Polycrystalline cell [7]

### 2.2. Thin film cells (2<sup>nd</sup> generation)

Due to the high costs of the crystalline silicon wafers new light absorbing materials and less expensive production technologies were investigated. Amorphous silicon, Cu(In,Ga)Se<sub>2</sub> (CIGS) and CdTe are the most common thin film cells on the market. The advantage with the thin film technologies is that the materials can be deposited on top of large area flexible substrates by sputtering, plasma enhanced physical vapor deposition and physical vapor deposition, which simplifies high volume manufacturing. The current world market share of thin film technology cells compared to mono and polycrystalline cells is about 10-20%. [4]

**Amorphous silicon cells** have a dark brown to purple coloring (see figure 4). The simplest cell structure consists of three layers (p-i-n). The production is cost effective but the cell efficiencies are only about 6-8% [7], whereas heat stabilized amorphous Si cells achieve 12.5% (see figure 7).

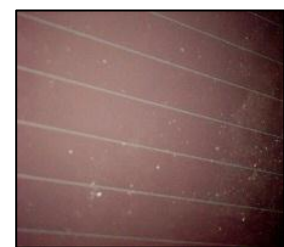


Figure 4 Amorphous silicon [7]



**Cadmium telluride (CdTe)** cells, shown in figure 5, have efficiencies of about 17.3 % (see figure 7). The limiting factor for these cells is the supply of the material Tellurium. In 2009 the USA, with a total output of 50 tons tellurium, was the highest producer followed by Japan with 40 tons. [8] Also the metal cadmium is extremely toxic and recycling of the old CdTe cells is an issue.



Figure 5 Flexible CdTe cells  
<http://gotpowered.com/2011/ge-develops-thin-film-photovoltaic-panels/> (19.04.2012)

**Copper indium gallium selenide solar cells (Cu(In,Ga)Se<sub>2</sub>)** (see figure 6) have the highest efficiency of the thin film cells with a power conversion efficiency of about 20.3% (see figure 7). Current disadvantages are the higher production costs compared to the other thin film technologies. [9] Other second generation technologies are multi junction cells which are containing several p-n junctions. The current efficiencies for different multi junction cells are in the range of 32.6 – 43.5% (see figure 7). In multi junction cells, different p-n junctions are configured to absorb different wavelength of light and are placed upon each other. With some restrictions to the material choices this technique can be applied to silicon crystalline cells and thin film cells. Unfortunately production costs of the multilayer cells are very high and they are used in more specialized applications e.g. space industry or in desert areas with high sunlight concentration. The theoretical maximum of a cell with infinite number of layers using concentrated sunlight is about 86%. [10]

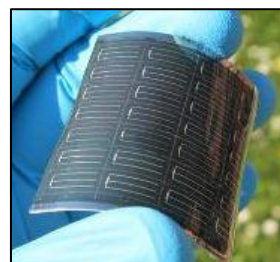


Figure 6 Flexible CIGS cells  
<http://www.azocleantech.com/news.aspx?newsID=15590> (19.04.2012)

### 2.3. Emerging photovoltaic technologies (3<sup>rd</sup> generation)

There are several emerging photovoltaic technologies, which try to reduce the material costs and increase the production efficiency. **Organic solar cells (OSCs)** and **dye sensitized cells (DSCs)** are currently the cells with most potential for the 3<sup>rd</sup> generation devices. OSCs use organic molecules or conductive organic polymers (carbon-compound based) as light absorbing- and charge transport materials, whereas DSCs use organic dyes for the photon absorption. The highest efficiency of OSCs (various types) is about 10% and for the DSCs it is about 11.4% (see figure 7). Advantages of the DSCs are that their performance increases with temperature, whereas on the other side OSCs have lower material and processing costs. Currently OSCs face problems concerning low power conversion efficiencies and short lifetime due to degradations. On the other side, OSCs can be made highly flexible which makes it possible to integrate them in various elements, shapes and sizes. Also they can be customized to various lengths and widths because it is possible to produce them with roll-to-roll manufacturing. They are thin and have a very low weight which makes them suitable for applications where low weight is desired and it makes storing and transporting more cost efficient. OSCs are tough, durable and they won't break like the conventional crystalline PV modules which are made on brittle



glass substrates. Furthermore a big plus is also that all OSCs materials are abundant and recyclable. [11] Organic material is compatible with a wide range of substrates, which makes the production methods very versatile. The manufacturing techniques involved have low temperature and energy demands compared to the silicon cells and could reduce costs significantly. Also material can be saved with the very thin OSCs (100nm) compared to standard silicon crystalline cell (300  $\mu\text{m}$ ) or thin film polycrystalline CuInSe<sub>2</sub> (1  $\mu\text{m}$ ). [11] Through molecular engineering it is possible to change the properties of the organic solution which is used for the OSCs, and influence the abilities to absorb photons and the ability to generate charges. This makes it possible to develop tailor made solutions with specialized molecular properties (e.g. different colorings of the OSCs). At the current level the use of the OSCs is more targeted towards specific applications for e.g. clothes, laptops, small portable devices. [12]

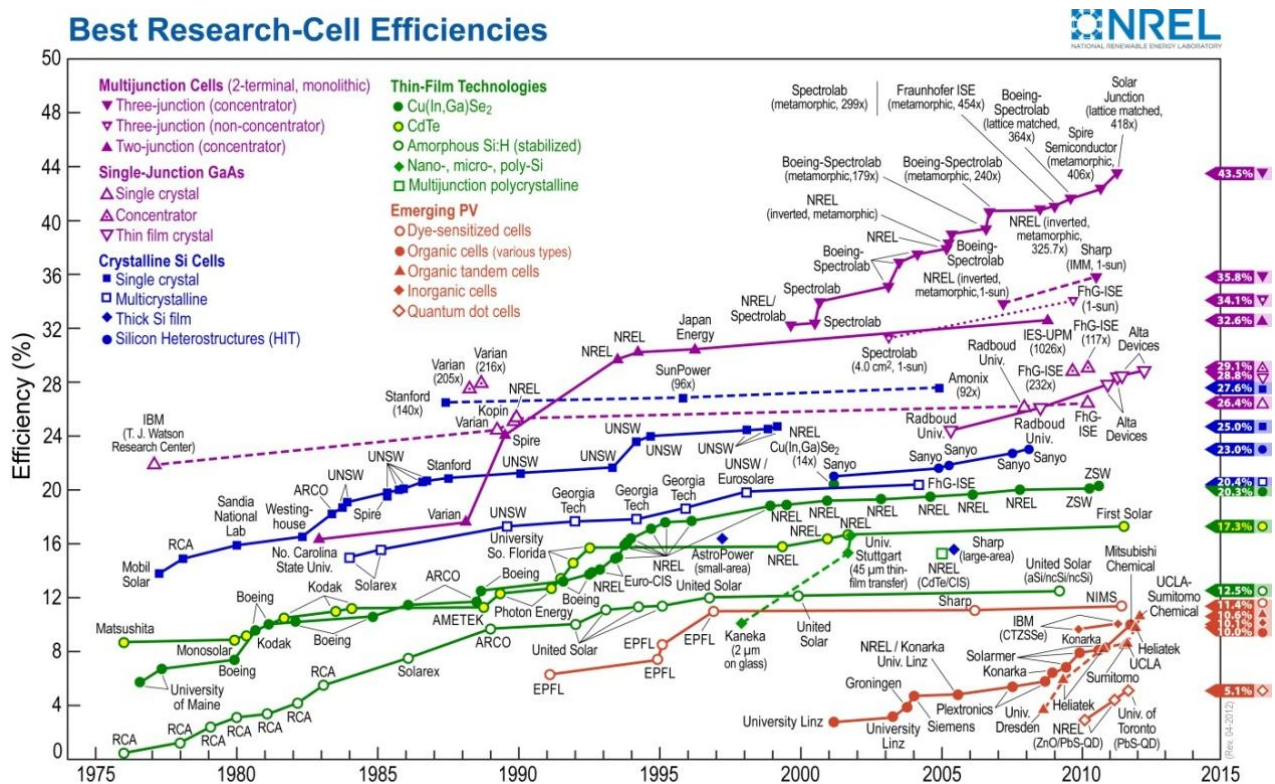


Figure 7 NREL – National Center for Photovoltaics – Latest cell efficiency records NREL  
[http://www.nrel.gov/ncpv/images/efficiency\\_chart.jpg](http://www.nrel.gov/ncpv/images/efficiency_chart.jpg) (17.04.2012)

### 3. Theory

This chapter will give a brief overview of the processes within inorganic and organic cells which convert photons from sunlight into an electrical current. Furthermore materials in OSCs, cell architectures, challenges, characterization and lifetime measurements will be discussed.

#### 3.1. Inorganic solar cells working principles

An inorganic solar cell consists of a positive (p-type) and a negative (n-type) layer of semiconductor materials such as silicon. To achieve the different polarities a process called doping is used (see figure 8). P-type silicon semiconductors are made by diffusing e.g. boron atoms into the silicon crystal lattice. Silicon atoms have four valence electrons whereas boron only has three valence electrons; the boron doping results in an extra hole or a positive net charge. For N-type silicon semiconductors e.g. phosphorus atoms are induced into the silicon crystal lattice. Phosphorus atoms have five valence electrons thus there will be an extra electron, which will result in a negative net charge.

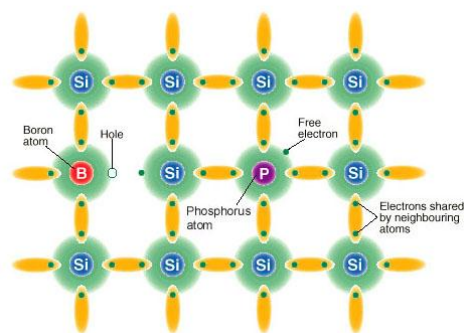


Figure 8 Doped Silicon Crystal Lattice  
<http://www.esdalcollege.nl/eos/vakken/na/zonnecel.htm> (21.04.2012)

The p-type and n-type semiconductor layers are put together and form the pn-junction (see figure 9). [13] When the pn-junction is formed free electrons from the n-type region near the junction interface diffuse into the p-type region, leaving positively charged ions in the n-region and free positive charges (holes) are diffusing from the p-type into the n-type region. Along the junction a charge is building up which creates an electric field that hinders the flow of electrons. At equilibrium the net flow of charge across the junction is zero. This area is called depletion region or space charge region.

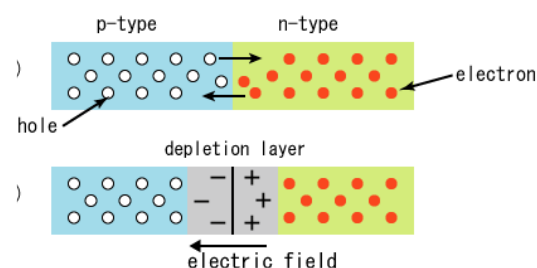


Figure 9 PN-junction  
<http://sv.wikipedia.org/wiki/File:PnJunction-PV-E.PNG> (21.04.2012)

Now when the semiconductor materials are exposed to electromagnetic radiation of very short wavelength (visible or UV-light) electrons will be emitted. The photons in the visible range of the light are absorbed by the valence electron if the photon energy ( $h \cdot \nu$ ) is equal or bigger to the threshold band gap of the semiconductor material. Photons with the needed energy (for silicon 1.11 eV @ 302 K) [14] excite electrons from the valence band into the conduction band, starting to conduct electricity (photovoltaic effect) (see figure 10). As free charge carriers electrons move toward

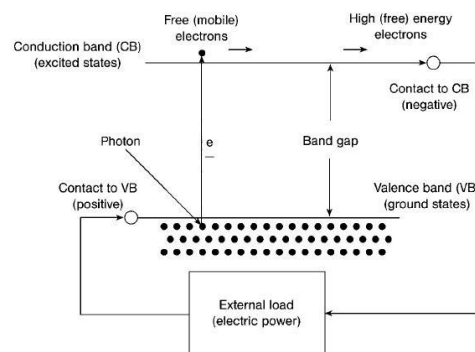


Figure 10 Pagliaro, Palmisano, Ciriminna – Flexible Solar Cells - WileyVCH page 33

the n-type side, where a contact drives the electrons to an external circuit where they lose energy doing work for a load (e.g. light bulb). The electrons return to the valence band of the semiconductor material through a second contact which closes the circuit. [11]

### 3.2. Organic solar cells

#### 3.2.1. Organic semiconductor theory

Organic solar cells use organic semiconducting materials for light absorption and electric current transportation. The ability of organic semiconductors to absorb light and transport electric current is based on the carbon atoms, which are ordered in a so called  $sp_2$ -hybridization configuration. To explain this concept figure 11 is used. In the  $sp_2$ -hybridization configuration the  $sp_2$  orbitals within a plane form a triangle. Another plane which contains the  $p_z$ -orbitals is orientated perpendicular to the  $sp_2$ -plane which results in the molecular structure shown in figure 11. The  $\sigma$ -bonds between the carbon-atoms (red spheres in figure 11) are formed by an orbital overlap of two  $sp_2$ -orbitals.

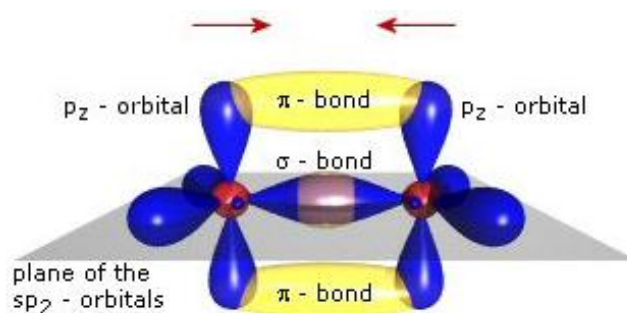


Figure 11 - Orbitals and bonds for two  $sp_2$ -hybridised carbon atoms [15]

In the case of long chains of bound atoms the energy gap between HOMO (highest occupied molecular orbital) and LUMO (lowest unoccupied molecular orbital) is very large which results in insulating properties. But in the case of the  $sp_2$ -hybridization,  $\pi$ -bonds between the  $p_z$ -orbitals are forming. These  $\pi$ -bonds have a much smaller energy difference between HOMO and LUMO, which makes absorption of the visible and near visible light spectra possible and adds the semiconducting properties to the organic material.

A semi-conducting polymer forms a long chain of carbon atoms, where the electrons in the  $p_z$ -orbitals of each  $sp_2$ -hybridized carbon atom, will form  $\pi$ -bonds with neighboring  $p_z$ -orbitals, in a linear chain of  $sp_2$ -hybridized carbon atoms with a delocalized  $\pi$ -electrons system. This will result in an alternating single and double bond structure like in figure 12.

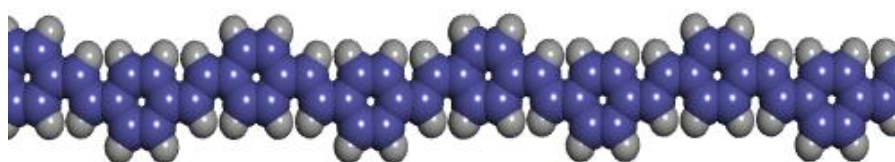


Figure 12 Polymer subunit [15]

The delocalized  $\pi$ -electrons are contained in an orbit that extends across several adjacent atoms. This makes it possible for electrons to move via the  $\pi$ -electron cloud through overlaps by hopping,

tunneling and other mechanisms, which give the polymer conductive properties. The hopping of the charge carriers depends on the energy gap between the HOMO and LUMO levels of the  $\pi$ -bonds. The system described above is also called conjugated system which leads to the name conjugated polymers. [15] [16]

### 3.2.2. Materials and processes

The most prominent materials at the time are the conjugated polymer “poly 3-hexylthiophene” (**P3HT**) and the fullerene derivative “1-(3-methoxycarbonyl) propyl-1-phenyl [6.6] C<sub>61</sub>” (**PCBM**) (see figure 13). [17]

P3HT comes from the polythiophene group and is a soluble electron donor type semiconducting polymer, which provides at the same time a conductive network for the transport of remaining holes (positive charges). [18] It is an excellent absorber of light, which make active layers of about 100-200 nm absorb most of the incident light within its absorption spectrum (see figure 15). PCBM is a soluble fullerene derivative, which acts as an electron acceptor material and has a conductive network for transporting electrons (see figure 14). [19]

The most common processing techniques for the OSC thin film production are “evaporation” and “wet processing”. For the evaporation approach the materials must be thermally stable and for the “wet processing” the material needs to be soluble. At too high temperatures long conjugated polymers will decompose. Also their molar mass is too high for thermal evaporation whereas small molecules are more suitable for the thermal evaporation approach. For semiconducting polymers the wet processing approach is more suitable. Due to their solubility these materials can be processed by spin coating, inject printing or roll-to-roll. Concerning the absorption of photons it would be best to have a material that absorbs as broadly and intensely as possible across the solar light spectrum (see figure 15). Many organic semiconductors have an optical band gap of around 2eV which limits the absorption of the solar spectrum yet chemical flexibility for the modification of the organic semiconductors leaves a lot of options to optimize the materials absorption rate. [16]

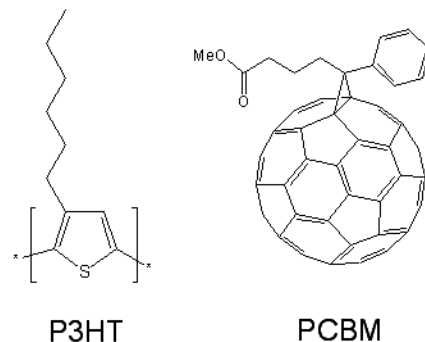


Figure 13 Molecular structures of P3HT & PCBM <http://www.light.t.u-tokyo.ac.jp/english/photovoltaic/Introduction.html> (22.04.2012)

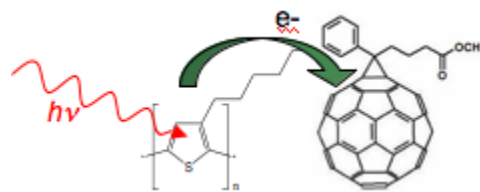


Figure 14 Electron transfer from P3HT to PCBM [http://photonicswiki.org/index.php?title=File:ET\\_P3HT\\_to\\_PCMB.png](http://photonicswiki.org/index.php?title=File:ET_P3HT_to_PCMB.png) (04.05.2012)

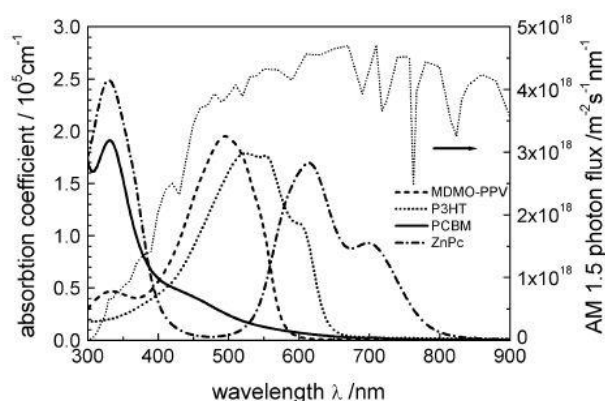


Figure 15 Absorption coefficients of P3HT and PCBM in comparison with the standard AM 1.5 terrestrial solar spectrums. [16]



### 3.2.3. Photo conversion in organic solar cells

The photo conversion process of organic solar cells is slightly different compared to inorganic solar cells. In organic semiconductors the dielectric constant is low and exciton binding energy is high, which means that free charge carriers are not created at room temperature because the exciton binding energy is too large to initiate a separation by thermal energy. On the other side, for inorganic solar cells the exciton binding energy is low and the dielectric constant is high, which means that excitons, which have been created by the absorption of photons, are separated at room temperatures in a positive and negative charge carrier, which will generate a current.

OSCs use two different materials, that differ in their electron donating and accepting properties, which make the creation of free charge carriers possible. The working principles are illustrated in figure 16:

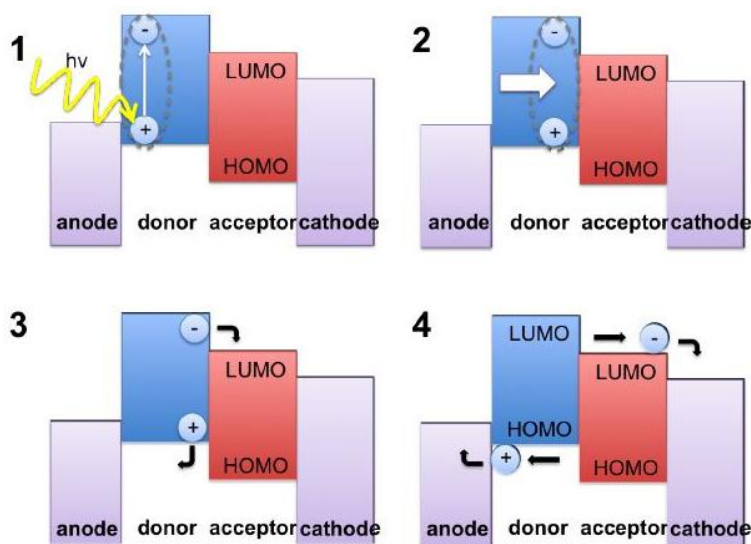


Figure 16: Frederik Krebs. Polymeric Solar Cells: Materials, Design, Manufacture.

DEStech Publications, Inc. (May 17, 2010) ISBN-10: 1605950173

#### 1. Absorption of light (exciton generation) (see figure 16 picture 1)

When the electron donor material is illuminated and the electrons, which occupy the highest molecular orbital (HOMO) absorb photons they are excited into the lowest unoccupied molecular orbital (LUMO) of the donor material. This creates a strongly bound electron-hole pair also called “exciton”.

The absorption coefficients of organic semiconductors are relatively strong ( $>10^5 \text{ cm}^{-1}$ ), so even for thin devices ( $<100 \text{ nm}$ ) almost all incident light is absorbed. [16] [20]

## 2. Diffusion of excitons to an active interface (see figure 16 picture 2)

In order to generate a current the exciton has to reach the interface of the electron donor and acceptor materials during its lifetime. A significant difference between organic and inorganic cells lies in the structure of the cell. Organic materials are amorphous and disordered, which makes the charge transport much more difficult compared to the structured crystalline cells, since the exciton diffusion length is limited to about 10 nm in organic semiconductors. In case when the exciton is generated e.g. 25 nm away from the interface, but it only is able to travel 10 nm during its lifetime, there will be no current production, because the exciton did not reach the interface. This is a common problem in e.g. the bilayer cell architecture. Excitons with a high diffusion coefficient have a longer lifetime and can travel longer distances before they decay back to the ground state, which will produce heat, vibration or release photons, which have been absorbed (photoluminescence). The balance between exciton diffusion lengths, film thickness and exciton lifetime has to be taken into consideration when engineering an organic solar cell. A promising cell design, which covers the mentioned problems, is the bulk heterojunction solar cell architecture (see chapter 3.2.4.). [16] [20]

## 3. Charge separation (see figure 16 picture 3)

Since the exciton binding energies are relatively high (0.1-1eV) the built in electric fields of the orders of  $10^6$ - $10^7$  V/m are not high enough to separate the exciton directly, but the separation of the exciton into free charge carriers can be achieved at the

interface of the electron donor/acceptor material by the sharp drop of potential. [16] Figure 17 shows the processes when an exciton arrives at the interface of the electron donor (D) and electron acceptor (A) materials. The ground state of the two materials is the lowest energy state. In this case it is assumed that the exciton is produced in the donor component which is labeled as  $D^*$  (excited state in the donor) in figure 17. If the exciton reaches the interface and there is a state and energy which corresponds to the exciton energy ( $D^*$ ), the exciton will transfer its electron to the electron acceptor material and the hole remains on the polymer

chains from the donor material. This creates the charge transfer state ( $D^+A^-$ ) in which the electron (negative charge) and a hole (positive charge) move away from each other, which results in a charge separated state. To produce an electric current a full charge separation of the electron and hole has to occur. One of the main reasons for low cell efficiency is the recombination of electron and hole ( $k_{CR}$ ) in the charge transfer state (CT state), which results in an efficiency loss. To maximize the efficiency

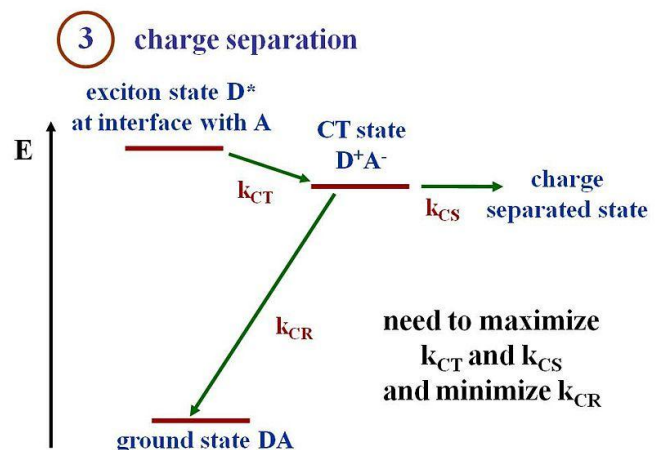


Figure 17 OSC Step 3 charge separation (exciton dissociation)  
[http://photonicswiki.org/index.php?title=File:Opv17\\_chargeseperation.JPG](http://photonicswiki.org/index.php?title=File:Opv17_chargeseperation.JPG) (04.05.2012)

the rate of charge transfer ( $k_{ct}$ ) and charge separation ( $k_{cs}$ ) have to be increased. Furthermore the rate of charge recombination ( $k_{cr}$ ) has to be reduced. [20]

#### 4. Charge transportation & collection (see figure 16 picture 4)

It usually takes a strong electric field to separate an exciton into free charge carriers because of the high exciton binding energy. After the separation of the electron and hole the difference in work functions of the electrodes, which created an electric field, will push the separated free charge carriers towards the electrodes. The electron will be drifting towards the cathode and the hole will drift to the anode. The charge carrier mobility in organic semiconductors is order of magnitudes lower than in inorganic semiconductors. This has a large effect on the efficiency and design of the organic solar cells. If the organic material in the solar cells is more ordered the mobility of the charge carriers will increase. This will result in a faster electron and hole separation because they can move fast away from each other. The charges carriers are collected at the electrodes and if an electrical circuit is connected to the electrodes an electrical current will flow through e.g. an external load where the electron lose energy while doing work. [16] [20]

#### 3.2.4. Cell Architecture

The focus in this project will be on the bulk heterojunction (BHJ) device architecture.

The bulk heterojunction type of photoactive layer is currently the most widely used one. In this device structure electron donating and electron accepting materials are mixed together to form the active layer of the organic solar cell (see figure 18). A phase separation of the two materials on nanometer scale creates many junctions throughout the bulk of the material. This solves the problem concerning the low exciton diffusion length, which makes it possible for the excitons to reach a donor-acceptor junction and separate in order to create free charge carriers. [11] Exciton loss and recombination rate are minimized in this structure. On the other side the exciton diffusion, separation and charge transport of the device is much influenced by the Nano-morphology in the blend, thus the morphology of the blend has a strong impact on the overall solar cell performance. [16]

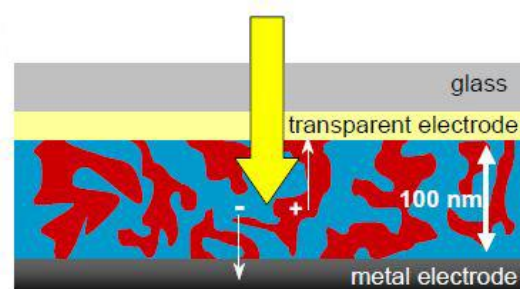


Figure 18 Bulk heterojunction, donor and acceptor materials mixed together <http://www.nrc-cnrc.gc.ca/eng/ibp/ims/enlighten/issue2/organic-photovoltaics.html> (22.04.2012)

The standard applied device structure for polymer/fullerene OSCs can be seen in figure 19. Many state of the art bulk heterojunction OSCs are constructed on substrates, which are coated with indium tin oxide (ITO), which acts as the anode. [21] On top of the ITO the material PEDOT:PSS (poly[3,4-(ethylenedioxy)-thiophene]:poly(styrene sulfonate)) is deposited. The PEDOT:PSS is a molecularly doped conjugated polymer. It acts as a hole-transport layer and blocks electrons from reaching the



anode. The photo active layer is then deposited on top of the PEDOT. [16] A PEDOT film thickness of about 70-350 nm results in a good compromise between light absorption and transport-loss due to charge carrier recombination. An aluminum cathode which collects the electrodes is deposited on top of the photoactive layer, which completes the solar cell. [18]

The drawback of this cell architecture is that the ITO is considerably increasing the production costs of the OSCs. To successfully commercialize the OSCs it's important to reduce their production costs and replace the ITO by another highly conductive, transparent and inexpensive material. Improved PEDOT:PSS with a higher conductivity and transparency makes it possible to fabricate cells without ITO. [21]

The inverted ITO-free bulk heterojunction OSC solves the cost related problems, which arise from ITO, by inverting the structure (see figure 20). The cathode becomes the bottom electrode and the PEDOT on top of the photo active material acts as an anode.

The different layer order creates interfaces with different chemistries which affect the stability of the cells. The standard structure uses low work function metals e.g. aluminum, whereas in the inverted cell geometry, higher work function metals (e.g. silver) can be used for the back electrodes. The use of silver as a back electrode makes the inverted structure much more stable compared to the standard structure, yet the efficiency of the standard structure is higher. [22]

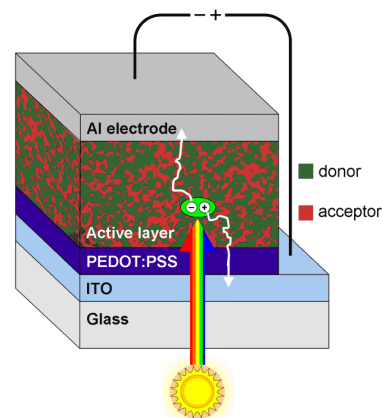


Figure 19 Bulk-heterojunction OSC  
<http://www-ssrl.slac.stanford.edu/science-summary/2011/january/effects-thermal-annealing-organic-solar-cells> (05.05.2012)

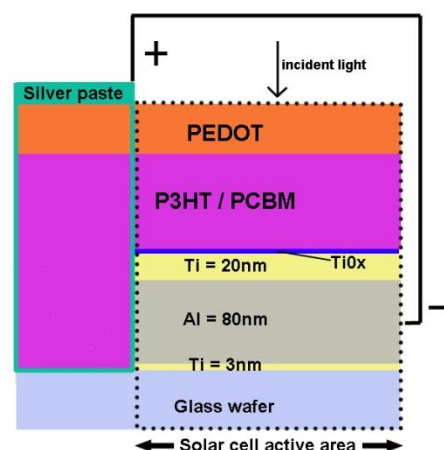


Figure 20 Section cut of inverted ITO-free bulk heterojunction organic solar cell (picture by Mathias Hausladen)

### 3.3. Challenges

Three main challenges have to be covered properly for a successful commercialization of OSCs (see figure 21). The challenge is to develop a high enough efficiency to compete with the more established photovoltaic devices, optimize the material and cell manufacturing processes including costs and achieve a stability which gives a long term operational lifetime.

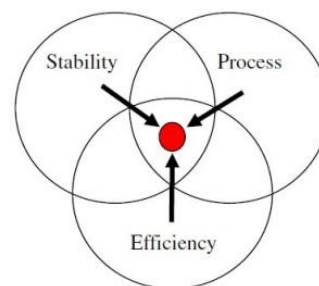


Figure 21 Unification challenge: source [23] p. 687

#### 3.3.1. Power conversion efficiencies

To further optimize the efficiencies of OSCs novel donor and acceptor materials have to be developed which are able to self-organize (enhanced order) and thus optimize the charge transport. Also the absorption spectrum of the light absorbing materials should be as wide as possible in order to harvest most of the incident light. [11] The purity of the organic materials and solvents is also an issue which has to be addressed. Currently various grades of PCBM with purities from 95% - 99.9% can be supplied. Also purification of P3HT is difficult and oligomers, monomers and various sub products are decreasing the charge-carrier transport and recombination rates, which in the end lowers the power conversion efficiencies. For example metal residues from catalysts can be found at levels from 1 to 200 ppm in P3HT. Another problem is photo oxidation of the P3HT which lowers the molecular weight. In case of the P3HT the molecular weight is a crucial parameter. The higher the molecular weight of the P3HT is, the higher the hole-mobility gets. [17]

#### 3.3.2. Stability

During the last years a great amount of effort was made to increase the power conversion efficiencies of the OSCs by finding new materials and device structures, yet before a successful commercialization will be possible, both stability and reliability of the OSCs have to be understood and optimized in order to guarantee long operational lifetimes. There are many different causes for the degradation of OSCs; Mechanical stress can lead to electrode failure or delamination. Stress induced by temperature accelerates the degradation and can cause morphological changes. Electrical stress caused by the electric field or columbic charge can cause internal short circuits and localized heating. Light itself causes photochemical oxidation, photo bleaching and mechanical failure. Yet the most dominant cause for the degradation is due to oxygen and humidity (water), which oxidizes the donor/acceptor materials and electrodes, gives rise to interface failure and change in mobility of charge carriers. [19]

Organic materials are more prone to chemical degradation in comparison with the inorganic material. The complex degradation mechanisms can be divided into chemical and physical categories:

### 3.3.2.1. Chemical degradation

Chemical degradation in OSCs deals with the role of water ( $H_2O$ ), oxygen ( $O_2$ ), electrode material and their reactions with the active polymer layer (see figure 22).

#### Diffusion of oxygen and water into OSC device:

The performance of OSCs is degrading faster if the device is exposed to oxygen and water (ambient air). During the manufacturing process small amounts of water and oxygen can be absorbed in different layers but mostly water and oxygen is diffusing into the finished OSCs.

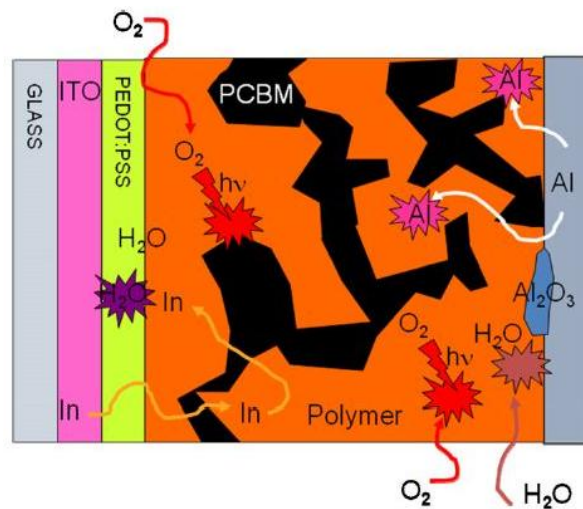


Figure 22 Cross section view of some degradation processes in standard bulk heterojunction devices, [23] p. 688

In a standard BHJ device the oxygen and water diffuses through the top electrode through microscopic pinholes (see figure 23). [23] (In the inverted BHJ structure the reactive low work function metal cathode was eliminated resulting in higher air stability.)

Degradation of the PEDOT:PSS layer due to the absorption of water from the atmosphere, which increases the sheet resistance of the PEDOT:PSS is also a problem.

In the case of the absorption of molecular water and oxygen the barrier effect of the individual materials, which is linked to the layer thickness, is also important. Also the order in how the different layers are stacked is important, because that will define the barrier effect at a given position/interface in the OSCs. [22]

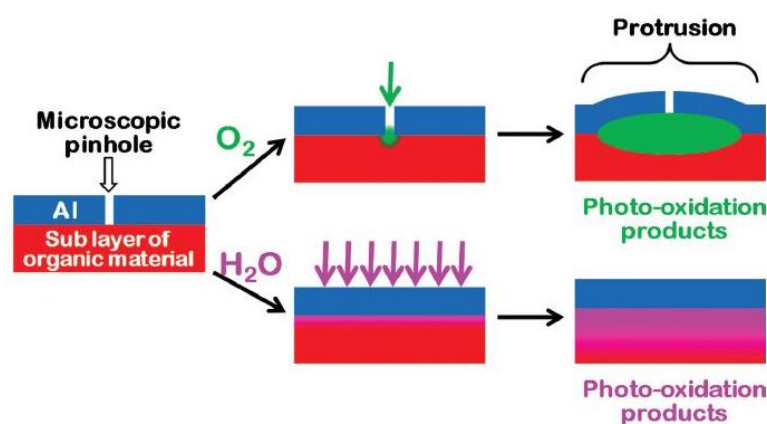


Figure 23: “Representation of the outer aluminum electrode showing two different entrance channels for water and molecular oxygen. Molecular oxygen mainly diffuses through microscopic pinholes. Water mainly diffuses in between the aluminum grains.” Source [22] page 591

Photo-oxidation of polymers: Organic materials are degrading when exposed to radiant energy e.g. UV light because of photolytic and photochemical reactions. The absorption of oxygen and water facilitates the photo oxidation process of the different OSCs layers such as oxidation of the electrodes or active layers. [23] Low work function electrodes e.g. aluminum can form metal oxides, which will work as an insulator and block the charge transport, which leads to a drop in cell efficiency. Also the active layer organic materials are degrading by photo oxidation. Another process could be that the metals in the cell will react with the organic material which leads to more reactions with oxygen and water. [22]

#### **3.3.2.2. Physical degradation**

The device efficiency depends on the precise thickness of the different material layers, which are responsible for photon absorption and charge carrier transportation. In BHJ cells the phase segregation of the active layer is another important point, which is influenced by the fabrication process. In case of a polymer/PCBM solution the solvent, concentration, ratio of donor and acceptor, spin coating parameters and annealing temperature/time have a major influence on the phase segregation and stability. Due to temperature changes morphological changes in the cell can occur, which ultimately influence the absorption and charge carrier transportation, thus a morphology which is thermally stable would be the optimum. [23]

#### **3.3.3. Encapsulation**

To achieve a high operating lifespan the cell main issue is the internal degradation of organic material due to photo-oxidation. Even in a vacuum the cell's efficiency degrades, which means that the best case scenario would be to solve the internal degradation issues and find materials with stable electro optical properties, which are resistant to chemical and photochemical degradation. Yet at the current time, an encapsulation would be a good solution for achieving a successful initial commercialization of OSCs in consumer electronics with an operating lifespan of 3-5 years. The encapsulations also will increase the mechanical stability, scratch resistance and furthermore they can work as UV-filters to minimize the photo-oxidation processes. [22]

There are many different organic and inorganic materials, which can be used for encapsulating the OSCs. The encapsulation materials should have a low water vapor transmission rate (WVTR) and a low oxygen transmission rate (OTR). To achieve a lifetime of about 10.000 h, the estimated WVTR should be around  $10^{-6}$  g/m<sup>2</sup>/day and the OTR should be around  $10^{-3}$  cm<sup>3</sup>/m<sup>2</sup>/day at room temperature. [24]

It is important that the encapsulation as a passive component is not minimizing the appealing qualities of the OSCs, thus the encapsulation should be flexible, transparent, light weight and cost efficient. Furthermore the encapsulation needs to be targeted for the specific cell architecture and targeted lifetime. [25]

Processing methods for encapsulations depend on the materials and include deposition techniques like e.g. thermal evaporation, *plasma enhanced chemical & physical vapor deposition (PECVD & PEPVD)* and atomic layer deposition (ALD). Also low cost processing techniques such as lamination and coating can be used to create encapsulation films.

In general the processing temperature has to be compatible with the temperature limits of the polymer materials which are used in the OSC. Due to the lower processing temperatures intrinsic defects in the film give water and oxygen the opportunity to diffuse through the film defects. High barrier multilayer films are a promising solution where e.g. PECVD is used to deposit a base film and ALD is used to close small pin-holes (defects) in the base film by depositing an ultrathin layer of another material on top of the base film. [26] Also barrier films from food and packaging industry can be used to encapsulate OSCs. There is a direct relationship between cost and barrier performance, so it is key to know the barrier requirements.

### 3.4. Characterization

To obtain information about the performance of a solar cell, the cell's current is measured as a function of voltage and the data are plotted as an IV-curve. In dark the solar cell shows the same electrical characteristics like a large diode (see figure 24 black-curve).

When illuminated the IV curve of the solar cell shifts because it starts to generate power (see figure 24 red curve). [27] As the intensity of the incident light increases, more current is generated by the solar cell and the shift  $I_L$  becomes greater. [28]

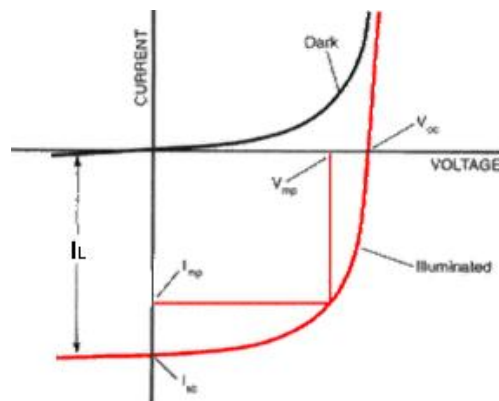


Figure 24 - IV curve of solar cell

[http://stuff.mit.edu/afs/athena.mit.edu/course/3/3.082/www/team2\\_f02/Pages/background.html](http://stuff.mit.edu/afs/athena.mit.edu/course/3/3.082/www/team2_f02/Pages/background.html) (13.05.2012)

The most important factors to characterize a solar cells performance are the open circuit voltage ( $V_{oc}$ ), the short circuit current ( $I_{sc}$ ), the fill factor and the power conversion efficiency (PCE).

The open circuit voltage ( $V_{oc}$ ) is the voltage when the two terminal of the solar cell are isolated. It occurs when no current is passing through the cell:  $V \text{ (at } I=0) = V_{oc}$ .

The short circuit current ( $I_{sc}$ ) is the current which flows when the two solar cell terminals are connected with each other.  $I_{sc}$  occurs when the voltage across the solar cell is zero:  $I$  (at  $V=0$ ) =  $I_{sc}$  (see figure 25). [28]

The current of a solar cell depends on the cells area. To be able to compare cells with different cell areas the current density is used, which is defined as:

$$J_{sc} = \frac{I_{sc}}{\text{solar cell areas}}$$

The cells operating regime is in the range between  $V=0$  and  $V_{oc}$ , during which the cell delivers the power density:

$$P = J_{sc} \cdot V$$

The maximum power point (see figure 25) is the point where the solar cell delivers most power. It occurs at the voltage  $V_{MPP}$  and the corresponding current density  $J_{MPP}$ .

$$P_{max} = V_{MPP} \cdot J_{MPP}$$

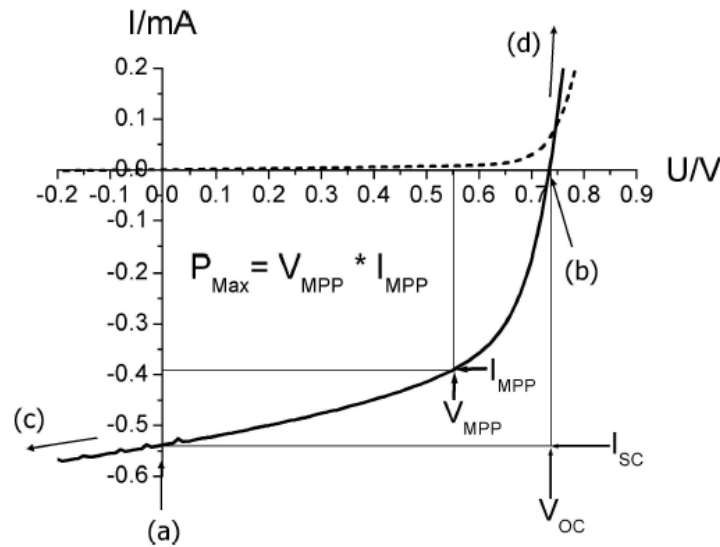


Figure 25 – IV curve of organic solar cell (dark dashed line and illuminated full line) [16]

The letters in figure 25 describe the different working conditions of the cell. At (a) the cell is illuminated and photo generated charges drift toward the contacts (closed circuit condition). At (b) the current becomes zero and the open circuit condition takes over. At (c) the cell operates under reverse bias and photo generated charges travel in strong electric fields. The cell works as a photo detector in this mode. In (d) the cell operates in forward bias which is larger than  $V_{oc}$ . The injection increases and the diode will open up. [16]

The Fill Factor (FF) measures basically the quality of a solar cell. It is calculated by taking the ratio between the maximum power (see figure 26 blue box) and the theoretical power ( $P_T$ ) which is the product of the open circuit voltage and short circuit current (see figure 26 green box). The FF is often stated as a percentage and it is desirable to achieve a large FF, which would correspond to a more square-like IV curve. [28] The FF is calculated by the following formula:

$$FF = \frac{J_{MPP} V_{MPP}}{J_{sc} V_{OC}} = \frac{P_{max}}{J_{sc} V_{OC}}$$

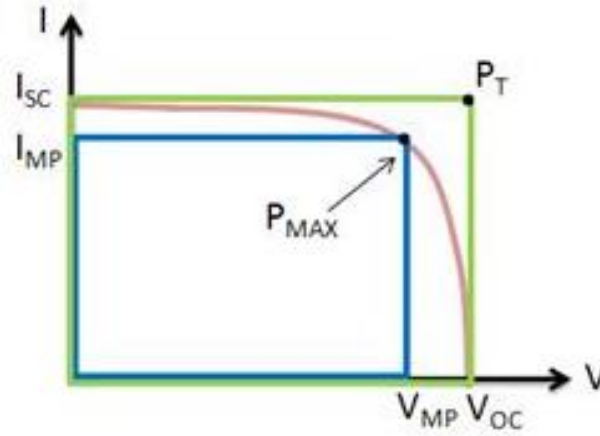


Figure 26 Fill Factor (blue). <http://www.ni.com/white-paper/7230/en#toc1> (12.05.2012)

Note that the current axis in figure 26 has been inverted. This is a convention since the cell is generating power. [27]

The solar cells efficiency is the ratio between the maximum power output and the power density of the incident light  $P_s$ :

$$\eta_{max} = \frac{P_{max}}{P_s} = \frac{J_{MPP} V_{MPP}}{P_s} = \frac{J_{sc} V_{OC} FF}{P_s}$$

In this project  $P_s$  is measured in  $mW/cm^2$  or in one sun which equals  $100 mW/cm^2$ . [28]

The Fill Factor and thus the efficiency of the solar cell are minimized by power dissipations across internal cell resistances. The parasitic resistances are modeled as a series resistance ( $R_s$ ) and parallel shunt resistance ( $R_{SH}$ ) (see figure 27). In an ideal case the parallel resistance ( $R_{SH}$ ) will be infinite, so there will be no other path for the current to flow (no leakage currents). The series resistance ideally should be zero which would result in no voltage drop before the load. [28]



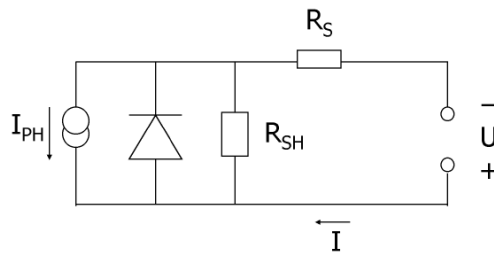


Figure 27 equivalent circuit of solar cell, source: [16] page 1930

The series resistance adds up from all the different series resistances which are coming from the bulk transport, interface transport and transports through the contacts. [16]

If  $R_s$  is increasing and  $R_{sh}$  is decreasing, the FF of the solar cell will decrease and  $P_{max}$  will shift to a lower position. In the case where there is a lot of leakage current in the cell so  $R_{SH}$  is decreasing a lot,  $V_{oc}$  will also drop. In the other case where there is a high series resistance in the cell and  $R_s$  is increasing excessively,  $I_{sc}$  could drop instead (see figure 28). [28]

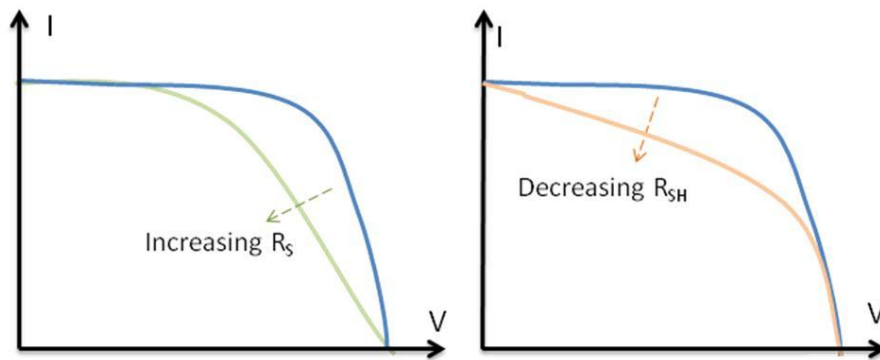


Figure 28 series and parallel resistances [28]

### 3.5. Lifetime measurements

The most common and simplest measurement of the OSC lifetime is the electrical measurement of the OSCs during illumination, to obtain the IV-curves. This gives information about the electrical transport and power generation of the device. From the IV-curves information about  $V_{oc}$ , FF, PCE,  $J_{sc}$ ,  $R_{sh}$  and  $R_s$  can be obtained. The most useful parameters for evaluating the lifetime of a cell are the PCE and  $J_{sc}$ , because they directly reflect the ability of the device to convert photons into electrical energy. The open circuit voltage  $V_{oc}$  is also degrading over time, but its decay doesn't always happen as straightforward as for the PCE and  $J_{sc}$ . [23]

If a chosen parameter of the OSC (e.g. PCE) is plotted as a function of time, one can obtain information based on the general shape of the curve, about how the degradation influences the PCE over time (see figure 29). The shape of the curve is influenced by the different degradation mechanism and combinations of them. Commonly the curves will follow an exponential decay, a linear decay or a combination of them. It is also often seen that the device performance improves during the first part of the device lifetime, which could be due to annealing effects in the cell structure. [23]

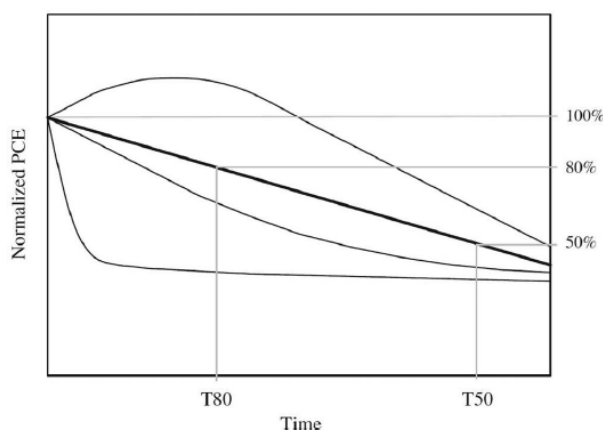


Figure 29 - Example of various decay curves that have been commonly reported. Source [22] p.605

The benefits and purpose of measuring the device lifetime by a decay curve is to obtain information whether the device is stable and how it degrades. More importantly it gives the opportunity to compare different devices, which are made from different materials. This measuring method helps to improve the OSCs stability by finding and fine-tuning the design errors and flaws of the device architecture, materials used in cell & encapsulation and the fabrication methods. [23]

#### 3.5.1. Standardized measurements

In the past years more and more publications about the lifetime of organic solar cells have been published. Also just in the last few years scientists started working more intensely to establish common measuring standards for the organic solar cell life time characterizations, so different groups around the world are able to compare their results. The ISOS-3 summit has recently been established.

This standard provides detailed information on how to perform and report indoor and outdoor lifetime measurements for OSCs<sup>3</sup>. This standard is divided into different levels; basic, intermediate and advanced. The basic level is for research facilities using simplest measurement equipment (hand-held) and few testing conditions. The intermediate level uses protocols and fixed measurement conditions. This level is suited for most laboratories. The advanced level is using standardized testing in certified laboratories that employ an extended range of parameter to monitor the OSCs. [22]

In general it is important that different science groups around the world employ standards, so the results of their OSCs can be compared with each other. For indoor weathering testing often solar simulator in combination with weathering chambers are used for aging the OSC at indoor conditions. Here the spectrum of the light source significantly affects the rate of decay (see figure 30). Especially the UV radiation is contributing to the degradation of the OSC. Based on the ISOS-3 standard it is mandatory for the intermediate research facility level to use a light source with close match to the AM 1.5G in order to achieve accurate and more realistic measurements. [22]

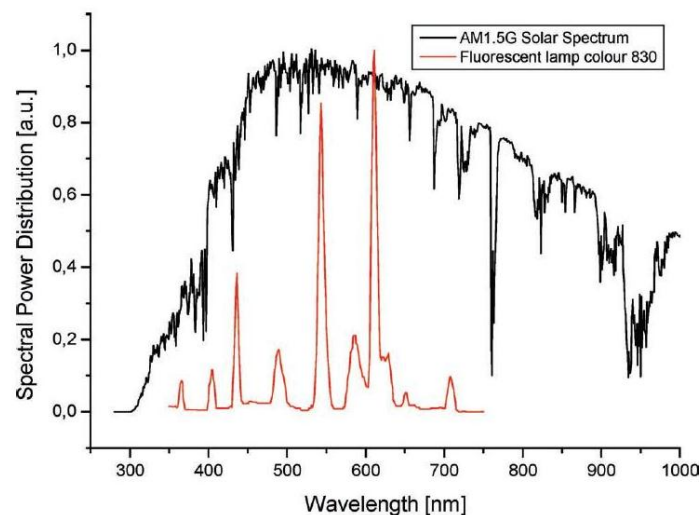


**Figure 30 – “Comparison of the spectrum of a fluorescent lamp with the light color 830 and the AM1.5 spectrum of the sun.” source [22] p.605**

Also the reporting of the operational lifetime has been evaluated and a set of parameters has been established to describe the device lifetime (see figure 31).

<sup>3</sup> See appendix „ISOS 3 – OSC lifetime measuring standard“ page 2

$E_0, T_0$	$E_0$ is the initial testing measurement of an OPV device immediately after final fabrication of the device, at time = 0, $T_0$ .
$E_S, T_S$	$E_S$ is a second testing measurement of an OPV device, defined arbitrarily by the user as some time, $T_S$ , after the fabrication of a device.
$E_{80}, T_{80}$	$E_{80}$ is the testing measurement of an OPV device after the device has decayed 20% from the initial testing measurement, $E_0$ . $T_{80}$ is the time it took to decay to $E_{80}$ .
$E_{S80}, T_{S80}$	$E_{S80}$ is the testing measurement of an OPV device after the device has decayed 20% from the second testing measurement, $E_S$ . $T_{S80}$ is the time it took to decay to $E_{S80}$ .

Figure 31 "Four pairs of parameters needed to define OSC device stability" Source [22] p.605

Figure 32 shows the parameters applied from figure 31 in a decay curve where the PCE as a function of time is displayed.

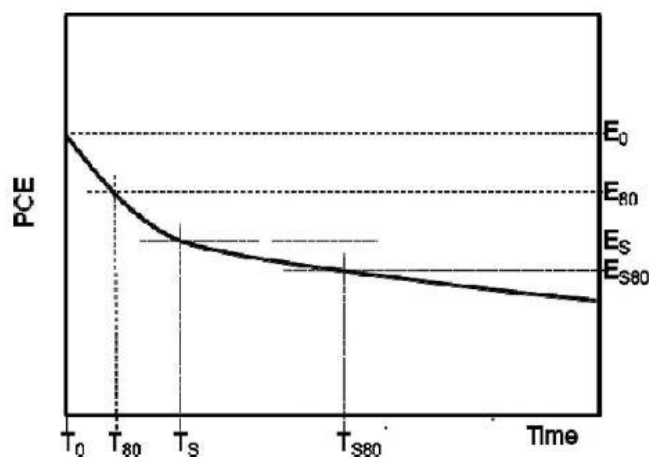


Figure 32 – “Representative figure defining the parameters to be included in the reporting of OSC stability data.” Source [22] p.605

It is also recommended to report the “device handling” history which also improves comparability of the results. Generally all parameters which could influence the lifetime of the device should be reported. This includes information about device encapsulation, device layout and geometric sizes, methods for contacting device anode and electrode, layer thicknesses of device electrode and the substrate and so on. [22]

## 4. Fabrication & characterization of inverted ITO free BHJ organic solar cells

This chapter summarizes all experimental details concerning the fabrication and characterization of the organic solar cells during this project. In this project the inverted ITO free bulk heterojunction (BHJ) organic solar cell (OSC) architecture is used as show in figure 33.

A glass wafer functions as the substrate of the solar cell. The electrodes are patterned onto the wafer substrate by photolithography steps and metal deposition. A 3nm layer of titanium is deposited to increase the adhesion of the 80 nm aluminum electrode. On top of the aluminum electrode a 20 nm thick layer of Ti is deposited. This layer acts as an anti-oxidation layer for the aluminum layer. Aluminum oxide decreases the conductivity of the aluminum electrode and thus the PCE of the OSC. A thin layer of titanium oxide ( $\text{TiO}_x$ ) forms naturally on top of the 20 nm titanium layer and acts as an electron transport and hole blocking layer (cathode). Then the active layer is deposited, which consists of P3HT/PCBM. P3HT is an electron donor and PCBM is an electron acceptor material. On top of the active material a layer of PEDOT is deposited. The PEDOT layer acts as a hole-transport layer and blocks electrons (anode). Finally a layer of silver paste is applied. In the following chapter the different production processes are explained and supplemented with detail production recipes in the appendix.

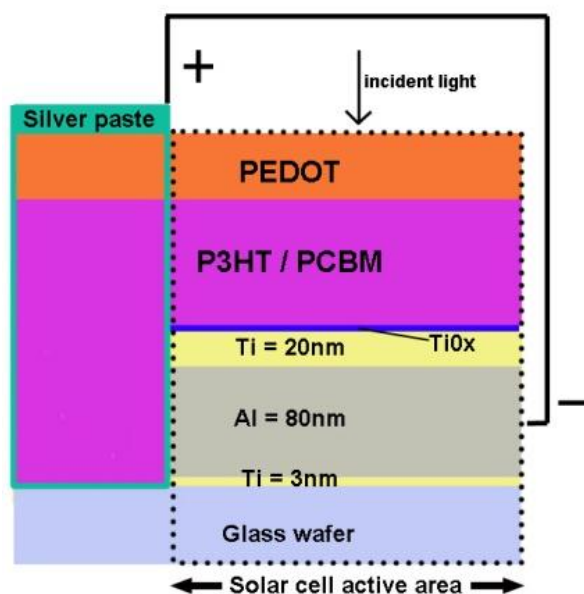


Figure 33 - Section cut of inverted ITO-free BHJ OSC

### 4.1. Production of the OSC substrate with metal bottom electrodes

The production of the metal bottom electrodes has been performed in the NanoSyd<sup>4</sup> class 100 cleanroom. To produce the bottom electrode a polished BK7 glass wafer has been cleaned and treated by a negative photolithographic process, according to a pre-made recipe<sup>5</sup>, to generate a pattern of the electrodes, on top of the glass wafer.

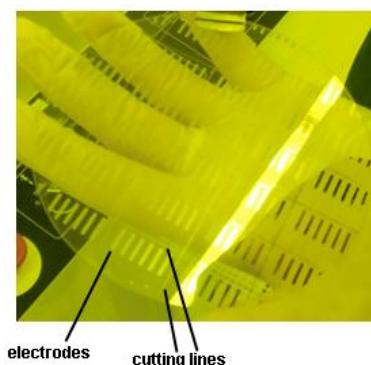


Figure 34 - finished wafer bottom electrodes

<sup>4</sup> <http://www.nanosyd.dk/cleanroom/en/page/facilities> (15.05.2012)

<sup>5</sup> See appendix "Process recipe for wafers bottom electrodes" on page 5-6

After the photolithographic processes the metal electrodes (3 nm Ti, 80 nm Al, 20 nm Ti) have been deposited with the “Cryofox Explorer 600 LT”.<sup>6</sup> The final step was to lift-off the remaining photoresist with acetone in a wet bench to achieve the finished structures on the glass wafer (see figure 34).

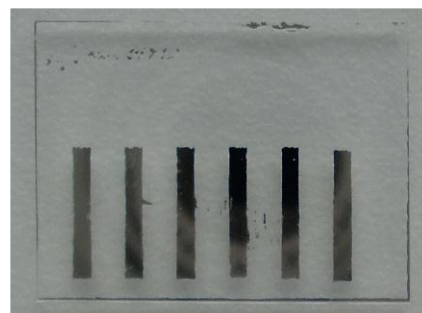


Figure 35 - OSC bottom substrate with 6 electrodes

Finally the wafer was cut along the wafer cutting lines (see figure 34) into small substrates with a wafer cutting Dicing saw (Disco DAD-2H5) which uses a diamond blade for the cutting process. Figure 35 shows the finished OSC glass substrate with 6 bottom electrodes. Note that during the project the design of the bottom electrodes has been changed which is discussed in chapter 4.5 on p.30.

## 4.2. Cleaning of “OSC substrates with bottom electrodes”

Before the OSCs are produced the glass substrates with the bottom electrodes have to be cleaned from dust, glass particles from the cutting process and other contaminations. This procedure is done in the cleanroom under a fume hood from “PM plast technology AB”. The substrates are put into a glass beaker which is filled with acetone and ultrasonicated with the “Branson 3510” for 2 minutes, which will remove organic and inorganic particles. Afterwards the acetone is rinsed off by Isopropanol. Then the isopropanol is removed with distilled water and the sample is blow dried with nitrogen. The process is finished by putting the samples into a plasma asher (Branson IPC 3000) for 6 min. During this process the chamber of the plasma asher pumps down to about 0.5 torr pressure. A flow of 60 sccm oxygen and RF power of 100 W was applied. The RF energy is creating an oxygen-plasma, which will react with organic materials on the sample surface and at the end the oxidized organics are pumped out of the chamber as exhaust gas.<sup>7</sup> After the cleaning procedure is completed, each substrate is individually stored in small 73x73x30mm plastic boxes, so contamination during the transport from the cleanroom facility to the external glove box facility is minimized.

## 4.3. Active material and PEDOT solution preparation

### 4.3.1. Active layer material (P3HT/PCBM) preparation

The active layer is a mixture of poly (3-hexylthiophene-2,5-diyl) (P3HT) and phenyl C61 butyric Acid Methyl Ester ([60]PCBM) (99.5% purity) (PCBM). For this 200 mg P3HT and 200 mg PCBM (ratio 1:1) have been diluted in 10 ml of dichlorobenzene.<sup>8</sup> The mixture was stirred overnight at 600 rpm at 65 °C. See appendix “Recipe for P3HT/PCBM blend” page 7 for detailed information.

<sup>6</sup> See appendix “Recipe for Cryofox Explorer 600LT” p. 6

<sup>7</sup> <http://www.nanosyd.dk/cleanroom/en/page/plasma-asher> (15.05.2012)

<sup>8</sup> Note: during the first 9 weeks of the project chlorobenzene has been used as a solvent. Later on the production switched to dichlorobenzene, which was expected to result in a better Nano-morphology of the P3HT/PCBM film. Experiments have shown minor changes for the PCE, FF, Voc and Jsc using this solvent.

#### 4.3.2. PEDOT solution preparation

In this project two different PEDOT solutions have been used. During the first 7 weeks a PEDOT blend based on a high-conductivity formulation of PEDOT:PSS (H.C. Starck CLEVIOS PH-1000) and another formulation of PEDOT:PSS (H.C. Starck CLEVIOS CPP 105D) mixed at a ratio of 3:1. [29] To increase the conductivity of the 3:1 PH1000:CPP PEDOT mixture, 5% “dimethyl sulfoxide (DMSO)” has been added to the solution. The mixture was stirred overnight at 300 rpm at room temperature. See Appendix „Recipe for PEDOT blends – PH1000:CPP PEDOT” page 8. The issue with this PEDOT mixture was, that in order to process it, it needed to be ultra-sonicated for about 60-120 min to enhance the wettability on the hydrophobic P3HT:PCBM layer. The ultra-sonication process significantly increased the production time of the OSCs, so the 3:1 PH1000:CPP PEDOT mixture was substituted with a new mixture.

The new solution is mixed together from Mix Clevios™ HTL Solar PEDOT with PEDOT:PSS (H.C. Starck CLEVIOS CPP 105D) at a ratio of 1:1. It has a very good wettability and it's not necessary to ultrasonicate the solutions before processing it, which saves a significant amount of time. See Appendix „Recipe for PEDOT blends - HTL:CPP PEDOT” page 8.

The properties of the new mixture can be controlled; HTL is increasing the adhesion to the active layer in case of bad wettability and CPP will act as electron blocking layer (or hole transport layer), making a good charge selection. Due to the high work function of the CPP PEDOT it is energetically non-favorable for electrons to be collected and conducted by this material. Roana Melina de Oliveira Hansen (postdoc, MCI SDU Sønderborg) has measured the sheet resistance of the different PEDOT:PSS types to be; CPP PEDOT: 400 ohm/sq, HTL solar: 250 ohm/sq and HTL solar: CPP PEDOT (mixture) : 230 ohm/sq. Furthermore an experiment has been conducted, to verify if the change to the HTL:CPP PEDOT mixture results in any significant differences concerning the stability of the cells (see chapter 5.2.2. p.37).

#### 4.4. OSC manufacturing in glove box

The complete production of the cells was performed inside a glove box from “GS Glovebox Systemtechnik”.<sup>9</sup> Pressurized nitrogen in bottles supplied by “YaraPraxair”<sup>10</sup> was used to create an inert atmosphere in the glove box. This was done to avoid oxygen and H<sub>2</sub>O, which would degrade the OSCs during the production.

The substrate was cleaned with acetone while spin coating it at 1000 rpm for 45s. The transport from the cleanroom to the glove box could have contaminated the samples, thus the spin coating with acetone cleans the substrates before the application of the active layer. After the spin coating the acetone is evaporated by placing the substrate on a hotplate for 2 min at 90 °C.

<sup>9</sup> <http://www.glovebox-systemtechnik.de/gs-glovebox-plexiglas.htm> (17.05.2012)

<sup>10</sup> <http://www.yarapraxair.no/gass/nitrogen/> (17.05.2012)



After the cleaning procedure the substrate is ready for further processing and a blue glue tape is applied to cover part of the Ti/Al electrodes (see figure 36). The blue glue tape covers part of the electrodes from the active layer (P3HT/PCBM), so it's possible to characterize the cell later by probing the bare Ti/Al electrodes.

With a plastic pipette a few drops of active layer material (P3HT/PCBM) are applied on top of the substrate with the blue glue stripe. By spin coating at 1000 rpm for 45s, it was measured that an active layer thickness of about 180 nm is reached (see figure 37).<sup>11</sup>

After spin coating, the blue glue tape is removed and the substrate is placed on the hotplate and annealed for 25 minutes at 140 °C (see figure 38)<sup>12</sup>. The annealing process improves the active layer morphology, creating a better interface between donor and acceptor thus improving the efficiency of the cell. This step has to be done in nitrogen atmosphere, since the presence of oxygen and water molecules can damage the layer during the annealing process.

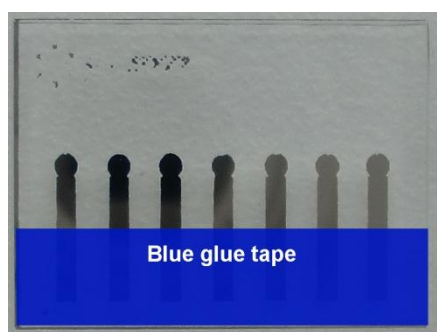


Figure 36 - blue glue tape covering part of the Ti/Al electrodes

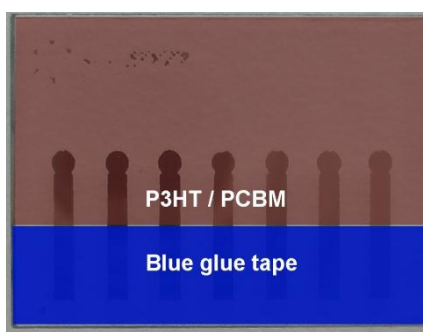


Figure 37 - Blue glue tape and active layer material

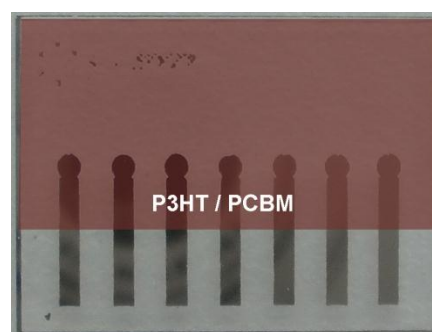


Figure 38 - blue glue tape removed after active layer deposition

After the baking process another blue glue tape is applied. The blue glue stripe should cover the bare electrodes and a part of the active layer in order to avoid contact of the PEDOT with the bottom electrodes, which would cause a short circuit. The position of the blue glue stripe will determine the size of the active solar cell (see figure 39).

After the blue glue tape is posited, a few drops of the PEDOT mixture are applied with a plastic pipette on top of the active layer and the glue tape. It has been measured that, spin coating of 1000 rpm for 45s will result in a PEDOT layer thickness of about 150 nm (see figure 40).<sup>11</sup> The PEDOT layer has to be thin enough to keep its transparent properties and if the layer of PEDOT is too thick it will increase the device resistance, which is not recommended. After the PEDOT mixture has been deposited, the substrate is annealed for 2 minutes at 140 °C on the hotplate. The annealing drives off moisture and makes the PEDOT layer stick to the active layer substrate.

<sup>11</sup> P3HT/PCBM and PEDOT layer thickness measured by Roana Melina de Oliveira Hansen (Postdoc, MCI SDU Sønderborg) with "Veeco Dektak 150" profilometer

<sup>12</sup> The annealing time and temperature was experimentally determined and optimized by Roana Melina de Olivera Hansen (Postdoc, MCI SDU Sønderborg)

The finished version of the inverted ITO free bulk-heterojunction organic solar cell can be seen in figure 41.



Figure 39 – blue glue stripe controlling solar cell size



Figure 40 - deposition of PEDOT

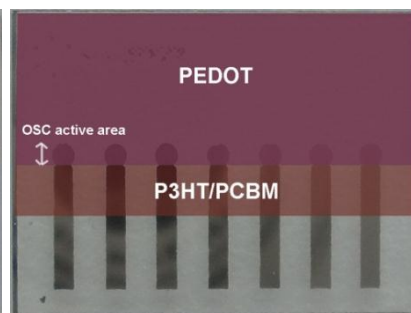


Figure 41 - finished inverted BHJ OSC

Finally to make the characterization of the cell easier a layer of silver paste is applied (outside the solar cell active area). The probing needles used for electrical measurements would damage the PEDOT layer, thus the silver paste acts as a conductor material for the anode (see figure 42 and 43).

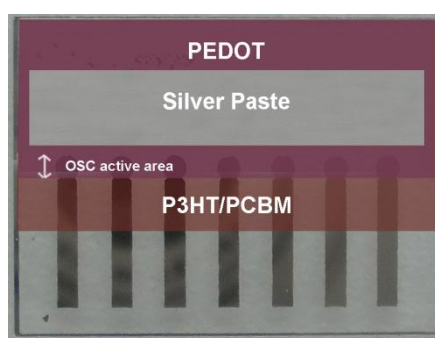


Figure 42 – finished inverted BHJ OSC with silver paste (model)

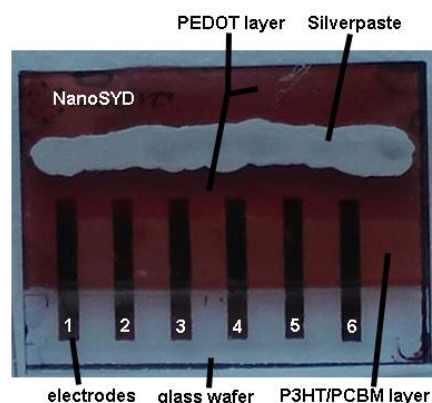


Figure 43 - real produced cell

All spin coating processes in this chapter have been performed with the “Laurell WS-400BZ-6NPP/Lite” spin coater. The hotplate used for the annealing processes in the glove box is the “RCT basic IKAMAG® safety control”. For the timing of the processes the “Unilab Digital Stopclock” was used. See appendix “Recipe for the production of inverted ITO-free BHJ OSCs” p.9 for extra processing information.

#### 4.5. Characterization of organic solar cells

After the production of the OSC is finished, the solar cell active area is measured with a vernier. To verify if this mechanical measurement is precise enough a comparison with computer aided cell size measurements has been performed. For this, digital pictures have been taken directly from an optical microscope and with the help of Photoshop 11 and pixel conversion factors, the areas of two cells have been determined. The two methods (vernier & computer aided cell size measurement) resulted in about the same cell areas for the measured cells, which means that the vernier is a reliable tool to measure the cell areas (see appendix “Optical microscope cell area measurements” page 10-11).

Twelve weeks into the project, the wafer substrate design has been changed from a pure rectangular bottom electrode with a width of 1 mm (see figure 44) to a rectangular bottom electrode with a width of 1 mm and a circle at the end of the rectangular electrode with an area of 1 mm<sup>2</sup> (see figure 45). The change was an optimization, which should make the cell size measurement easier, if the production process of the OSCs is done like in figure 39-41, where in the end the active solar cell area will be limited to the circle.

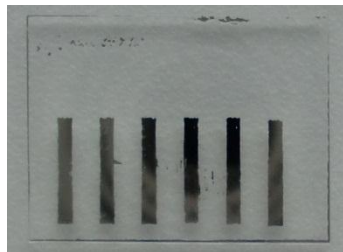


Figure 44 – Old design – 6 solid rectangular bottom electrodes

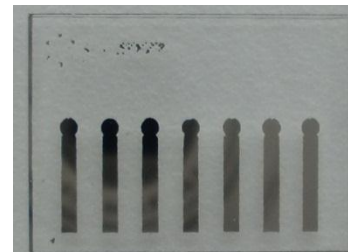


Figure 45 – New design – 7 rectangular bottom electrode with 1 mm<sup>2</sup> dot

#### 4.5.1. Electrical characterization

The solar generator setup consists of the “Universal Arc Lamp Power Supply, model 69907”, a “250 W Oriel Research Arc Lamp Housing” and a “150 Watt Xenon, Ozone Free Arc Lamp”. The illumination intensity for each measurement has been calibrated to 100 mW/cm<sup>2</sup> with a reference solar cell and a meter from Newport using an AM 1.5G filter. The distance between the light source and the reference cell is adjusted by a custom made adjustable platform (see figure 46)



Figure 46 - measurement setup for reference solar cell

The electrical characterization of the OSCs was performed by using a custom made LabVIEW measurement application (see appendix “Voltage sweeps with LabVIEW” p.12).

The voltage is controlled by a 16 bit National Instruments DAQ card. The DAQ card is also sampling the current which is measured by a Stanford Research SR 570 current amplifier. The probing itself is done with probes from “Micromanipulator Co., Inc.” (see figure 47). The probe which is connected to the DAQ unit, is contacting the anode (silver-paste) and the probe, which is connected to the current amplifier, contacts the cathode (Ti-layer) of the OSC. By using the custom made LabVIEW application the IV-curves of the cells were obtained. See appendix “Measuring IV-curves step by step procedure” on p.13 for a detail description of the characterization procedure.



Figure 47 - measurement setup for measuring OSCs

## 5. Lifetime measurement of non-encapsulated cell

This chapter summarizes the results of the lifetime measurements which were performed on non-encapsulated cells.

### 5.1. Development of a standardized measuring procedure

First a measuring standard was created which had the purpose of creating somehow equal conditions for each measurement. The finished version of the measurement standard can be found in appendix “Measurement standards for OSCs samples” p.14).

A key question which is addressed by the measuring standard is, in how far the illumination of the solar light generator is influencing the non-encapsulated organic solar cells efficiencies. The following two experiments show the difference between a sample which is constantly illuminated and one sample which is only illuminated when measured.

#### 5.1.1. Experimental setup

In experiment 9.1 a fresh produced sample (M4) with 6 individual cells (see figure 48) was placed under a constant illumination of 1 sun. In total 21 measurements were conducted on cell 2 (see figure 48) and the timespan between each measurement was kept at 3 minutes and was timed with a stopwatch. Each measurement takes 20 s and sweeps from 0V to 1V and back from 1V to 0V. The active layer was spin-coated from a solution of P3HT/PCBM dissolved in chlorobenzene and for the PEDOT the 3:1 PH1000:CPP PEDOT mixture (old version) was used. With a venire the cell area was measured to 1 mm<sup>2</sup>. Both background illumination and room temperature were measured with the reference solar cell from Newport to be at 0.010 sun and 23.98 °C respectively.

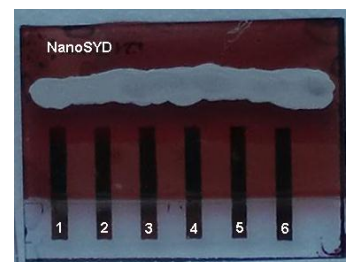


Figure 48 - Sample M4 - continuous illumination

In experiment 9.2 another fresh produced sample (M5) with 6 individual cells was used. A total of 21 measurements were conducted on cell 2 (see figure 49). The same solar generator configuration was used as in experiment 9.1, but now between each measurement the light was blocked for 3 minutes, so the sample was just illuminated during the active measurement period, which takes 20s. Sample M5 was produced together with sample M4 and the same P3HT/PCBM and PEDOT mixtures were used. During experiment 9.1 sample M5 was put in a small plastic box which was wrapped in aluminum foil and stored in the glove box to avoid degradation. The cell area was measured with a venire to be 1 mm<sup>2</sup>. Both background illumination and room temperature were measured with the reference solar cell from Newport to be at 0.018 sun and 24.29 °C respectively.

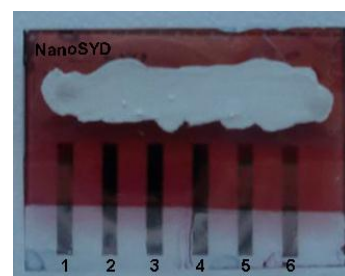


Figure 49 - Sample M5 - short illumination

### 5.1.2. Results and result treatment

Figure 50 shows the power conversion efficiencies of sample M4 and M5 plotted versus time in minutes. The PCEs of the samples are normalized so it is easier to compare the two samples. Also the measuring standard from figure 31 on page 25 was applied to measure the device stabilities.

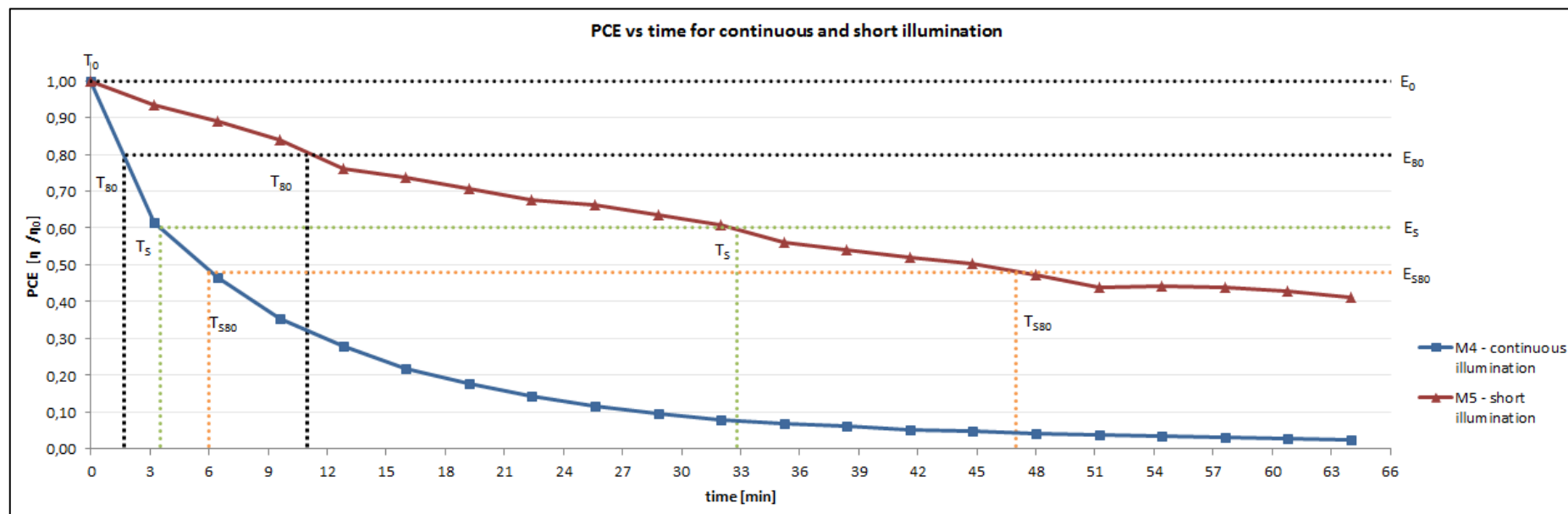


Figure 50 – Comparison between continuous and short illumination for non-encapsulated

It can be seen from figure 50 that the PCE of sample M4 (constant illumination) is decreasing faster than for sample M5 (short illumination).

From table 7 appendix “Sample M4 and M5 calculations” page 15, the calculated values show that sample M4 decayed 20% from its initial PCE ( $E_0$  to  $E_{80}$ ) within 1 min 42s. Sample M5 decayed from  $E_0$  to  $E_{80}$  in about 11 min, which is about 6.5 times slower than M4.

The second testing measurement  $E_s$  was arbitrarily defined to start at 60% of the OPV device performance.  $T_{s80}$  is the time it takes for  $E_s$  to decay 20% to the point  $E_{s80}$ . Sample M4 decayed from  $E_s$  to  $E_{s80}$  in 2 min 30s and sample M5 did this in 14 min 12s, which is about a factor of 5.7 slower.



The degradation of the cells PCE is linked to  $V_{oc}$ , FF and  $J_{sc}$ . Figure 51 shows the open circuit voltage vs. time for sample M4 and M5. It can be seen that the open circuit voltage of M4 is degrading faster compared to M5. After 64 minutes the open circuit voltage dropped by about 57% for M4 and about 23% for M5.

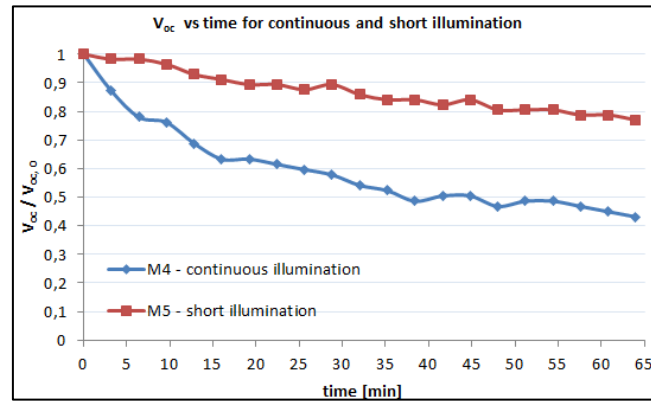


Figure 51 - Normalized open circuit voltage ( $V_{oc}$ ) vs. time - continuous vs. short illumination

Figure 52 shows the fill factor versus time for M4 and M5. For M4 the FF decreased 34% and for M5 33% after 64 minutes illumination. Also note the recovery for the FF of M4.

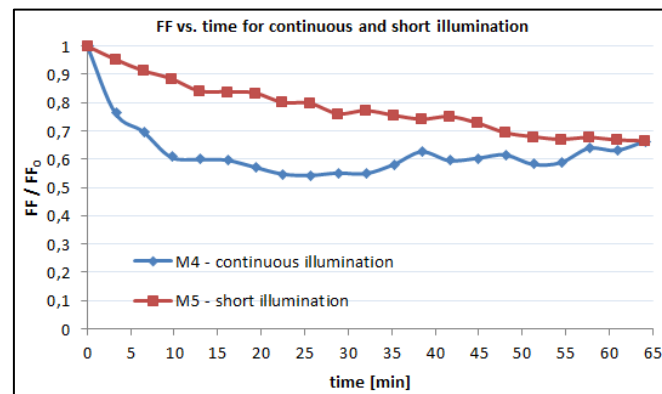


Figure 52 - Normalized Fill Factor (FF) vs. time - continuous vs. short illumination

Figure 53 shows the current density ( $J_{sc}$ ) vs. time for sample M4 and M5. For sample M4 the current density dropped about 91% and for M5 it dropped about 20% after 64 minutes.

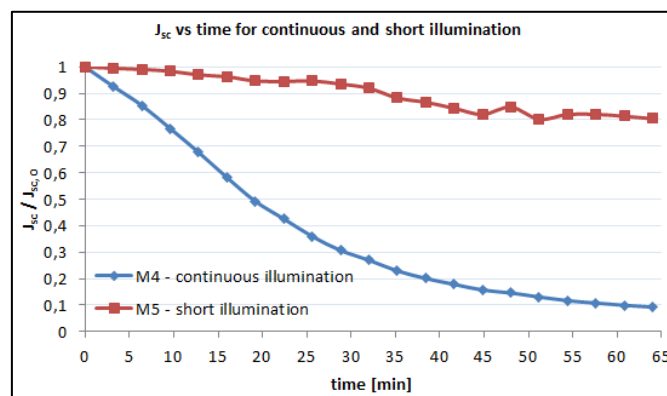


Figure 53 - Normalized current density ( $J_{sc}$ ) vs. time for continuous vs. short illumination

### 5.1.3. Discussion and conclusion

Generally from experiment 9.1 and 9.2 it can be seen that the efficiency of the non-encapsulated cells decreases when the sample is illuminated.

It also can be seen that there is a difference when a sample is constantly illuminated or just for a short period of time. M5 decays by a factor of 6.5 slower from  $E_0$  to  $E_{80}$  and a factor 5.7 slower from  $E_s$  to  $E_{s80}$  compared to sample M4. Also Figure 50 shows that after 64 minutes the PCE of sample M4, which was illuminated continuously, dropped more than 90%, whereas the PCE of sample M5 dropped by about 60% from its initial value, which indicated that for the short illumination the sample M5 degrades slower than M4.

Figure 51-53 display the decay of the  $V_{oc}$ , FF and  $J_{sc}$  respectively. Out of these three key parameters the current density  $J_{sc}$  decays the most over the 64 minutes. Interestingly the Fill Factor (figure 52) for sample M4 was recovering during the experiment. It is also notable that for sample M5 the PCE decreased by 26% after 6 measurement have been done, despite of that the sample was only illuminated during the measurements (see figure 50). In order to be able to compare results for different cells from the same substrate and to minimize the effects of the measuring process on the cells efficiencies, it is advisable to avoid constant illumination of all the OSC's when just one is measured. Based on the results from figure 51-53, it seems that the current density is the parameter which is most vulnerable to the constant illumination compared to the FF and  $V_{oc}$ . The  $J_{sc}$  for M4 dropped by 91% after 64 minutes constant illumination and the current density for M5 dropped by only 20%, which is a difference of 71%.  $V_{oc}$  showed a drop of 57% for M4 and 23% for M5 after 64 minutes, which is a difference of 34%. The difference in FF for the M4 and M5 was only 1% after 64min, which shows that the  $J_{sc}$  has the biggest impact followed by the  $V_{oc}$ . The slower degradation of M5's PCE can be linked to the slower degradation of M5's current density and open circuit voltage.

### 5.1.4. Avoiding error sources

Experiment 9.1 and 9.2 showed that the samples are degrading faster when exposed to continuous illumination compared to if they just are illuminated for short intervals. Still if more than one cell is measured on a sample, a device should be used which blocks the light from the cells, which are not measured at that point. For this purpose a device was designed with “Siemens PLM NX 7.5” (see figure 54) and printed with the “Fortus 250mc Stratasys” 3D printer (see attached CD for CAD files and drawings).

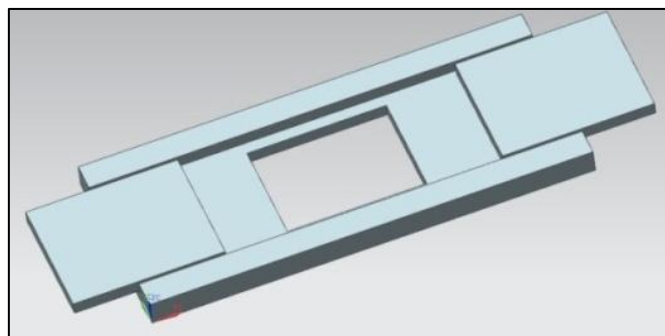


Figure 54 - CAD model of light shutting device



The cell sample is placed into the middle and the top plates can be shifted over the cell. Figure 55 shows the light shutter in action; Cell 1 of the sample is ready to be measured and cell 2-6 are covered from the light. Also to minimize the error when making several lifetime measurements on the same sample over a longer period of time, it would be good to measure the cells always in the same order to ensure better comparability of the results.



Figure 55 - Printed light shutter in action

#### 5.1.4.1. Other guidelines

Furthermore the solar generator and the setup are calibrated, so that the reference solar cell from Newport is measuring 1 sun. It is necessary to wait about 5 minutes until the solar generator readings are stable, after switching on the lamp of the solar generator. Also the position of the solar cell is important. Both the reference solar cell and the sample which is about to be measured, should be aligned in the center of the light cone from the solar generator. Furthermore the cells are always put individually in small plastic boxes, which are wrapped in aluminum foil to block the light, and stored in a drawer.

## 5.2. Minor device structure change

As mentioned in chapter 4.3.2 “PEDOT solution preparation” p.28, there was a change in the PEDOT:PSS mixture, which was used as top electrode at that point. To be aware of the consequences that the change results in, an experiment was conducted with a fresh sample (M8), which used the new “1:1 HTL:CPP PEDOT” and got compared with sample M4 from experiment 9.1 on p.32. The testing setup was kept like in experiment 9.1, so it is possible to compare sample M4 with M8.

#### 5.2.1. Experimental setup

Sample M8 is placed under a constant illumination of 1 sun. The active layer was spin-coated from a solution of P3HT/PCBM dissolved in chlorobenzene. In total 21 measurements were conducted on cell 4. With a venire the cell area was measured to be about  $0.5 \text{ mm}^2$ . The timespan between each measurement was kept at 3 minutes and was timed with a stopwatch. Each measurement takes 20 s and sweeps from 0V to 1V and back from 1V to 0V. Both background illumination and room temperature were measured with the reference solar cell from Newport to be at 0.013 sun and  $23.50^\circ\text{C}$  respectively.

### 5.2.2. Results and result treatment

Figure 56 shows the normalized power conversion efficiencies of sample M4 and M8 plotted versus time in minutes.

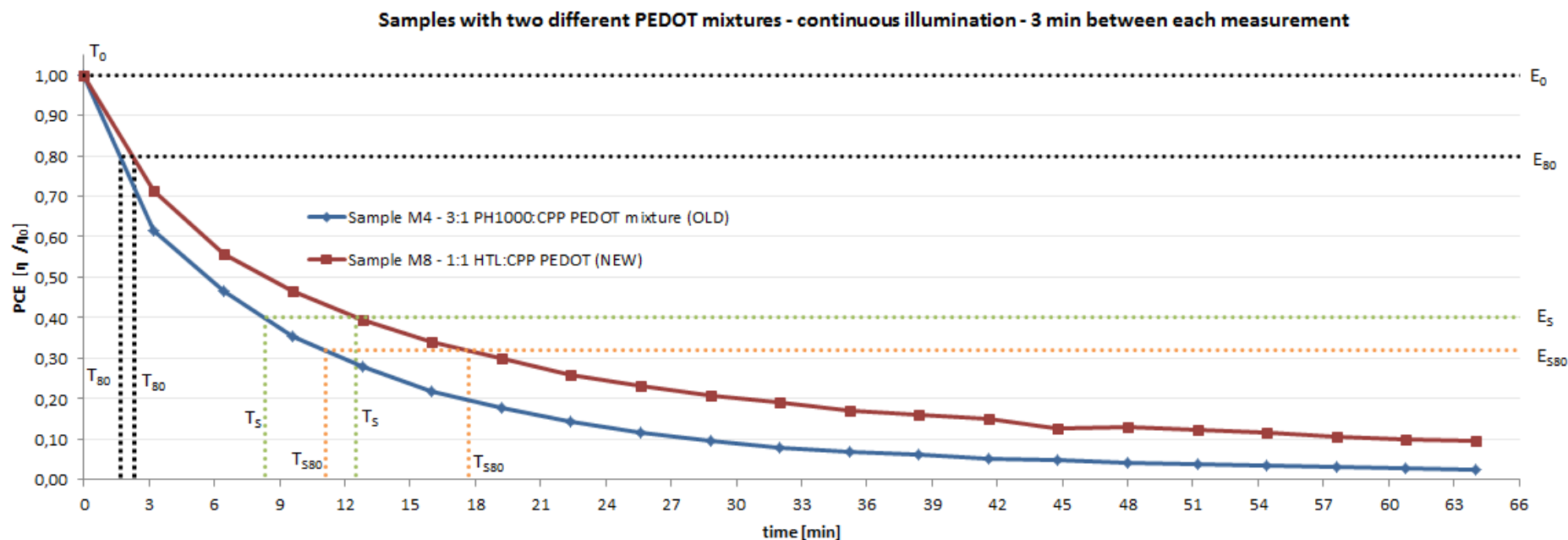


Figure 56 - comparison between old and new PEDOT mixtures

It can be seen from figure 56 that the PCE of sample M4, is decreasing a bit faster than for sample M8. From table 8 appendix “Sample M4 and M8 calculations” page 15, the calculated values show that sample M4 is decaying by 20% of its initial PCE ( $E_0$  to  $E_{80}$ ) within 1 min 42s under constant illumination. Sample M8 decayed in about 2 min 18s, from  $E_0$  to  $E_{80}$ , which is about 1.4 times slower than M4.

The second testing measurement  $E_s$  has been arbitrarily defined to start at 40% of the OPV device performance. Sample M4 decays from  $E_s$  to  $E_{s80}$  in 2 min 58s and sample M8 does this in 5 min 3s, which is a factor 1.7 slower.

### 5.2.3. Discussion and conclusion

The experiment showed that the new 1:1 HTL: CPP PEDOT is a little bit more stable compared to the old PEDOT mixture, which is a nice improvement. M8 decays by a factor of 1.4 slower from  $E_0$  to  $E_{80}$  and a factor 1.7 slower from  $E_S$  to  $E_{S80}$  compared to sample M4.

Also the experiment with sample M8 shows again the strong degradation of non-encapsulated cells under constant illumination. After 64 minutes of constant illumination, sample M8 lost more than 90% of its initial PCE, so generally the encapsulated cells are useless after about 1 hour constant illumination and for this reasons an encapsulation has to be developed which increases the cells stability under constant illumination.

## 5.3. Reproducibility experiments

In this chapter the final cell type, which was also used for the further encapsulation experiments was tested for its stability and reproducibility when exposed to illumination of 1 sun. As mentioned in chapter 4.3.1 p.27, there was a small modification in the P3HT/PCBM mixture from using chlorobenzene to dichlorobenzene as a solvent. The samples use dichlorobenzene as a solvent for the P3HT/PCBM mixture and the new “1:1 HTL:CPP PEDOT” as top electrode.

### 5.3.1. Experimental setup

The experimental setup is identical to the one in chapter 5.1.1 on p.32. Two samples (M34, M35) have been produced. On sample M34 two cells were measured and on sample M35 one cell was measured for 64 minutes under constant illumination of 1 sun. By using the light shutting device from chapter 5.1.4 p.35 for sample M35, only the cell which was actively measured was exposed to the incident light. In total 21 measurements were conducted on each cell with three minutes between each measurement. Both background illumination and room temperature were measured with the reference solar cell from Newport to be at 0.022 sun and 23.98 °C respectively.

The different cell areas and initial PCE in percentage are listed in table 1:

Sample	Cell	Cell area [cm <sup>2</sup> ]	Initial PCE
M34	1	0,011	0,50%
	6	0,012	0,58%
M35	3	0,009	0,41%

Table 1 - sample information M34, 35, 36

### 5.3.2. Results and result treatment

Figure 57 shows the normalized power conversion efficiencies of the three cells from sample M34 and M35

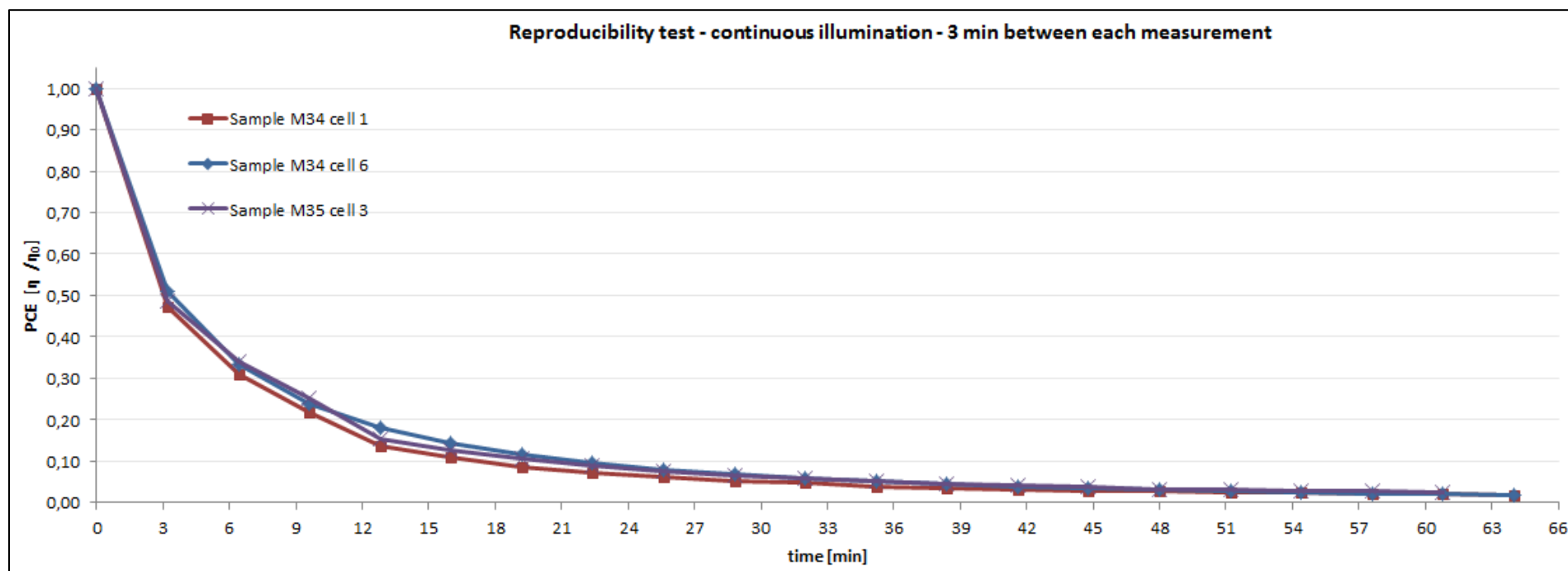


Figure 57 - comparison between samples using dichlorobenzene solvent for P3HT/PCBM and 1:1 HTL:CPP PEDOT

### 5.3.3. Discussion and conclusion

From Figure 57 it can be seen that the decay curves for the samples are similar to each other. After about 12 minutes under continuous illumination, all three cells lost about 80% of their initial PCE. At the end of the experiment, the cells have lost about 98% of their initial PCE. This shows that an encapsulation is needed to increase the cells stability and that the lifetime measurement for the non-encapsulated cells are reproducible.

## 6. Encapsulations

### 6.1. Requirements

Based on the requirements from the problem formulation on page 5, a suitable encapsulation material had to be found. The requirements which have to be fulfilled are that the material used has to have a high barrier to water or oxygen. Furthermore the material must be optical transparent to guarantee high transmission of the sun light. Secondary requirements, which are also important but can be excluded if necessary are, that the encapsulation should be mechanical flexible and the process and material costs should be low.

In general the barrier materials for organic solar cells should show a hydrophobic behavior, which makes them water repellent and the corrosion factor both to water and oxygen has to be small. Also the materials should have a high UV-stability, so no change in color (e.g. yellowing) or other photo induced corrosion of the material happen.

For the processing it is important to keep the defect levels in the thin films during deposition as low as possible, which can be achieved by using relatively low deposition rates and multilayers of both inorganic / organic materials.

First processing techniques at SDU Sønderborg were identified and for the encapsulation physical vapor deposition, spin coating and lamination techniques can be used in this project. Also a material research has been conducted to find materials, which fit to the above processing techniques and fulfill the needed encapsulation requirements. (See appendix “Initial material and process research for encapsulations” p.16-17)

### 6.2. Initial encapsulations

In this chapter a brief overview of the initial encapsulation, which lead to the final encapsulations used in this project, is given.

#### 6.2.1. Glass plate encapsulation

At first several samples have been encapsulated with a glass plate. For this a BK7 glass wafer was cut with the dicing saw into small 20mm x 7.5mm glass pieces. What was tried is to apply the glass plate directly at the start of the annealing process of the PEDOT in the glove box on top of the PEDOT layer (see figure 58). The result was that the adhesion was very little and it was very easy for the glass plate to slip of.



Figure 58 - glass plate encapsulation

Another experiment was conducted where the small wafer glass plate was spin coated at 1000 rpm for 45 s with PEDOT and the glass plate was directly applied on top of the PEDOT top electrode of the OSC at the start of the annealing process in the glove box. The idea was that when the moisture of the PEDOT is driven off by the hotplate that the PEDOT would bind to the glass plate. The adhesion between glass plate and substrate with this procedure was a little bit better, but after some time the glass plate lost contact to the substrate and fell off. Another problem was that, there is still a small gap between the glass plate and

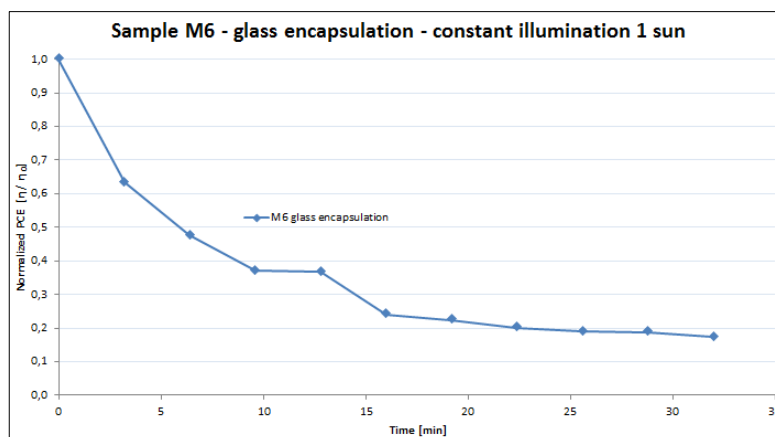


Figure 59 - Lifetime measurement Glass-PEDOT encapsulation

the PEDOT, which became clear when the silver paste was carefully applied to the cell and it diffused under the glass plate which resulted in a short circuit of some of the cells. Lifetime measurements on cell 4 showed, that the cell was degrading over 80% of its initial PCE in about 34 minutes (see figure 59), so it seems that it is important to also seal the edges of the encapsulation.

### 6.2.2. Glass plate / PMMA encapsulation

To increase the adhesion between the glass plate and the OSC, the glass plate was spin coated with PMMA (Plexiglas) at 1000 rpm for 45 s. The glass slide with PMMA was then put on top of the cell and annealed for 5 min @ 90 °C. All this was done in the glove box with a nitrogen atmosphere. The idea was, that when the PMMA hardens it will stick to the substrate. The result was that the adhesion between the glass plate and the OSC was better, but during the annealing process small bubbles formed under the glass, which could be

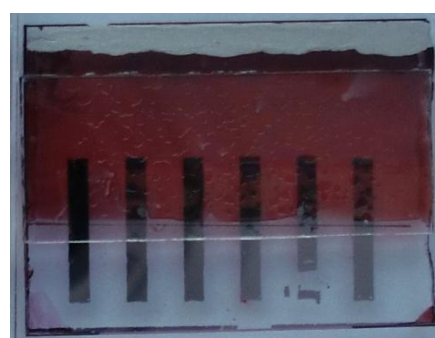


Figure 60 - glass plate / PMMA encapsulation

due to entrapped nitrogen (see figure 60). Also the edges of the encapsulation need to be sealed, to prevent the penetration of O<sub>2</sub> and H<sub>2</sub>O. Based on this encapsulation and an article about coating of Nano fibers with PMMA and SiO<sub>x</sub> [30], the idea to spin coat the OSC with PMMA and then deposit a thin film of SiO<sub>x</sub> on top of the PMMA was created, which is presented in chapter 6.3 p.43.



### 6.2.3. Glass plate with epoxy encapsulation

To overcome the low adhesion problems between the glass plate and the substrate, the glass plate was put on top of the OSC and the sides were dipped into a two-component epoxy glue from UHU (see figure 61). This encapsulation needs optimization and it is hard to work in a clean way with the two-component glue. Another problem is that there is still a small gap between the glass plate and the substrate, which makes it possible for  $H_2O$  and  $O_2$  to degrade the cells. Based on this encapsulation the idea was created to investigate a commercial high barrier solvent free epoxy glue which could be spin coated on top of the inverted OSC. This idea is presented in chapter 6.4 p.57.



Figure 61 - glass plate / epoxy encapsulation

### 6.2.4. Wire bonding experiments

It was also investigated if it's possible to create an encapsulation which completely encapsulates the sample with PDMS (see figure 62). For this kind of encapsulation it was necessary to develop a method for getting contact to the anode and cathode. So wires were attached by silver paste to the OSC and characterized under 1 sun illumination (see figure 63). It was found through experiments that a copper wire with a diameter of 0,30mm, which has been dipped into silver paste works very well and it is easy to achieve electrical contact with the probes for characterizing the cells.

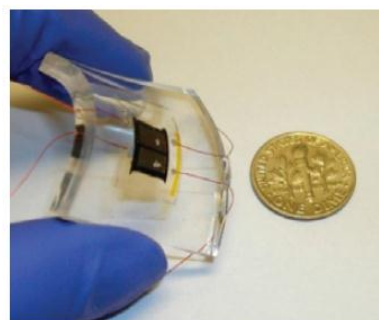


Figure 62 - device embedded in PDMS [35]

It was found that PDMS would significantly increase the production time, so after the solvent free epoxy glue, which was mentioned in chapter 6.2.3. arrived, it was applied directly to the sample together with the wire bonding (see figure 64), and illuminated for 5 min with the solar generator (without AM 1.5 G filter was removed to increase the UV-light output). The result was that the glue hardened, but it is hard to standardize this method because the thickness can't be controlled without a dispenser unit. Also this encapsulation process has potential, it was decided to go with an encapsulation which is more time effective and simpler to realize.

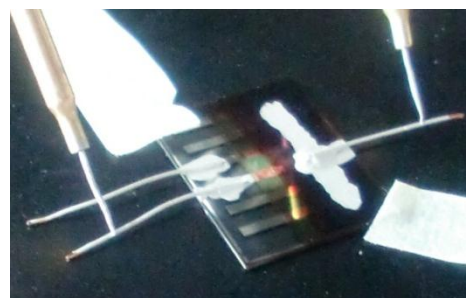


Figure 63 - OSC sample with wires bonded by silver paste to anode and cathode

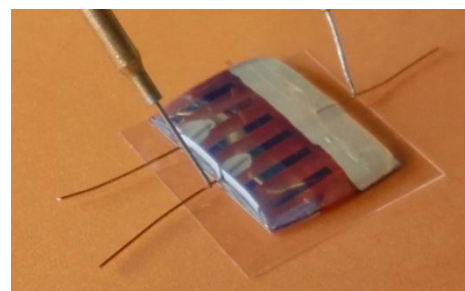


Figure 64 - Epoxy + wirebonding encapsulation

### 6.3. PMMA/SiO<sub>x</sub> encapsulation

In the following chapter the materials and processing, the lifetime measurements and a discussion of the results for the PMMA/SiO<sub>x</sub> encapsulation are presented.

#### 6.3.1. Materials and encapsulation concept

The materials used for this encapsulation are Polymethyl Methacrylate (PMMA) and Silicon dioxide (SiO<sub>2</sub>). PMMA is an organic polymer and also known as Plexiglas. Based on the data from “Granta CES Edupack 2011” material database, PMMA has a water vapor transmission (WVTR) of  $1.62 \cdot 10^{-3}$  to  $1.79 \cdot 10^{-3}$  g/m<sup>2</sup>/day, which is three magnitudes larger than the recommend WVTR of  $10^{-6}$  g/m<sup>2</sup>/day. The oxygen transmission rate (OTR) for PMMA is  $4.31 \cdot 10^{-3}$  to  $7.19 \cdot 10^{-3}$  cm<sup>3</sup>/m<sup>2</sup>/day at room temperature, which is about 4-7 times larger than the recommended  $1 \cdot 10^{-3}$  cm<sup>3</sup>/m<sup>2</sup>/day at room temperature. It is relatively flexible (elongation of 2-7% strain), light weight, low costs and it can be easy processed by e.g. spin coating and furthermore it got good outdoor stability (e.g. good weathering resistance. [30] The transmission for visible light is 92% at (3 mm thickness) [31] and concerning UV radiation, PMMA filters ultraviolet (UV) light at wavelengths below about 300 nm (similar to ordinary window glass) [31] and has good UV radiation stability, so minimal changes in color or photo induced corrosion will appear. The PMMA used for this encapsulation is called PMMA 950 A4 from “NanoChem”, which is used for imaging and non-imaging microelectronic applications. Most commonly it is used for high resolution positive resist for e-beam, x-ray and deep UV microlithography processes. Furthermore it can also be used as a protective coating and a bonding adhesive. [31]

The silicon dioxide (SiO<sub>2</sub>) or normally denoted as SiO<sub>x</sub> is also known as glass. Thin films of SiO<sub>x</sub> are used in the food packaging and microelectronics industry for products, which require excellent barrier abilities and transparency. SiO<sub>x</sub> thin films have a low moisture and oxygen permeability; they are good insulators, a high wear resistance and a good chemical resistance. [32] The SiO<sub>x</sub> thin film, which is used for this encapsulation is deposited by the Cryofox Explorer 600 LT using RF sputtering physical vapor deposition with a pure SiO<sub>2</sub> target.

The idea is to use a combination of PMMA and SiO<sub>x</sub> to create a bilayer encapsulation, which increases the OSC stability. The concept for this encapsulation is shown in figure 65. PMMA functions in this case as a buffer layer to protect the OSC during the SiO<sub>x</sub> deposition, which is done with RF sputtering physical vapor deposition process, which would damage the top electrode.

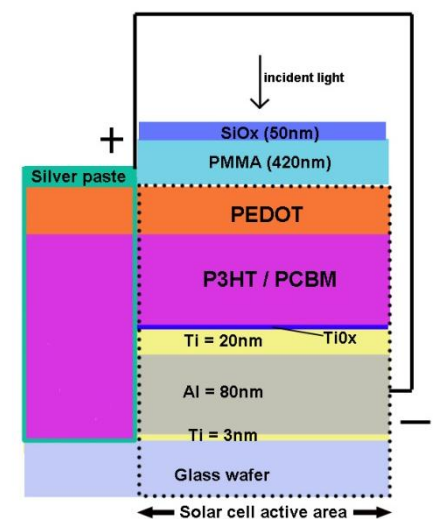


Figure 65 OSC with PMMA/SiO<sub>x</sub> encapsulation

### 6.3.2. Initial experiments

The PMMA was tested together with the inverted OSC, since it was not clear how the solvent “Anisole” in the PMMA will react with the PEDOT top electrode or whether it will diffuse through pinholes in the PEDOT and destroy the P3HT/PCBM active layer. The goal was to see if morphological or electrical changes occur when the PMMA is applied.

#### 6.3.2.1. PMMA effect on OSC

First a non-encapsulated OSC was investigated under an optical microscope<sup>13</sup> to get a reference picture of a normal cell structure (see figure 66 left). After that the same OSC was spin coated<sup>14</sup> with a layer of about 420 nm<sup>15</sup> “950 PMMA A4” from “NanoChem” at 1000 rpm for 30s and annealed for 5 min at 90°C on a hotplate<sup>16</sup>. The OSC was then examined again with the optical microscope (see figure 66 right), to see if the anisole was dissolving the active or PEDOT layers, which could result in morphological changes at the borders of the PEDOT and P3HT/PCBM layers.

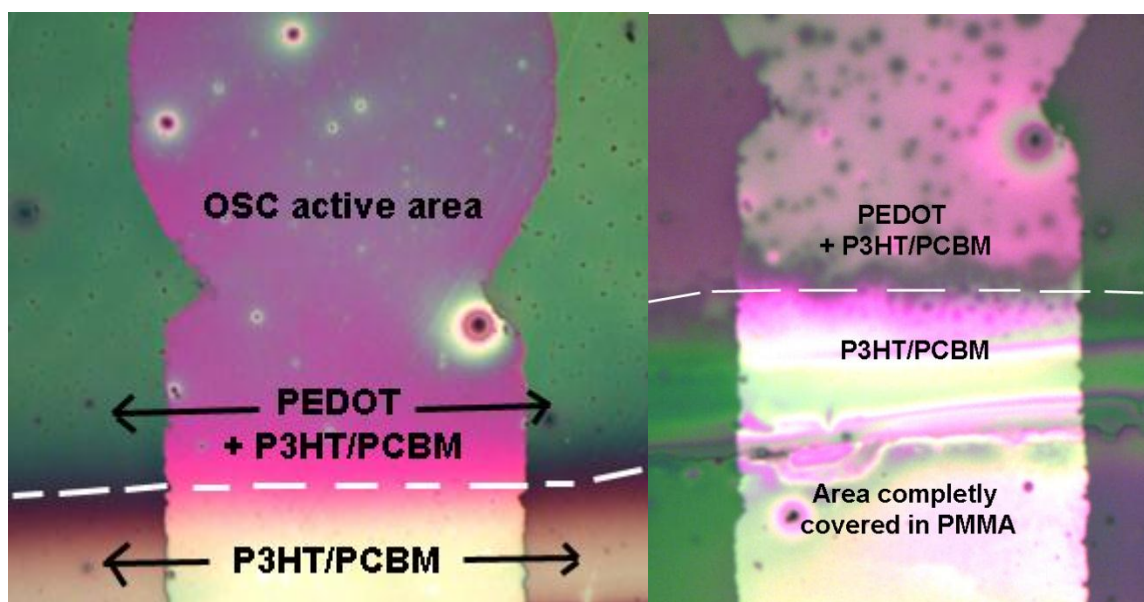


Figure 66 – Left picture shows OSC without PMMA and right picture shows OSC with PMMA

The borders of the P3HT/PCBM and PEDOT are still visible after the PMMA has been applied and annealed, so no dissolving occurred. It can be seen on figure 66 left that there seems to be holes in the PEDOT layer. To see if the PMMA diffuses through the holes and causes damage to the active layer, the cell was characterized with the standard procedure (chapter 4.5.1. p.31) and the cell exhibited the standard diode characteristics in dark and working photovoltaic effect of around 0.5% under 1 sun illumination, which means that the active layer and PEDOT were not destroyed by the PMMA.

<sup>13</sup> Digital inspection microscope (Nikon LV100D)

<sup>14</sup> Spin Coater (RRT Lanz EBS 11)

<sup>15</sup> See appendix „PMMA film thickness (Å) vs. Spin speed (rpm)” p.18

<sup>16</sup> Hotplate H. Gestigkeit PZ28-2SR

### 6.3.2.2. PMMA transmission experiment

The transmission spectrum of the PMMA thin film was analyzed with “TEProbe spectroscopy ellipsometer” from Ångström Sun Technologies Inc.. A thin film of 420 nm PMMA was spin coated at 1000 rpm for 30 s on top of a bare glass bottom substrate and annealed for 5 min at 90 °C.

Figure 67 shows the transmission spectrum for the 420 nm PMMA thin film (green) and the reference signal (blue) which was taken with a bare glass bottom substrate.

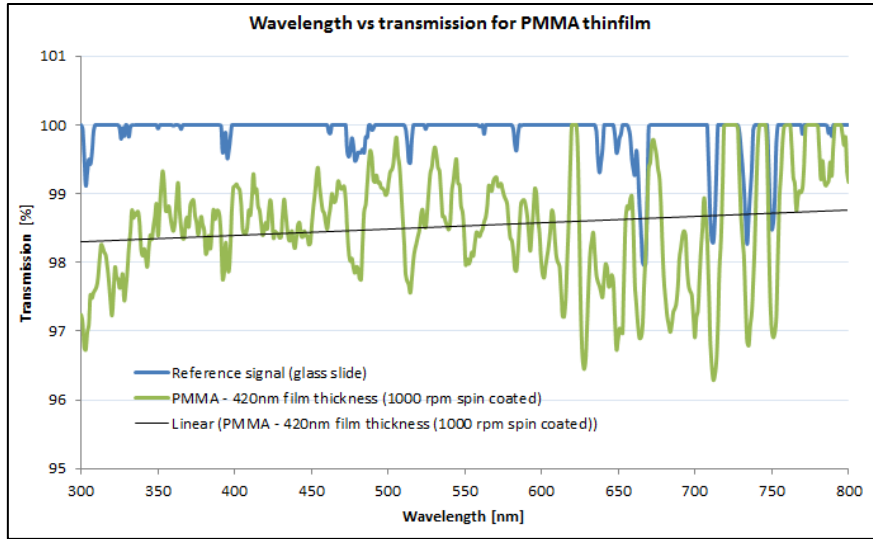


Figure 67 - Transmission [%] vs. wavelength [nm] for bare glass and PMMA thin film

It can be seen from figure 67 that over 96% of the incident light across the wavelength of 300-800nm is transmitted through the PMMA thin film of 420 nm, which means that the transparency of this material is good enough for the encapsulation.

### 6.3.3. Encapsulation procedure

In this chapter the encapsulation procedure for the PMMA/SiO<sub>x</sub> encapsulation is presented.

The entire encapsulation procedure is done in the clean room, which minimizes the chance of contaminations getting entrapped in the encapsulation and it also speeds up the process since all needed equipment is localized.

First, silver paste was applied close to the electrodes, which was done to increase the conductivity of the top layer (see figure 68). In the next step the blue glue tape was used to cover part of the top layer (anode) and part of the Ti/Al electrodes (cathode) to be able to characterize the cells also after the encapsulation is done (see figure 69). In this step it was helpful to weaken the glue tape, by applying and removing it a few times to a bare surface, before it is applied to the cell, otherwise the glue tape would take of some off the silver paste after it is removed at the end of the process. Furthermore it was found out during the process optimization that it is enough to just slightly push the edges of the glue



tape onto the substrate, which also makes it easier to remove the tape after the process, without ripping off the underlying silver paste. The next step is to spin coat the substrate with the “950 PMMA A4” at 1000 rpm for 30s using the spin coater from “Reinraumtechnik Lanz EBS 11”. The spin coating will result in a thin film of about 420 nm according to the datasheet (see appendix “PMMA film thickness (Å) vs. Spin speed (rpm)” p.18) (see figure 70).

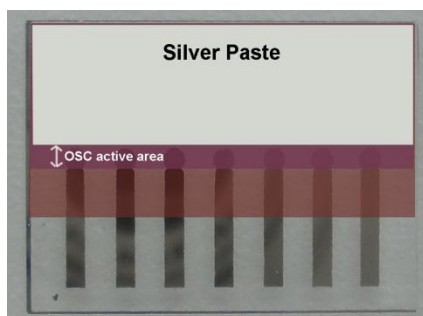


Figure 68 - Applying silver paste close to bottom electrodes

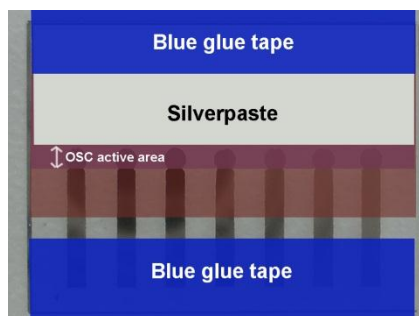


Figure 69 - Blue glue tape covering part of the Ti/Al electrodes and silver paste

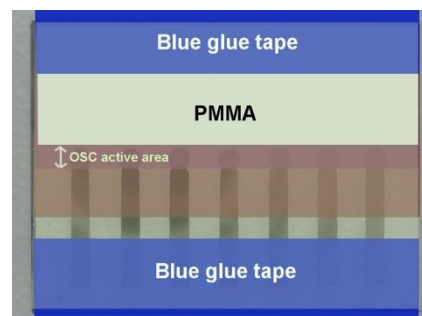


Figure 70 – Spin coating PMMA

After the PMMA was applied the blue glue tape was carefully removed with a tweezer. In case some of the silver paste layer is removed by the tape new silver paste can easily be applied again. The sample was then placed on a hotplate (Gestigkeit PZ28-2SR), where the PMMA got annealed for 5 min at 90 °C (see figure 71). The spin coating parameters have been determined after several process optimizations and it was found that, if the PMMA layer is too thick it will take longer to anneal the PMMA in order to harden it. Also the annealing time was determined based on information from the PMMA datasheet<sup>17</sup>, which lists a pre-bake time of 50-90s for a hotplate at 180 °C. The applied temperature has to be compatible with the temperature limits of the organic and polymer substrate (about 120°C) [26], so the process was set to 5 min at 90 °C.

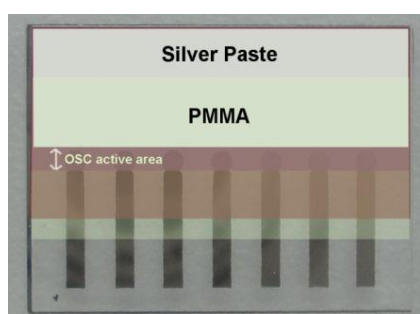


Figure 71 - Removing blue glue tape + annealing PMMA

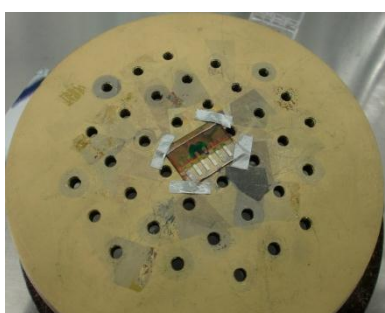


Figure 72 – Cell mounted with tape to Cryofox sample holder



Figure 73 –cover foil applied to the Cryofox sample holder

After this the sample was ready for the SiO<sub>x</sub> deposition, which was done with the Cryofox Explorer 600 LT using RF sputtering physical vapor deposition with a pure SiO<sub>2</sub> target. For this the sample was placed onto a sample holder and each corner of the sample was fixed with tape (see figure 72). Then a

<sup>17</sup> [http://www.microchem.com/pdf/PMMA\\_Data\\_Sheet.pdf](http://www.microchem.com/pdf/PMMA_Data_Sheet.pdf) (27.05.2012)

cover foil was applied, so the  $\text{SiO}_x$  is not deposited onto the anode and cathode areas which are needed for the characterization of the sample (see figure 73).

The parameters for the deposition with the Cryofox Explorer 600 LT are listed in table 2.

Parameters	Values
Base pressure	$5 \cdot 10^{-5}$ mbar
Ignition pressure	$1.5 \cdot 10^{-2}$ mbar
Sputter pressure	$3 \cdot 10^{-3}$ mbar
Thickness [nm]	50
Rate [ $\text{\AA}/\text{s}$ ]	0.5
Tooling factor	20

Table 2 – Cryofox deposition parameters using RF sputtering

The base, ignition and sputter pressure were all pre-installed values with which the Cryofox normally operates at MCI SDU Sønderborg. The thickness, tooling factor and deposition rate of the  $\text{SiO}_x$  thin film were determined after a conversion with Luciana Tavares [Researcher at MCI SDU Sønderborg] and Kirill Bordo [Researcher at MCI SDU Sønderborg], who both have experience with the deposition of  $\text{SiO}_x$ . The deposition rate influences the morphology of the thin film and a deposition rate higher than  $0.5 \text{ \AA}/\text{s}$  would result in a yellowish color for the thin film. The thickness was set to 50 nm because the complete deposition process for that thickness, from loading the sample to unloading the sample, will take about 30 minutes. Yet a thicker layer of  $\text{SiO}_x$  could increase the barrier effect of the encapsulation and thus the stability of the cell, but it also would prologue the production process and increases the costs, which is why this parameter combination seems to make a good compromise between time, costs and barrier effect.

After the deposition was done the sample was unloaded from the Cryofox and the cover foil was removed (see figure 74). A short recipe was created for this encapsulation process, which can be found in appendix “Process recipe for PMMA/ $\text{SiO}_x$  encapsulation” p.19



Figure 74 - (left) Sample after the  $\text{SiO}_x$  film deposition, (right) finished sample with removed cover foil



### 6.3.4. Lifetime measurement results

In this chapter the PMMA/SiO<sub>x</sub> encapsulation is tested with the characterization setup from chapter 4.5.1. “Electrical characterization” p.31.

### 6.3.5. Experimental setup

All samples were measured under continues illumination of 1 sun. The time between each measurement is 6 minutes and the samples and probes have not been repositioned during the experiment. Table 3 summarizes information about the samples which have been measured.

Sample	Cell	Cell area [cm <sup>2</sup> ]	Initial PCE after encapsulation
M15	4	0,01	0,983%
M25	5	0,009	0,567%
M37	3	0,01	1,540%

Table 3 - Sample information

Sample M15 was the first successful encapsulation attempted, but only measured for 64 min. Sample M25 checks the reproducibility of M15 and was furthermore measured for 6 hours and 12 minutes. M37 was not measured directly after the production. The difference is that sample 37 was previously pre-illuminated for 1 hour and it was stored in a small plastic box wrapped in aluminum foil for 3 days, before it was measured again for 6 hours and 12 minutes under continuous illumination.

### 6.3.6. Results and result treatment

Figure 75 shows the normalized power conversion efficiencies of the encapsulated samples M15, M25 and M37 plotted versus time in minutes. From the graphs it can be seen that the initial PCE increases for all three samples.

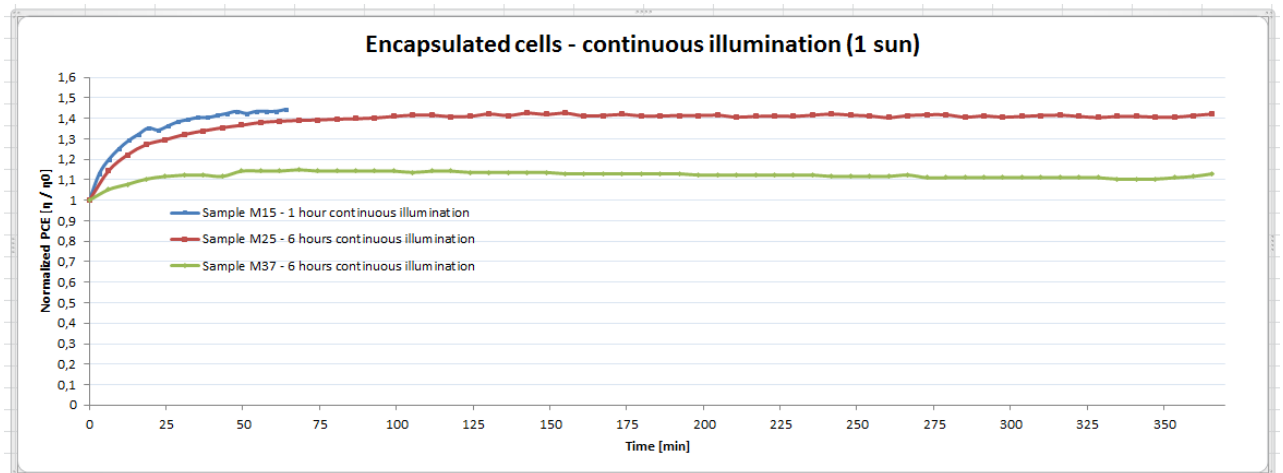


Figure 75 –PMMA/SiO<sub>x</sub> encapsulated cell Normalized PCE vs. time measurement results

It is not possible to use the measurement standard from chapter 3.5.1. “Standardized measurements” p.25, because the power conversion efficiency over the tested time frame, is not degrading enough to use the standard. To characterize the stability of the cells, a system has been applied which measured the PCE after every past hour from T0, which is the time at the initial PCE to T6, which is the PCE after 6 hours of measurement (see figure 76). Figure 76 shows a close-up of the PCE vs. time graphs of figure 75 with the previous described stability characterization system.

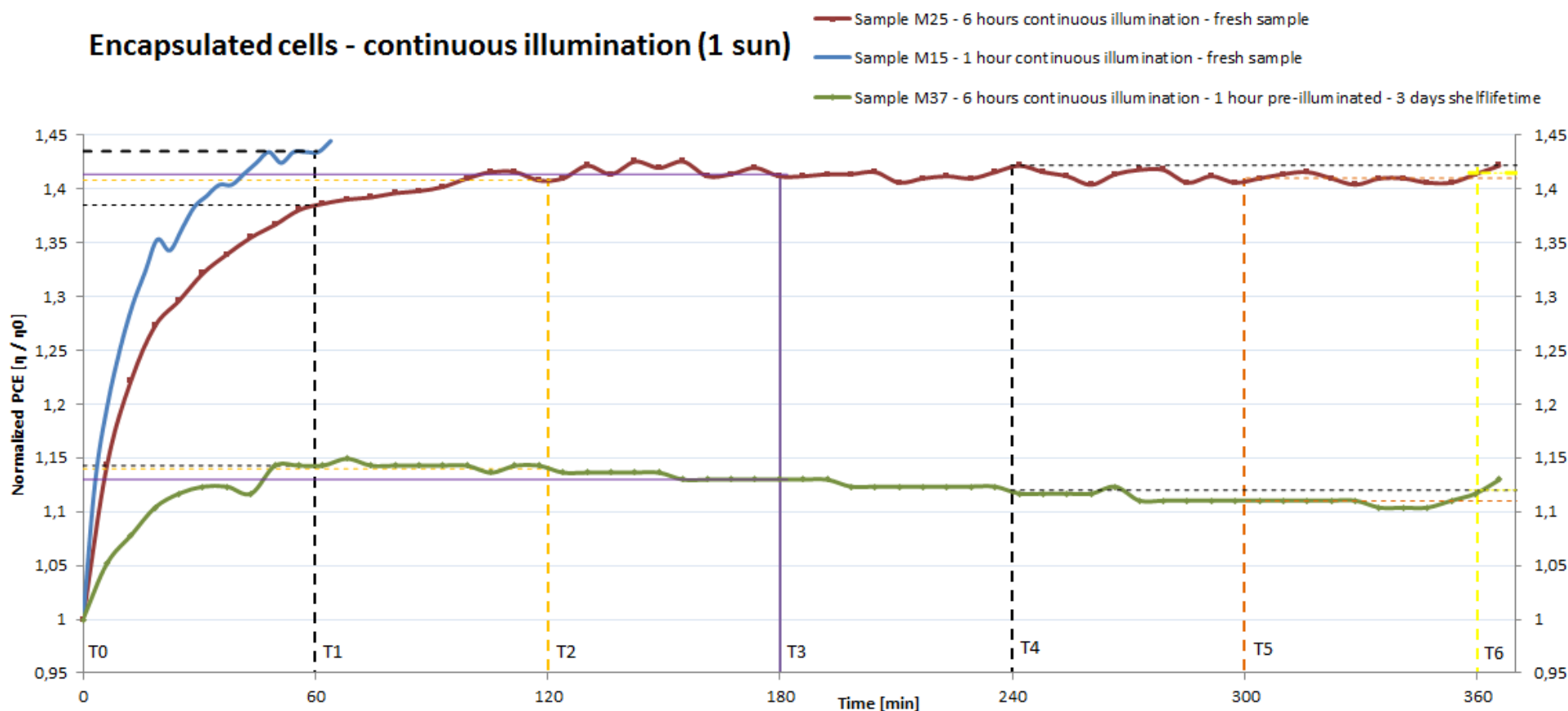


Figure 76 –PMMA/SiO<sub>x</sub> encapsulated cells – Normalized PCE vs. time - stability analysis

Table 4 shows the normalized PCE's at the given points of time from T0 to T6 from figure 76:

Time [min]	Sample M15 (blue)		Sample M25 (red)		Sample M37 (green)	
	Normalized PCE [ $\eta$ / $\eta_0$ ]	Growth of initial PCE	Normalized PCE [ $\eta$ / $\eta_0$ ]	Growth of initial PCE	Normalized PCE [ $\eta$ / $\eta_0$ ]	Growth of initial PCE
T0 = 0	1	0 %	1	0 %	1	0 %
T1 = 60	1,44	44%	1,39	39 %	1,14	14 %
T2 = 120	-	-	1,41	41 %	1,14	14 %
T3 = 180	-	-	1,41	41 %	1,13	13 %
T4 = 240	-	-	1,42	42 %	1,12	12 %
T5 = 300	-	-	1,41	41 %	1,11	11 %
T6 = 360	-	-	1,42	42 %	1,12	12 %

Table 4 Table with normalized PCE's for given point of time T0 to T6 from figure 76

Sample M15 and M25 show a strong growth of the initial PCE, with about 44% and 39% respectively, during the first 60 minutes of the constant illumination.

For M25 the PCE after 6 hours of illumination has grown by about 42%.

Sample M37 only increased by about 14% during the first 60 minutes of illumination. The earlier described pre-illumination and shelf storage of 3 days of sample 37 is believed to be connected to the lower growth of the initial PCE, yet after 6 hours of illumination the PCE still increased by 12,0% from its initial value.

Figure 77 shows the normalized  $V_{oc}$  vs. time for the encapsulated samples under constant illumination.

For M15 the normalized  $V_{oc}$  at  $t=60$  min is 1,07 (about 7% higher than its initial value). It can be seen that during the first 6 minutes the  $V_{oc,M15}$  is climbing to 1,07 and then it stays constant for the rest of the time.

For M25 the  $V_{oc}$  is at 1,12 at  $t=60$  min and at  $t=360$ min it is at 1,16. The graph for M25 shows that  $V_{oc,M25}$  is increasing most during the first 85 minutes and then getting fairly stable at around 1,13-1,16 for the rest of the time (fluctuations can be seen from  $t=240$ min to  $t=360$ min). For M37 the  $V_{oc}$  was stable at its initial value for the first 60 min. At  $t=360$ min the  $V_{oc,M37}$  had slowly declined to 0,984 which corresponds to a 1,6% drop from its initial value. Also fluctuations at  $t=240$ min to  $t=360$ min are visible.

Figure 78 shows the fill factor versus time for the encapsulated samples under constant illumination. All three samples show an improvement of their FF during the first 60 minutes.

For M15 the FF increased by 33% after 60 minutes. For M25 the FF increased by 23% from after 60 minutes from its initial measurement. At  $t=360$ min the FF for M25 was at about 23% again.

For sample M37 the FF increased by about 11% after 60 minutes from its initial measurement and at  $t=360$ min it was at about 12%. Both for M25 and M37, which have been measured for 6 hours, the behavior of the normalized FF is fairly constant from  $t=60$ min to  $t=360$ min (some small fluctuations are visible in this time frame)

Figure 79 shows the current density  $J_{sc}$  vs. time for the encapsulated samples under constant illumination. It can be seen from the plotted results that  $J_{sc}$  is fairly constant for all three samples. For M15 and M25 the  $J_{sc}$  stays constant at their initial values. For M37  $J_{sc}$  increases during the first 20 minutes by about 2,5% and then also stays fairly constant for the rest of the time.

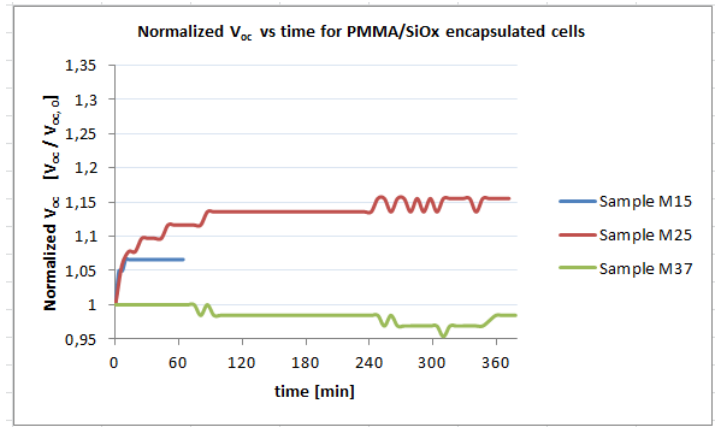


Figure 77 - Normalized open circuit voltage ( $V_{oc}$ ) vs. time for encapsulated cells

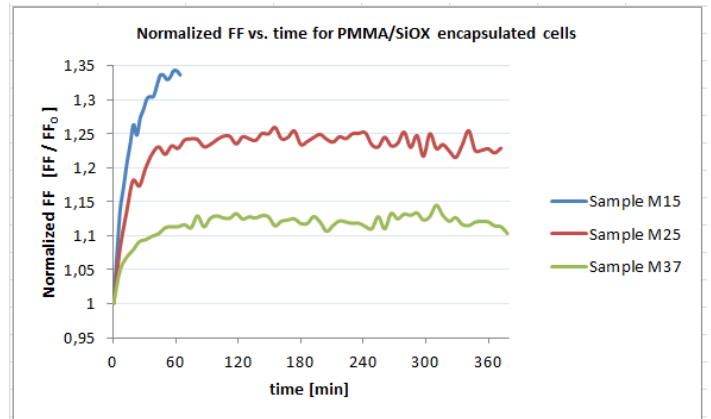


Figure 78 - Normalized Fill Factor (FF) vs. time for encapsulated cells

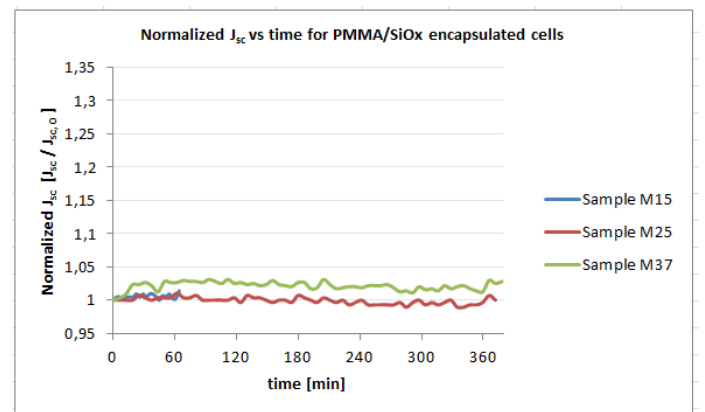


Figure 79 - Normalized current density ( $J_{sc}$ ) vs. time for encapsulated cell

### 6.3.7. Discussion

From results it can be seen that the encapsulation is increasing the stability of the inverted OSCs, yet interestingly the PCE is also enhanced (see figure 76 & table 4).

It is suggested that the enhanced PCE is related to an improvement in the  $\text{TiO}_x$ /organic material interface. When the OSC is illuminated with UV light for longer time, it can be observed from the IV-curves that the s-shape is vanishing (see figure 80 & 81), the Fill factor is increasing (see figure 78), the maximum power point is shifted to a higher level and  $V_{oc}$  increases a bit (see figure 77). The s-shape comes from an interfacial barrier for charge transport at the  $\text{TiO}_x$ /organic interface and it is believed that this barrier is removed due to the photo generated electrons in the  $\text{TiO}_x$  layer upon UV illumination. [33] In the case of the encapsulated cell a longer illumination period is possible without degrading the cell, so it is possible to observe this effect.

Taking a look at the IV-curve from figure 80 it can be seen for M15, that the interfacial charge barrier (s-shape) disappears. The IV characteristic after 1 hour of illumination (red curve) is closer to the characteristic shape of an IV-curve for a solar cell (see figure 25 on p20). A similar behavior as for M15 can be seen in figure 81 for M25.

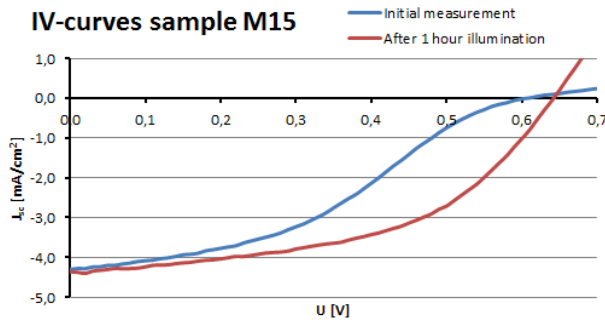


Figure 80 - IV curves M15

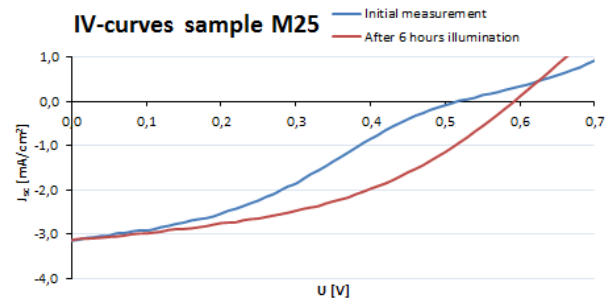


Figure 81 - IV curves M25

The increasing Fill Factor in figure 78 is the result of the improvement of the  $\text{TiO}_x$ /organic interface and it seems, that the improvement of the interfacial barrier at the  $\text{TiO}_x$ /organic interface by photo generated electron is strongest during the first 60 minutes of UV illumination, because during this time span, the FF is increasing very rapidly. Figure 78 also shows that the FF of M37 is not increasing as much

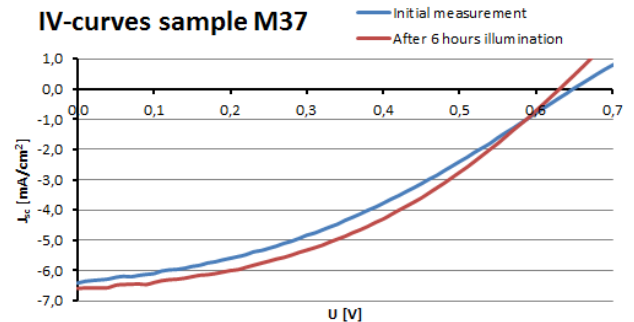


Figure 82 - IV curves M37

as for M15 and M25, which also can be seen in figure 82. Sample M37 had been previously pre-illuminated and it had been observed, that after the  $\text{TiO}_x$ /organic interface is improved the s-shape disappeared and was not observed again upon illumination. [33] So it seems that the improvement of the  $\text{TiO}_x$  layer is permanent, with possibly a small reversibility but this needs further investigations.

Now that there is a solution for the interfacial barrier for charge transport, which results in that the s-shape of the IV-curve disappears, the next step would be to find out how to even more improve the PCE of the OSC. Taking a look at the shape of the IV-curves after illumination from figure 80-82 it seems, that a further optimization could be done by decreasing the internal serial resistance ( $R_S$ ) and increasing the internal parallel resistance ( $R_{SH}$ ) of the OSCs, which would bring the IV-curves closer to a more ideal IV-curve like in figure 25 on p.20. By decreasing the  $R_S$  and increasing  $R_{SH}$ , the Fill factor would even more increase and the maximum power point would shift to a higher position. To achieve this one could e.g. further optimize the cleaning procedure, which could result in a better film structure and interface, due to less film defects caused by external particles (see figure 66 on p.44). Also the charge transport to the contacts could be improved (improves  $R_S$ ) by further optimizing the PEDOT mixture by finding a more accurate way of producing the mixture, which could yield in a higher reproducibility and conductivity.

To explain the behavior of the open circuit voltages for M15, M25 and M37 in figure 77 it is helpful to take a look at the non-normalized graphs in figure 83.

The  $V_{oc}$  depends on the materials HOMO and LUMO levels. For P3HT:PCBM the  $V_{oc}$  should be about 0.5-0.6 V [34], and this factor doesn't normally change so much from cell to cell, since it is an intrinsic characteristic of the material.

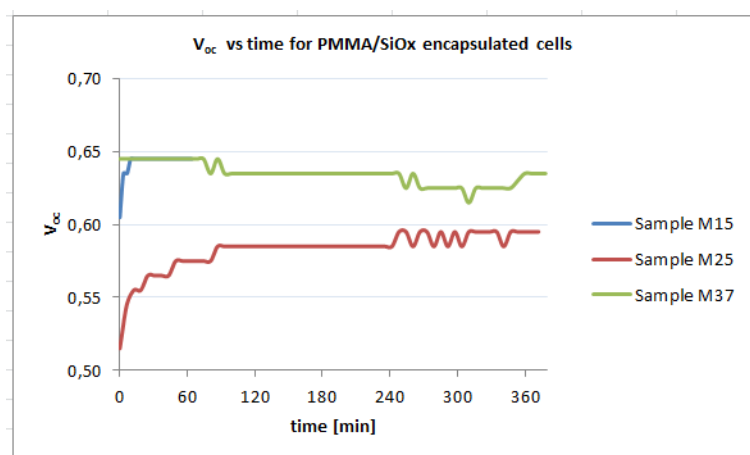


Figure 83 –  $V_{oc}$  vs. time for PMMA/SiO<sub>x</sub> encapsulated cells

From figure 83 it can be seen that the  $V_{oc}$  for samples M15 and M25 are increasing. This increase seems to be connected to the earlier described conductivity improvement of the TiO<sub>x</sub> layer, which resulted in a higher Fill Factor. It can be seen from figure 80 & 81 how  $V_{oc}$  is changing from before to after illumination for sample M15 and M25. Another observation is that  $V_{oc}$  is not increasing for sample M37 (figure 82), for which the TiO<sub>x</sub>/organic material interface already had been improved by the previous pre-illumination, which could also explain the relative high initial value of  $V_{oc}$  for sample M37 (see figure 83). So it seems that upon UV illumination the conductivity improvement of the TiO<sub>x</sub>/organic material interface also improves the  $V_{oc}$  of the OSC permanently. Further experiments could be conducted, to investigate this observed behavior. E.g. one experiment could be, to produce a few samples, illuminate them so the TiO<sub>x</sub>/organic material interface improves, measure the IV-characteristics and store them on the shelf in the dark. After a few days the cells are re-measured and the before after characteristics are compared in order to see if the improvement of the TiO<sub>x</sub>/organic interface is reversible over time.



Looking at the current density in figure 79 it can be seen that  $J_{sc}$  stays fairly constant for all samples at around their initial values. The slightly increased current density upon illumination for sample M37 could have different reasons. E.g. between the lifetime measurements of sample M25 and M37 the PEDOT and P3HT/PCBM solutions were re-filled with fresh produced solutions, which could have resulted in a slightly better Nano-morphology in the P3HT/PCBM blend upon annealing due to illumination, which would positively impact the exciton diffusion, separation and charge transport of sample M37 compared to M25, and increase the charge carrier collected at the electrodes, thus increasing the current density.

### Encapsulation improvements

The improvements of the PCE are a nice side effect of the encapsulation. Concerning the PMMA/SiO<sub>x</sub> encapsulation itself, there is a lot of room for improvements.

From figure 76 and table 4, it can be seen that the encapsulation works for a minimum of 6 hours of continuous illumination (1 sun). The encapsulation needs to be tested in an environment with harsher conditions (increased temperature and humidity), so the lifetime measurement can be accelerated (see appendix “accelerated lifetime measurements” p.4). This will also make it possible to apply the measurement standard from chapter 3.5.1 on p.25 for analyzing the OSC stability.

Furthermore a UV-filter should be applied to the cells after the improvement of the TiO<sub>x</sub>/organic material interface. This will also increase the stability of the cell, since it's not recommended to expose the OSC to UV-light, because this will degrade the cells. The SiO<sub>x</sub> thin film layer should act as a UV-filter (like normal window glass does), but it needs to be determined at which thickness this UV-filtering property will work most effectively. Also further experiments should be done where the SiO<sub>x</sub> thickness is increased and decreased to gain an understanding of the importance of the SiO<sub>x</sub> thin film thickness. Also the SiO<sub>x</sub> thin film should be investigated for defects like cracks or pinholes, with the goal to determine the optimum deposition parameters (e.g. rate, pressure, thickness) to improve the SiO<sub>x</sub> film morphology.

Another area which needs some further investigation is the PMMA, which is used as a protective layer during the RF-sputtering. It should be investigated if there are solvent free materials, which could be used as a buffer instead of PMMA, since the PMMA uses Anisole as solvent and it is not fully clear if the Anisole is reacting with the PEDOT or active layer, causing a decrease of the absolute OSC PCE.

Also the use of multilayer encapsulation should be considered. For the PMMA/SiO<sub>x</sub> encapsulation another layer of PMMA on top of SiO<sub>x</sub> could protect the SiO<sub>x</sub> layer and counterbalance defects in the SiO<sub>x</sub> thin film. An experiment should also be conducted where Al<sub>2</sub>O<sub>3</sub> (Aluminum oxide) is used as encapsulation after the deposition process with the “Edwards Auto 500” will be optimized, to see how that material functions as a barrier material.

Furthermore the minimum thickness of the PMMA layer, where it still works as protective layer could be investigated. If the PMMA layer is too thick compared to the SiO<sub>x</sub> layer, it will make it possible for H<sub>2</sub>O and O<sub>2</sub> to bypass the SiO<sub>x</sub> layer and diffuse through the PMMA side walls (see figure 84). In case the PMMA can be spin coated with a film thickness of 30 nm and 50 nm of SiO<sub>x</sub> are deposited on top of the 30 nm PMMA, then the SiO<sub>x</sub> should seal the sidewalls of the PMMA and completely encapsulate the underlying OSC (see figure 85). The biggest obstacle with a very thin PMMA layer could be particles on the substrate, which leave holes in the PMMA thin film, exposing the active layer to the RF sputtering which would cause damage to the active layer. This means that this procedure has to be done in the clean room and possible extra cleaning procedures should be established.

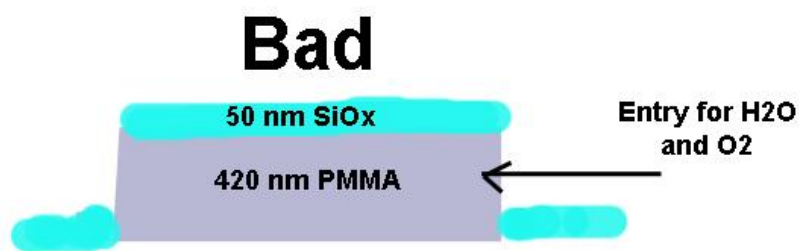


Figure 84 – Too high side walls – not fully encapsulated



Figure 85 – Side wall coverage - good encapsulation

## 6.4. Epoxy encapsulation

After the encapsulation attempt with the glass/epoxy combination in “chapter 6.2.3. p.42”, further research had been conducted on the idea to use an adhesive for the OSC encapsulation.

It was found that the German based company named “DELO”<sup>18</sup> offers a variety of different adhesives and some of them which are suitable for the encapsulation of OSCs. The requirements for the adhesive are that it should be solvent free, in order to minimize the chances of any reactions with the PEDOT top electrode of the OSC. Furthermore the glue should have a very low WVTR and OTR, so it functions as a barrier for H<sub>2</sub>O and O<sub>2</sub>. For simplifying the processing, multi-component adhesives should be avoided. Our contact person for this project was the sales engineer Helge Jürgensen who was supplying us with two free test samples of the glue “DELO-KATIOBOND LP VE 110484”, which is normally used for the sealing of sensitive component like flexible OSCs or for edge sealing and flat bonding. The adhesive is supplied so it is ready for use right away. It is made from a modified epoxy resin, which consists of only one component (easier processing), it is solvent free and it is cured by UV-/light. From the datasheet (see attached CD), it can be seen that the WVTR is 6.2 g/m<sup>2</sup>/day at 60 °C and 90% relative humidity for a layer thickness of 1mm, yet the OTR is unknown.

### 6.4.1. Encapsulation procedure

The adhesive has to be stored cool at 0 to +10 °C immediately after receipt and before the use of the adhesive, it is important that the container is conditioned to room temperature. Furthermore it's good to know that the adhesive can easily be removed with acetone and isopropanol in case of cleaning.

The encapsulation procedure is similar to the one for the PMMA/SiO<sub>x</sub> encapsulation. The entire encapsulation is done in the glove box and the curing of the adhesive is done with the solar generator from chapter 4.5.1 p. 31. Before starting the encapsulation it is advisable to apply silver paste close to the cathodes of the OSC for increasing the conductivity (see figure 86).

To start the encapsulation, the anode and cathode of the OSC were covered partly with the blue glue tape (see figure 86) to be able to characterize the OSC after the encapsulation has been applied.

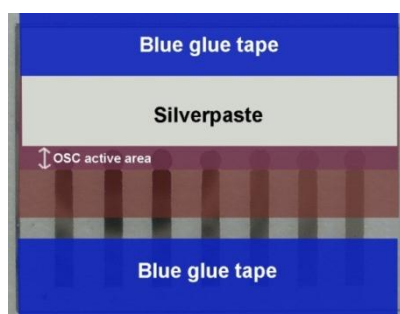


Figure 86 - OSC covered with blue glue tape

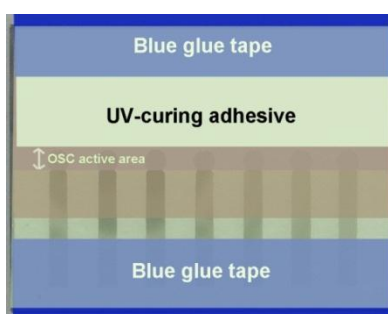


Figure 87 Spin coating adhesive

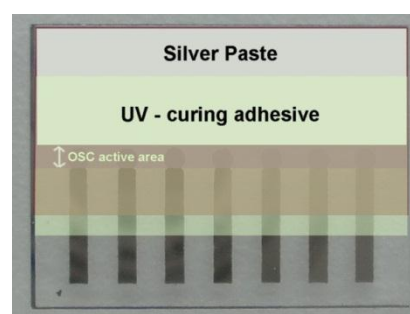


Figure 88 - Removing blue glue tape

<sup>18</sup> <http://www.delo.de/en/> (29.05.2012)

The next step was to spin coat the OSC with the adhesive using the “Laurell WS-400BZ-6NPP/Lite”. Unfortunately the company could not supply any spinning vs. film thickness data, but through experiments it had been found that at above 1000 rpm, it frequently occurred that the adhesive film showed areas on the OSC, which were not covered with the adhesive. The adhesive was spin coated at 1000 rpm for 45 s (see figure 87) and after the spin coating process the blue glue tape was carefully removed with tweezers (see figure 88).

The final step was to cure the adhesive; the curing parameters are depending on the material thickness and absorption, lamp type and distance between lamp and adhesive layer.

For the curing the AM 1.5 G filter was removed, the sample was placed at a distance of about 20 cm to the light source and the solar generator was calibrated to run with 5.5 A. The sample was then exposed for 2 minutes to the light (see figure 89). After the exposure the light was shut and the adhesive got 20 minutes to cure without illumination, which resulted in a hard surface. (This procedure was found through optimizations experiments.) (see figure 90)

From the datasheet it can be seen, that for an irradiation at 55 to 60 mW/cm<sup>2</sup> the minimal curing time is 16 seconds and the recommended curing time is 60 seconds for a layer of 0,2 mm thickness. Again this depends on previous mentioned curing parameters (e.g. material thickness, lamp type), which means that for different parameters the curing time has to be adjusted so the adhesive receives a sufficient radiation for starting the curing process. See appendix: “Process recipe for epoxy adhesive encapsulation” p.20).

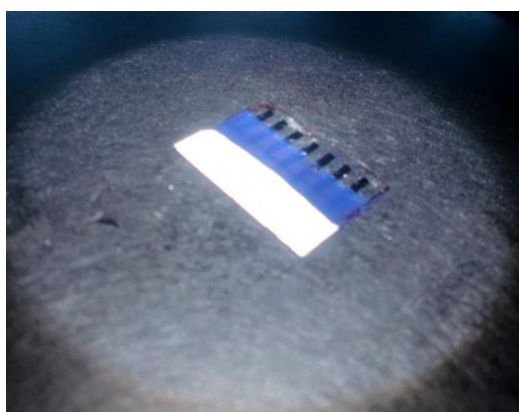


Figure 89 - OSC sample with epoxy glue (epoxy shining blue when illuminated)



Figure 90 - OSC encapsulated with adhesive

After the OSC was encapsulated, the solar cell profile and film thickness of the adhesive had been measured with the “Veeco Dektak 150” profilometer (see figure 91). The measurement showed an average surface height of 51.4  $\mu\text{m}$  for the measurement point in figure 91 (green line).

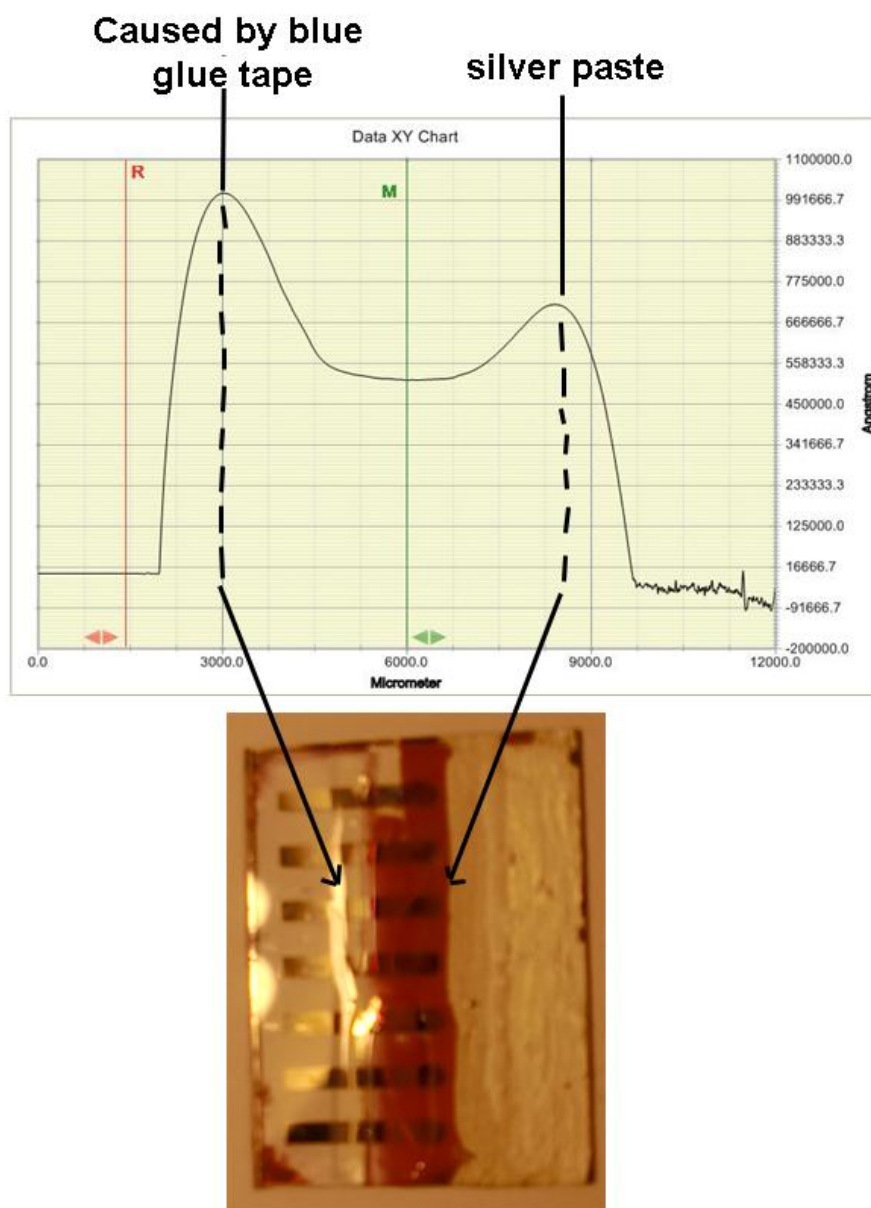


Figure 91 - Adhesive thickness (spin coated at 1000 rpm, 45 s)

## 6.4.2. Lifetime measurement results

### 6.4.2.1. Experimental setup

All samples were measured under continuous illumination of 1 sun with the standard solar generator setup described in chapter 4.5.1 on p.31. The time between each measurement is 6 minutes and the samples and probes have not been repositioned during the experiment. Table 5 summarizes information about the measured samples.

Sample	Cell	Cell area [cm <sup>2</sup> ]	Initial PCE after encapsulation
M32	3	0,01	0,42%
M38	4	0,011	0,88%

Table 5 - Sample information

Sample M32 was the first lifetime measurement done with the adhesive and only measured for 64 minutes. Sample M38 was produced to check for the reproducibility of the method and was measured for 6 hours. Both samples were produced according to the same procedures, yet for M38 a fresh sample of the PEDOT and P3HT/PCBM mixture was used.

### 6.4.2.2. Results and result treatment

Figure 92 shows the normalized power conversion efficiencies of the encapsulated samples M32 and M38 plotted versus time in minutes. From the graphs it can be seen that the initial PCE stays rather constant for M32 (red) and declines a bit over the course of 6 hours for M38.

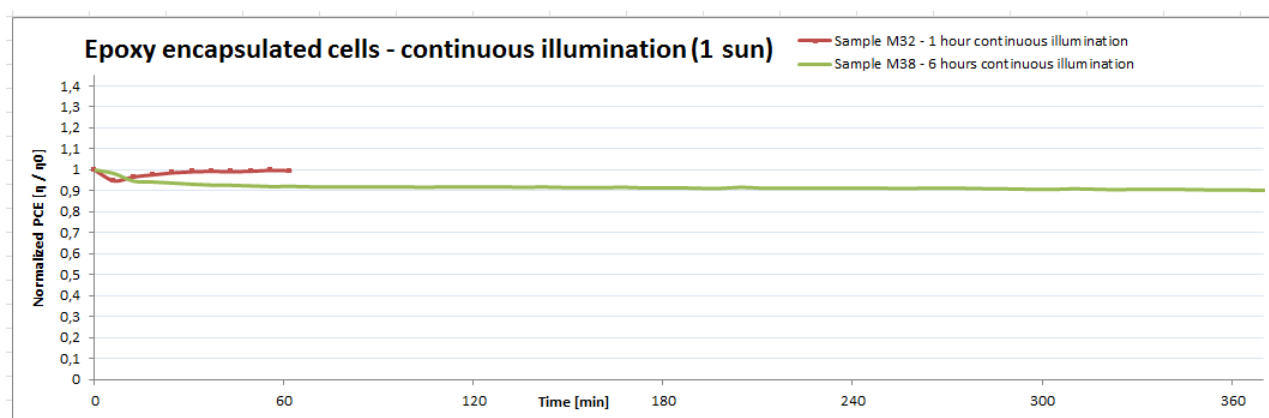


Figure 92 - Encapsulated cell PCE vs. time measurement results



For measuring the stability of the epoxy encapsulated OSCs, the same measurement system will be applied like for the PMMA/SiO<sub>x</sub> encapsulation in chapter 6.3.6 p.48), since the epoxy encapsulated cells are not degrading enough to use the common measurement standard (chapter 3.5.1 p.25). Figure 93 shows a close-up of the PCE vs. time graphs of figure 92 with the measurement standard from chapter 6.3.6 p.48.

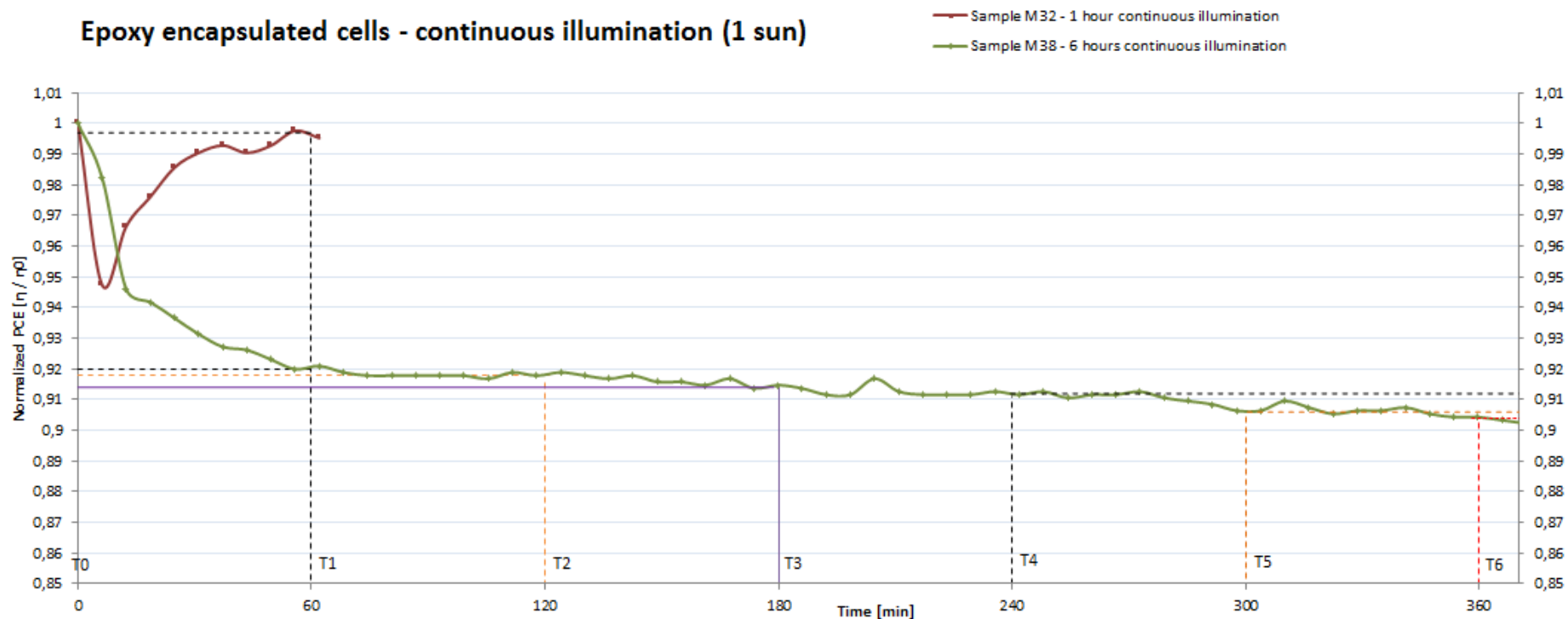


Figure 93 - Epoxy encapsulated cells – PCE vs. time - stability analysis

Table 6 shows the normalized PCE's at the given points of time from T0 to T6 from figure 93:

M32 (red)	Normalized PCE	M38 (green)	Normalized PCE
T0	0	T0	0
T1	0,997	T1	0,92
		T2	0,918
		T3	0,914
		T4	0,912
		T5	0,906
		T6	0,904

Table 6 - Table with normalized PCE's for given point of time T0 to T6 from figure 93

From figure 93 and table 6 it can be seen that both sample M32 and M38 show no improvement of their initial PCE. For M32 the normalized PCE is dropping during the first few minutes but then recovering to about its initial PCE again. Sample M38 is dropping by 8% during the first 60 minutes and drops about 10% from its initial PCE after 6 hour's constant illumination.

Figure 94 shows the  $V_{oc}$  vs. time for the encapsulated samples under constant illumination. It can be seen that both for sample M32 and M38 the  $V_{oc}$  is constant. The small fluctuations can be attributed to other sources of measurements errors.

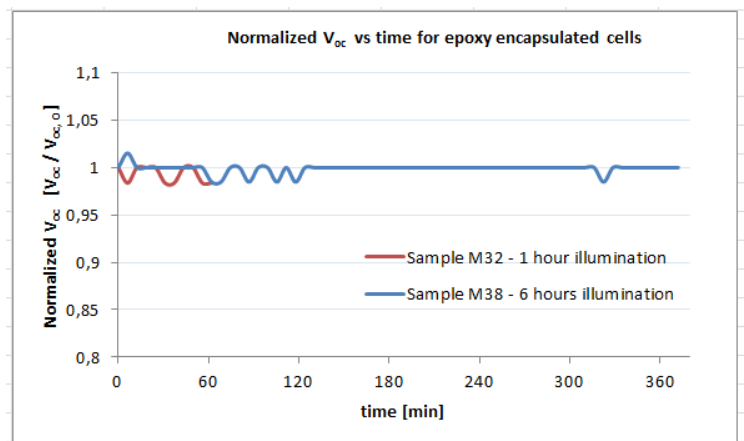


Figure 94 - Normalized  $V_{oc}$  vs. time for epoxy encapsulated cells

Figure 95 shows the fill factor versus time for the encapsulated samples under constant illumination and no significant increase can be seen. The FF of sample M32 is at 5% at  $t=60$  minutes. Also the FF for sample M38 is slightly increasing (around 2% from  $t=0$  to  $t=360$ ).

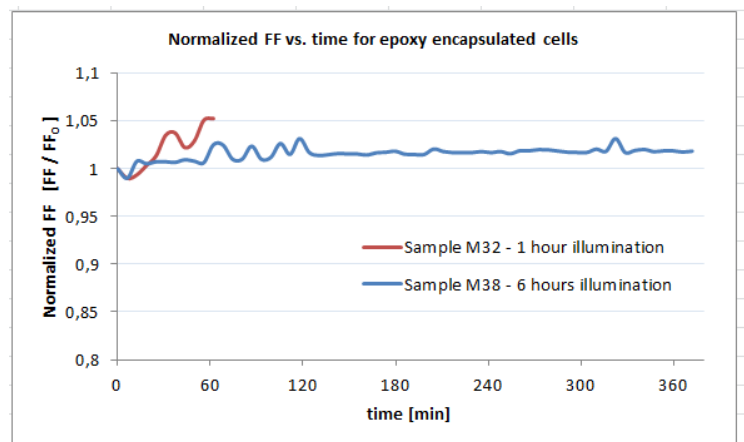


Figure 95 - Normalized FF vs. time for epoxy encapsulated cells

Figure 96 shows the current density  $J_{sc}$  vs. time for the encapsulated samples under constant illumination. Both sample M32 and M38 show a reduction in their short circuit current during the measurement. Sample M32 has decreased by 4% at  $t=60$  minutes and sample M38 decreased by 8% at  $t=60$  minutes. At  $t=360$  minutes sample M38 lost about 12% of its initial  $J_{sc}$ .

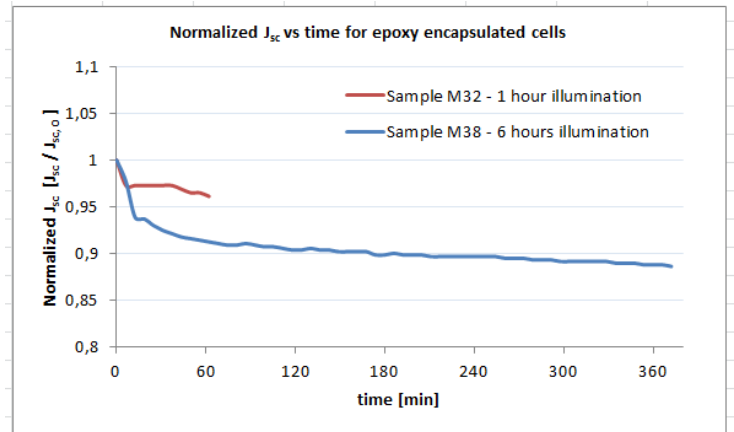


Figure 96 - Normalized  $J_{sc}$  vs. time for epoxy encapsulated cells

Also taking a look at the IV-curves of sample M32 and M38 in figure 97 and 98 it can be seen that they are very linear and no increase in the Fill Factor is seen like for the PMMA/SiO<sub>x</sub> encapsulation from chapter 6.3.7 p.52.

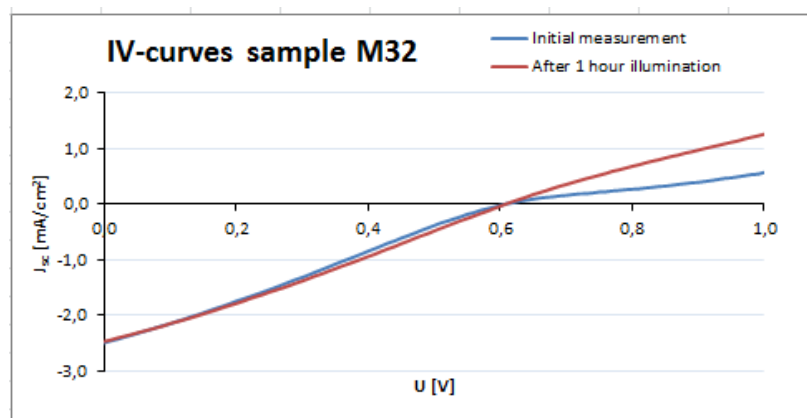


Figure 97 IV curves sample M32 (before and after illumination)

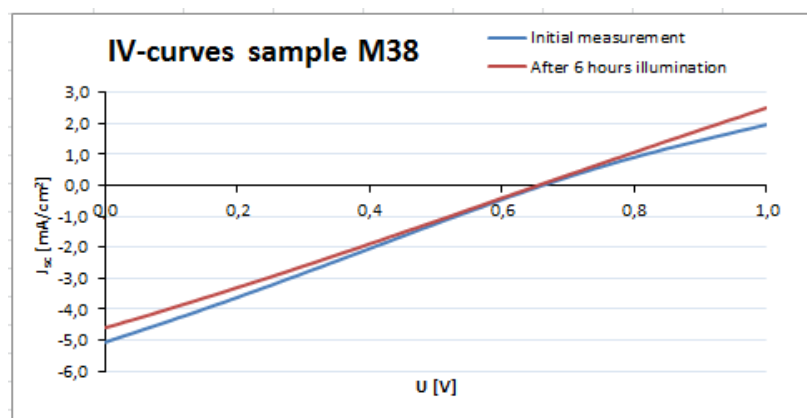


Figure 98 IV curves sample M38 (before and after illumination)

### 6.4.2.3. Discussion

Based on the results in figure 93, table 6 and figure 96-98 it seems that the epoxy encapsulation still needs optimization in order to make the OSCs more stable.

From figure 96 it can be seen that  $J_{sc}$  for both samples is decreasing, which results in a decrease of the PCE. From figure 95 it can be seen that the FF is only increasing very little for both samples and  $V_{oc}$  in figure 94 stays constant for both samples.

As the PCE is decreasing a little in figure 93 it would be expected to see a decrease in both FF and  $J_{sc}$ , yet only a decrease in  $J_{sc}$  is observed. It could be that the FF stays constant (instead of decreasing) due to the improvement of the  $TiO_2$  conductivity discussed in chapter 6.3.7 p.52, which would improve the interface between the bottom electrode and active layer and result in an improved FF. The decreasing  $J_{sc}$  and constant FF seem to balance each other out and this could cause the IV curve shape to have the constant linear behavior (see figure 97 & 98). The linearity after longer illumination could be due to the improvement of the  $TiO_2$ /active layer interface due to the UV light. The curves from the initial measurements for M32 and M38 in figure 97 & 98 are becoming less s-shaped upon illumination, and in the case where there would be an improvement of the FF, the curves would look like the ones in chapter 6.3.7 p.52. It can also be said that the curves are becoming linear in a "try" to overcome the s-shape and have the diode behavior but are stopped due to the non-improvement of the Fill Factor (due to degradation of  $J_{sc}$ ).

In figure 89 p.57 it can be seen that when the UV-curable adhesive is illuminated, it reflects blue light. It absorbs the UV light (see figure 99) and the glue's properties make it reflect part of the blue light, which may also cause a small decrease of the PCE, but a transmission experiment should be done, to verify the transmission spectrum of the glue for the given thickness.

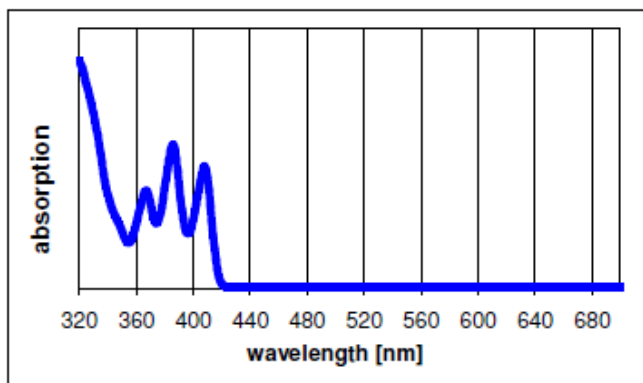


Figure 99 - absorption spectrum DELO-KATIOBOND LP VE 110484

Also the linearity of the initial IV-curves (blue) in figure 97 & 98 for sample M32 and M38 could be caused by a mixture of leakage currents (low parallel resistance) and low conductivity (high series resistance). The reason for the linear behavior of the initial IV-curves is believed to come from the adhesive. During the curing phase the adhesive will shrink<sup>19</sup>, which could cause damage to the PEDOT top electrode or during the spin coating process, the adhesive could cause damage through the

<sup>19</sup> From the "DELO-KATIOBOND LP VE 110484" datasheet: shrinkage volume [%] = 2.8

rotational forces, because it adheres very well to the top electrode. Both scenarios could cause leakage currents (decreases parallel resistance) and a lower conductivity for the active layer / PEDOT interface (increases serial resistance). To avoid damage to the top electrode a thin protective layer of PMMA could be used. For this further experiments are needed to show if the PMMA is strong enough to withstand damage from the adhesive and if the IV-curves of the OSCs will improve to a “normal” shape.

Another optimization which could be done is to achieve a more uniform film thickness of the glue across the OSC. Based on the thickness analysis from figure 91 p.58, it can be seen that there are two tops and one valley. The first top is created during the spin coating of the adhesive when the “blue glue tape” from figure 86 p.56 acts as a barrier and the adhesive accumulated along the “blue glue tape”. The second hill is caused by the silver paste. Future experiments could be done to determine the optimal parameters by varying spin coating speed and time, so a more uniform glue film thickness is achieved.

From figure 96 p.62 it can be seen that the  $J_{sc}$  is decreasing for both samples M32 and M38 for the measured time frame, so it seems like, that the glue layer thickness should be increased, to enhance the barrier effect of the encapsulation. Another possibility to improve the glue barrier effect is to use the glue as a protective layer for the OSC while  $SiO_x$  or  $Al_2O_3$  are deposited with the “Edwards Auto 500” on top of the glue layer, but first the layer uniformity of the glue has to be optimized.

Also there seems to be a problem with spin coating speeds of 1250 rpm and 1500 rpm, which will cause that the OSC is just partly covered in glue and partly there will be areas with no glue. This will make it hard to achieve very thin films with this particular glue. At spinning speeds of 1000 rpm and below the glue covered the whole OSC like it was intended. Further experiments could be conducted with glue layers spin coated at 500 rpm for 45 s, which would also yield in a thicker glue layer and probably a higher barrier effect.

## 7. Comparison

Figure 100 shows a comparison between the two encapsulations with PMMA/SiO<sub>x</sub> and epoxy. To highlight the stability of M25 and M38 a non-encapsulated sample is also included.

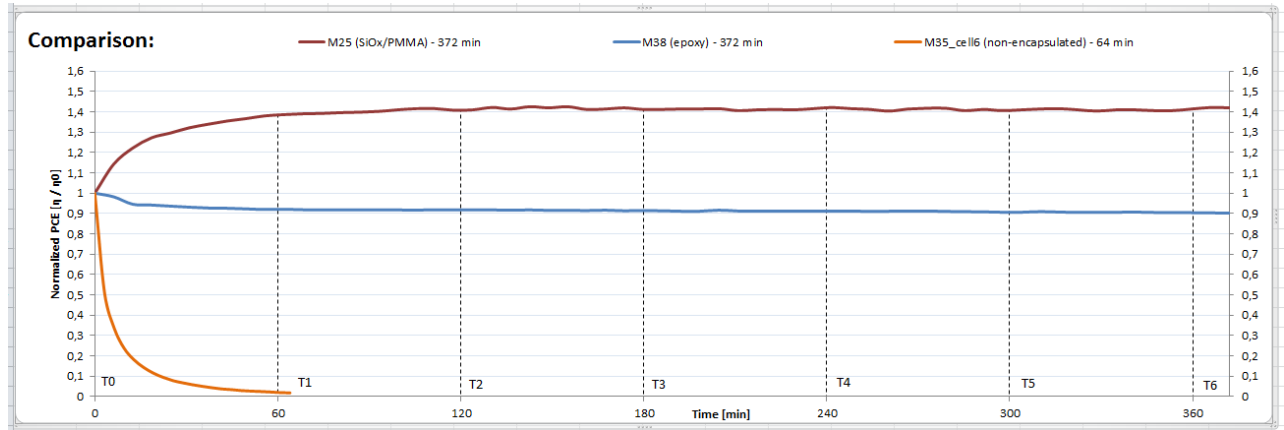


Figure 100

It can be seen that both the PMMA/SiO<sub>x</sub> and epoxy encapsulation prologue the lifetime of the original non-encapsulated OSCs. The samples with the PMMA/SiO<sub>x</sub> encapsulation even increase its initial PCE due to the previous discussed improvements in the TiO<sub>x</sub>/organic interface. The epoxy encapsulation doesn't show this initial PCE gain and the PCE decreases slightly over time.

### 7.1. Advantages and disadvantages

The advantage of the PMMA/SiO<sub>x</sub> encapsulation is that it seems to have good enough barrier properties to keep the initial parameters stable, so the effect of the improved TiO<sub>x</sub>/organic interface can be utilized, which results in a higher FF and thus an enhanced PCE. The epoxy encapsulation doesn't seem to have as good barrier qualities to counteract the degradation of  $J_{sc}$  (figure 96 p.62) and the PCE is not increasing above its initial value. Yet the epoxy encapsulation has a lot of potential and with the discussed process optimization from chapter 6.4.2.3.p.63 the encapsulation could possibly also make the OSC as stable as the PMMA/SiO<sub>x</sub> encapsulation does. From processing standpoint of view the epoxy encapsulation takes much less time to do and is also cheaper because less resources are used. The epoxy encapsulation can be applied to flexible materials and if further optimized it is probably possible to create a very effective encapsulation. This encapsulation has the potential for a very good balance between cost and barrier effect. The PMMA/SiO<sub>x</sub> encapsulation is more complex, involves more production steps and takes longer time to produce, which results also in higher production costs for the PMMA/SiO<sub>x</sub> compared to the epoxy encapsulation, but on the other side this encapsulation is effective, in the case if more than one cell is encapsulated, since it's possible to deposit SiO<sub>x</sub> on top of many cells at the same time with the Cryofox, the costs can be divided and the process gets accelerated.



## 8. Future projects

Besides of the improvements and further experiments discussed in the discussion of chapter 6.3.7 p.52 and chapter 6.4.2.3 on p.63 for the PMMA/SiOx and epoxy adhesive encapsulation there are a few more things which I would investigate.

### 8.1. Shelf lifetime

The next step would be to analyze the encapsulations under accelerated conditions and measure their shelf lifetime. One experiment has been done where the shelf lifetime of non-encapsulated cells was measured over 5 days (see appendix A – misc: shelf lifetime Sample M3 non-encapsulated p.3). A short description of the standard for shelf lifetime measurement can be found in appendix A – “ISOS-3: OSC lifetime measuring standard” p. 2 and appendix A – “Accelerated lifetime measurements” p.4.

### 8.2. Mathematical description

Further investigations can be done by fitting curves to the lifetime measurements by e.g. excel, so the behavior of the results can be expressed by a mathematical formula. This could help to identify key degradation variables, which are influencing the IV-curves shape. It has been tried to do fittings during this project and it was found that polynomials of the order of 4 to 6 fit the lifetime measurements of PMMA/SiOx and adhesives very well, yet further investigation was not possible due to the time frame of the project.

### 8.3. Miscellaneous

It would be interesting to analyze the PCE standard deviations for fresh produced samples over a certain time frame to see how they are varying.

Another thing which was observed are the particles which are seen in figure 101, which shows a picture of an OSC electrode taken with an optical microscope (Nikon ME600) with a 5x-0.1 microscope objective. It is not clear what these particles are and it could be further investigated if they have an effect on the conductivity of the PEDOT or other effects.

Also the pinholes in the PEDOT film (see figure 66 p.44) could be further investigated with the goal of establishing a PEDOT thin film which has less defects.

Also the encapsulations could be applied to flexible solar cells.

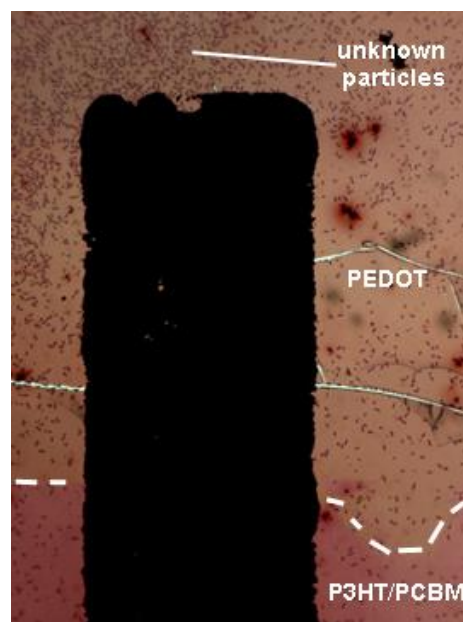


Figure 101 - picture of OSC electrode taken with optical microscope with a 5x-0.1 microscope objective

## 9. Conclusion and outlook

Organic solar cells are promising due to their low material and processing costs, flexibility, low weight and mechanical durability, however, the fast degradation hinders the practical use of the cells and therefore an encapsulation with a high barrier effect has to be applied to the OSC in order to increase their stability.

During this project the inverted bulk-heterojunction solar cells from P3HT:PCBM were successfully fabricated and several types of encapsulations were tested and evaluated. Experiments showed that the non-encapsulated cells degrade rapidly when placed under constant illumination, which can be mainly attributed to photo oxidation and absorption of oxygen and water.

It had been found that an encapsulation with PMMA/SiO<sub>x</sub> prologues the lifetime of the OSCs. Furthermore during the testing of the encapsulation an enhancement in the PCE had been observed, which is believed to come from improvements in the TiO<sub>x</sub>/organic interface due to photo generated electrons in the TiO<sub>x</sub> layer upon UV illumination, , which is not observed in non-encapsulated cells due to cell degradation.

A very simple method of encapsulating the OSC has been found by using the commercial product from DELO-adhesives, but this method needs further optimization concerning the layer thickness and protection of the top electrode of the OSC, during spin coating and curing process of the glue, in order to be as stable as the PMMA/SiO<sub>x</sub> encapsulation and to show the same improved IV-curves.

Future work should focus on the optimization of the glue layer thickness, to improve the barrier effect. Also the SiO<sub>x</sub> thin film should be analyzed for layer defects, so the deposition parameters can be optimized further, which could even more improve the barrier effect of the PMMA/SiO<sub>x</sub> encapsulation. Also it should be researched if the combination of the DELO-adhesive and SiO<sub>x</sub> (instead of PMMA/SiO<sub>x</sub>) can be made and if the combination yields in a higher stability of the OSCs. Finally a shelf lifetime research should be done with accelerated life time testing, to find out where the limits of the current encapsulations are.

## Bibliography

1. U.S. Energy Information Administration. *International Energy Outlook 2011*. [Online] [Cited: april 18, 2012.] <http://www.eia.gov/forecasts/ieo/world.cfm>.
2. **Smil, Vaclav**. *Energy: a beginner's guide*. s.l. : Oneworld, 2006. p. 12. 1851684522.
3. U.S. Energy Information Administration. *World Total Net Electricity Consumption, 1980-2006*. [Online] [Cited: 14 February 2012.] <http://www.eia.gov/pub/international/iealf/table62.xls>.
4. Solarbuzz - Solar market research and analysis. *Technologies*. [Online] [Cited: april 18, 2012.] <http://www.solarbuzz.com/going-solar/understanding/technologies>.
5. Renewable Energy World.com. *PV Costs Set to Plunge for 2009/10*. [Online] [Cited: april 18, 2012.] <http://www.renewableenergyworld.com/rea/news/article/2008/12/pv-costs-set-to-plunge-for-200910-54380>.
6. *Detailed Balance Limit of Efficiency of p-n Junction Solar Cells*. **Queisser, William Shockley and Hans J.** Vols. J. Appl. Phys. 32, 510 (1961) DOI: 10.1063/1.1736034.
7. Energieroute.de - Wegweiser zu erneuerbaren Energien im Raum Erfurt. *Solarzellenarten*. [Online] [Cited: april 17, 2012.] <http://www.energieroute.de/solar/solarzellen.php>.
8. *World mineral statistics British Geological Survey*. **Brown, TJ**. 2011, p. 95. 0852726775.
9. Solar facts and advice. *Sale of CIGS Solar Cell Panels Expected to Reach*. [Online] [Cited: april 19, 2012.] <http://www.solar-facts-and-advice.com/CIGS-solar-cell.html>.
10. *Detailed balance limit of the efficiency of tandem solar cells*. **Vos, A. De**. 1980, Vols. A De Vos 1980 J. Phys. D: Appl. Phys. 13 839 doi:10.1088/0022-3727/13/5/018.
11. **Mario Pagliaro, Giovanni Palmisano and Rosaria Ciriminna**. *Flexible Solar Cells*. s.l. : WILEY-VCH Verlag GmbH & Co. KGaA, 2008. pp. 1-54, 85-106. 978-3-527-32375-3.
12. Bright Hub. *Organic Solar Cells vs Semiconductor-based Solar Cells*. [Online] [Cited: april 19, 2012.] <http://www.brighthub.com/environment/renewable-energy/articles/95572.aspx>.
13. **James D. Plummer, Michael D. Deal, Peter B. Griffin**. *Silicon VLSI technology - Fundamentals, Practice and Modeling*. s.l. : Tom Robbins, 2000. pp. 15-17. 0130850373.
14. **Streetman, Ben G. and Banerjee, Sanjay**. *Solid State electronic Devices (5th ed.)*. New Jersey : s.n., 2000. p. 524. 0130255386.
15. **Leo, Prof.Dr. Karl**. Organic Semiconductor World. *What are organic semiconductors*. [Online] [Cited: mai 2, 2012.] [http://www.iapp.de/orgworld/?Basics:What\\_are\\_organic\\_semiconductors](http://www.iapp.de/orgworld/?Basics:What_are_organic_semiconductors).
16. *Organic solar cells: An overview*. **Harald Hoppe, Niyazi Serdar Sariciftci**. s.l. : Materials Research Society, Juli 2004, Vols. J. Mater. Res., Vol. 19, No. 7 DOI: 10.1557/JMR.2004.0252.
17. *P3HT:PCBM, Best Seller in Polymer Photovoltaic Research*. **Minh Trung Dang, Lionel Hirsch , and Guillaume Wantz**. Adv. Mater. 2011, 23, 3597–3602 DOI: 10.1002/adma.201100792,

18. *Organic solar cells using inverted layer sequence*. **M. Glatthaar a, b,\***, **M. Niggemann b**, **B. Zimmermann a**, **P. Lewer b**, **M. Riede a,b,**. Vols. Thin solid films 491 (2005), No.1-2, pp.298-300 DOI:10.1016/j.tsf.2005.06.006.
19. *Polymer–Fullerene Bulk-Heterojunction Solar Cells*. **By Christoph J. Brabec, \* Srinivas Gowrisanker , \* Jonathan J. M. Halls, \* Darin Laird**. Vols. Adv. Mater. 2010, 22, 3839–3856 DOI: 10.1002/adma.200903697.
20. Center for Materials and Devices for Information Technology Research (CMDITR)Photonics Wiki. *Major Processes in Organic Solar Cells*. [Online] [Cited: 5 4, 2012.] [http://photonicswiki.org/index.php?title=Major\\_Processes\\_in\\_Organic\\_Solar\\_Cells](http://photonicswiki.org/index.php?title=Major_Processes_in_Organic_Solar_Cells).
21. *Interlayer for Modified Cathode in Highly Efficient Inverted ITO-Free Organic Solar Cells*. **Zheng Tang, \* L. Mattias Andersson, Zandra George, Koen Vandewal, Kristofer Tvingstedt, Patrik Heriksson, Renee Kroon, Mats R. Andersson, and Olle Inganäs\***. Vols. Adv. Mater. 2012, 24, 554–558 DOI: 10.1002/adma.201104579.
22. *Stability of Polymer Solar Cells*. **Mikkel Jørgensen, Kion Norrman, Suren A. Gevorgyan, Thomas Tromholt, Birgitta Andreasen, and Frederik C. Krebs\***. Vols. Adv. Mater. 2012, 24, 580–612 DOI: 10.1002/adma.201104187.
23. *Stability/degradation of polymer solar cells*. **Mikkel Jørgensen, Kion Norrman, Frederik C. Krebs**. Vols. Solar Energy Materials & Solar Cells 92 (2008) 686–714 DOI:10.1016/j.solmat.2008.01.005.
24. *Thin-Film Permeation-Barrier Technology for Flexible Organic Light-Emitting*. **Lewis, J.S.** Vols. IEEE Journal of Selected Topics in Quantum Electronics. 10(2004)1. p. 45-57.
25. *Definition of encapsulation barrier requirements: A method applied to organic solarcells*. **S. Cros n, R. de Bettignies, S.Berson, S.Bailly, P.Maisse, N.Lemaitre, S.Guillerez**. Vols. Solar Energy Materials and Solar Cells Volume 95, Supplement 1, May 2011, Pages S65–S69 doi:10.1016/j.solmat.2011.01.035.
26. *The developmet of thin film barriers for encapsulating organic electronics*. **Yongjin Kim, Namsu Kim, Hyungchul Kim, Samuel Graham**. Vols. Electronic Components and Technology Conference (ECTC), 2011 IEEE 61st, pp. 2101-2105.
27. **Bowden, Christiana Honsberg and Stuart**. PVEDUCATION.ORG. *IV-curve*. [Online] University of new south wales Sydney, mai 13, 2012. <http://pveducation.org/pvcdrom/solar-cell-operation/iv-curve>.
28. National Instruments. *Part II – Photovoltaic Cell I-V Characterization Theory and LabVIEW Analysis Code*. [Online] [Cited: mai 13, 2012.] <http://www.ni.com/white-paper/7230/en#toc1>.
29. *Optimization of a polymer top electrode for inverted semitransparent organic solar cells*. **Yinhua Zhou, Hyeunseok Cheun, Seungkeun Choi, Canek Fuentes-Hernandez, Bernard Kippelen**. s.l. : Volume 12, Issue 5, May 2011, Pages 827–831 DOI: 10.1016/j.orgel.2011.02.017.
30. *Reduced bleaching in organic nanofibers by bilayer polymer/oxide coating*. **L. Tavares, J. Kjelstrup-Hansen, H.-G. Rubahn, and H. Sturm**. Vols. J. Appl. Phys. 107, 103521 (2010); doi: 10.1063/1.3427561.

31. **MicroChem.** *NANO<sup>TM</sup>PMMA and Copolymer*. [Online] [Cited: mai 24, 2012.] [http://www.microchem.com/pdf/PMMA\\_Data\\_Sheet.pdf](http://www.microchem.com/pdf/PMMA_Data_Sheet.pdf).
32. *Thin-Film High-Barrier Technology for New Type Packaging Material*. **Chun Wei Li, Xue Song Jiang, Qun Li Zhang, Shu Yan Xu, Gui Ying Wang**. Vols. *Advanced Materials Research (Volumes 113 - 116)*, 2333-2336, June 2010, DOI: 10.4028/www.scientific.net/AMR.113-116.2333.
33. *Highly Efficient Tandem Polymer Photovoltaic Cells*. **By Srinivas Sista, Mi-Hyae Park, Ziruo Hong,\* Yue Wu, Jianhui Hou,.** Vols. *Adv. Mater.* 2010, 22, 380–383 DOI: 10.1002/adma.200901624.
34. *Plastic photovoltaic devices*. **Sariciftci, Niyazi Serdar**. *Physical Chemistry*, Johannes Kepler University of Linz : ISSN:1369 7021 © Elsevier Ltd 2004.
35. *Three-dimensional nanopillar-array photovoltaics on low-cost and flexible substrates*. **Zhiyong Fan, Haleh Razavi, Jae-won Do [...]**. Vol. *NATURE MATERIALS VOL 8 AUGUST 2009* DOI: 10.1038/NMAT2493.

## Abbreviations

Commonly used abbreviations used in this thesis are:

BHJ = bulk heterojunction

FF = fill factor

$J_{sc}$  = current density

OSCs = organic solar cells

PCE = power conversion efficiency

$V_{oc}$  = open circuit voltage



## Appendix

### Contents

<b>A</b>	<b>Appendix: miscellaneous.....</b>	<b>74</b>
	ISOS-3: OSC lifetime measuring standard.....	74
	Shelf lifetime Sample M3 - non-encapsulated .....	75
	Accelerated lifetime measurements .....	76
	<b>Bibliography.....</b>	<b>76</b>
<b>B</b>	<b>Appendix: OSC substrate production .....</b>	<b>77</b>
	Process recipe for wafer bottom electrodes (NanoSyd) .....	77
	Process recipe for wafer bottom electrodes illustrations (M. Hausladen) .....	77
	Recipe for “Cryofox Explorer 600 LT” .....	78
<b>C</b>	<b>Appendix: Solution Preparation .....</b>	<b>79</b>
	Recipe for P3HT/PCBM blend.....	79
	Recipe for PEDOT blends .....	80
<b>D</b>	<b>Appendix: OSC fabrication and characterization.....</b>	<b>81</b>
	Recipe for the fabrication of inverted ITO-free BHJ OSCs .....	81
	Optical microscope cell area measurements.....	82
	Voltage sweeps with LabVIEW .....	84
	Measuring IV-curves – step by step procedure .....	85
<b>E</b>	<b>Appendix: Lifetime measurement non-encapsulated cells .....</b>	<b>86</b>
	Measurement standards for OSCs samples .....	86
	Sample M4 and M5 calculations .....	87
	Sample M4 and M8 calculations .....	87
<b>F</b>	<b>Appendix: Lifetime measurements encapsulated cells.....</b>	<b>88</b>
	Initial material and process research for encapsulations .....	88
	PMMA film thickness.....	90
	Process recipe for PMMA/SiO <sub>x</sub> encapsulation.....	91
	Process recipe for epoxy adhesive encapsulation.....	92

## A Appendix: miscellaneous

### ISOS-3: OSC lifetime measuring standard

<b>Three levels</b>						
Basic (Level 1):		"Hand held" measurements using the simplest equipment and few conditions.				
Intermediate (Level 2):		Fixed conditions and protocols suited for most labs.				
Advanced (Level 3):		Standardized tests applied in certified labs. Extended range of parameters to monitor etc.				
Test Type	<b>Dark</b>			<b>Outdoor</b>		
Test ID	ISOS-D-1 Shelf	ISOS-D-2 High temp. storage	ISOS-D-3 Damp heat	ISOS-O-1 Outdoor	ISOS-O-2 Outdoor	ISOS-O-3 Outdoor
Light Source	None	None	None	Sunlight	Sunlight	Sunlight
Temperature <sup>a)</sup>	Ambient	65 °C/85 °C	65 °C/85 °C	Ambient	Ambient	Ambient
Relative Humidity (R.H.) <sup>a)</sup>	Ambient	Ambient (low)	85%	Ambient	Ambient	Ambient
Environment <sup>b)</sup>	Ambient	Oven	Env. chamber	Outdoor	Outdoor	Outdoor
Characterization light source	Solar simulator or sunlight	Solar simulator	Solar simulator	Solar simulator	Sunlight	Sunlight & solar simulator
Load <sup>b)</sup>	Open Circuit	Open Circuit	Open Circuit	MPP or Open Circuit	MPP or Open Circuit	MPP
Test Type	<b>Laboratory Weathering Testing</b>			<b>Thermal Cycling</b>		
Test ID	ISOS-L-1 Laboratory weathering	ISOS-L-2 Laboratory weathering	ISOS-L-3 Laboratory weathering	ISOS-T-1 Thermal Cycling	ISOS-T-2 Thermal Cycling	ISOS-T-3 Thermal Cycling
Light Source	Simulator	Simulator	Simulator	None	None	None
Temperature <sup>a)</sup>	Ambient	65 °C/85 °C	65 °C/85 °C	Between room temp. and 65 °C/85 °C	Between room temp. and 65 °C/85 °C	−40 °C to +85 °C
Relative Humidity (R.H.) <sup>a)</sup>	Ambient	Ambient	Near 50%	Ambient	Ambient	Near 55%
Environment/setup	Light only	Light & Temp.	Light, Temp., R.H.	Hot plate/Oven	Oven/Env. Chamb.	Env. Chamb.
Characterization light source	Solar simulator	Solar simulator	Solar simulator	Solar simulator or sunlight	Solar simulator	Solar simulator
Load <sup>b)</sup>	MPP or Open Circuit	MPP or Open Circuit	MPP	Open Circuit	Open Circuit	Open Circuit
Test Type	<b>Solar-Thermal-Humidity Cycling</b>					
Test ID	ISOS-LT-1 Solar-Thermal Cycling		ISOS-LT-2 Solar-Thermal-Humidity Cycling		ISOS-LT-3 Solar-Thermal-Humidity-Freeze Cycling	
Light Source	Simulator		Simulator		Simulator	
Temperature	Linear or step ramping between room temp. and 65 °C		Linear ramping between 5 °C and 65 °C		Linear ramping between −25 °C and 65 °C	
Relative Humidity (R.H.)	Monitored, uncontrolled		Monitored, controlled at 50% beyond 40 °C		Monitored, controlled at 50% beyond 40 °C	
Environment/setup	W0eathering chamber		Env. Chamb. with sun simulation		Env. Chamb. with sun simulation and freezing	
Characterization light source	Solar simulator		Solar simulator		Solar simulator	
Load <sup>b)</sup>	MPP or Open Circuit		MPP or Open Circuit		MPP or Open Circuit	

<sup>a)</sup>The ambient conditions are defines as 23 °C/50% RH in general, and 27 °C/65% RH accepted in tropical countries according to ISO 291(2008): Plastics - Standard atmospheres for conditioning and testing; <sup>b)</sup>Open circuit refers to a simply disconnected device or device connected to a sourcemeter set to 0 current

## Shelf lifetime Sample M3 - non-encapsulated

Figure 0 shows the shelf life time for a non-encapsulated sample. The sample has been stored in a small plastic box which was wrapped in aluminum foil to block all light from the OSC. The plastic box was then stored in a drawer and re-measured every day. Figure 0 indicates the date and time when the IV-characterization of the OSC had been performed. Figure 0 shows that all measured cells on the sample are degrading more than 60% after about 5 days shelf time. Note that the decrease is also caused by the illumination during the characterization of the IV curves (see chapter 5.1.3.)

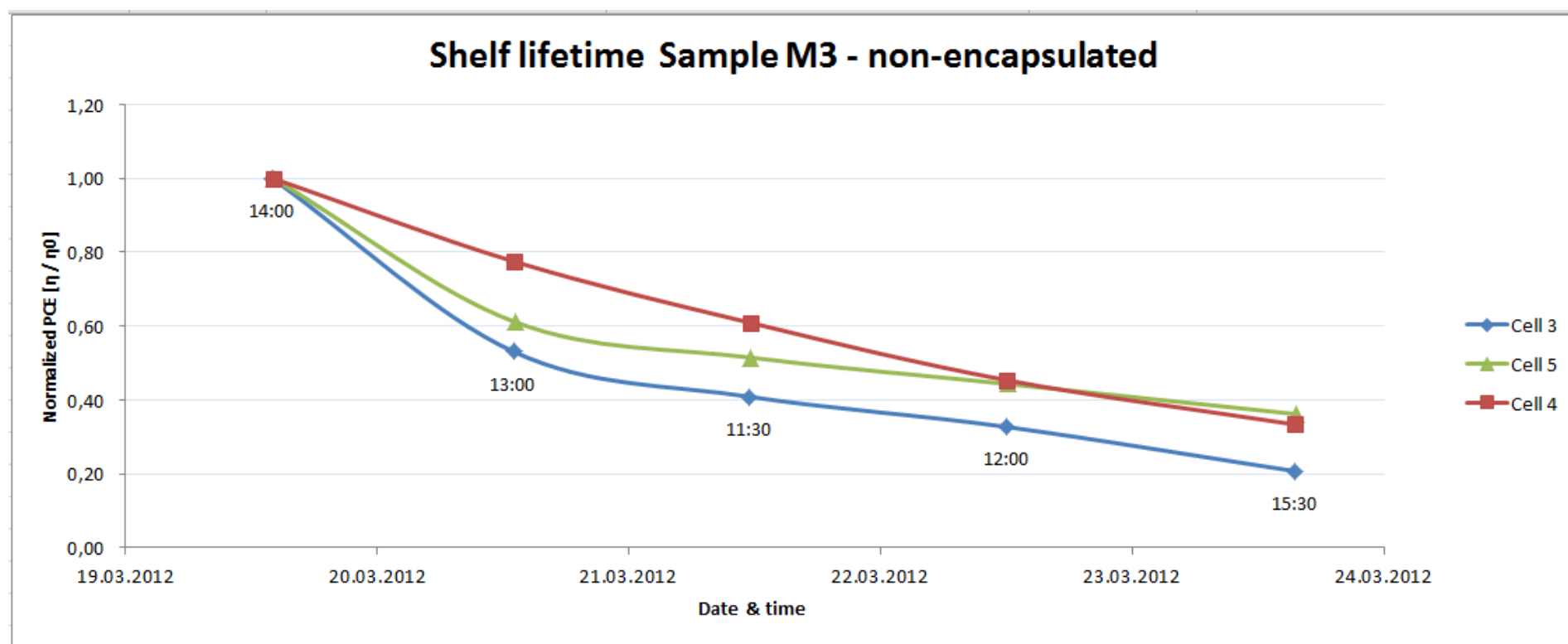


Figure 0 - shelf lifetime Sample M3

## Accelerated lifetime measurements

One simple method to obtain information about the lifetime of an OSC is the shelf life studies. The OSCs are simply stored in a dark room environment. The IV-curves are then periodically measured under a calibrated sun simulator. The highest reproducibility of this kind of method will be achieved if the samples are stored in a climate chamber for aging which has an accurate control of temperature and humidity levels.

In the case where a stable lifetime is achieved by encapsulation, accelerated lifetime measurements are appropriate, to achieve data in a more meaningful timeframe. During accelerated lifetime measurements harsher environmentally conditions are applied like e.g. increased temperature, increased humidity and increased solar irradiance.

A fairly new way of testing OSCs, which has become a rather common procedure, is with the help of a weathering or atmosphere chamber. The chambers provide accuracy and reducibility of the testing conditions. To be able to compare the results between different group the recommended temperature and humidity level combinations are 65 °C and 85 RH% or 85 °C and 85 RH%. It is possible to distinguish between the impact of different environmental factors, like humidity, temperature, oxygen and light on the power conversion efficiency of the OSCs. Unfortunately these machines are rather expensive and many scientific groups will not have the financial power to afford such a machine. [1]

## Bibliography



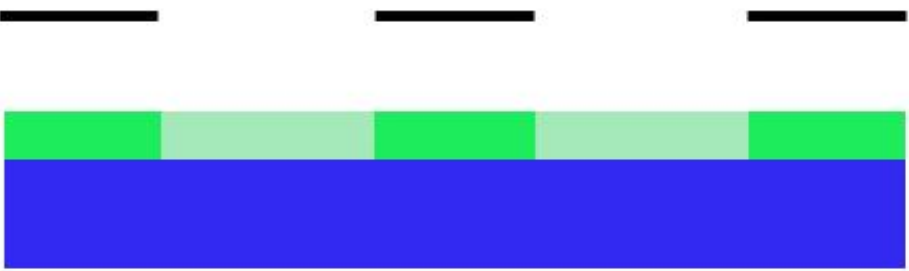
1. *Stability of Polymer Solar Cells*. Mikkel Jørgensen, Kion Norrman, Suren A. Gevorgyan, Thomas Tromholt, Birgitta Andreasen, and Frederik C. Krebs\*. Vols. Adv. Mater. 2012, 24, 580–612 DOI: 10.1002/adma.201104187.

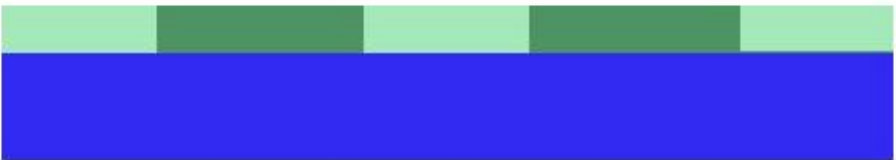




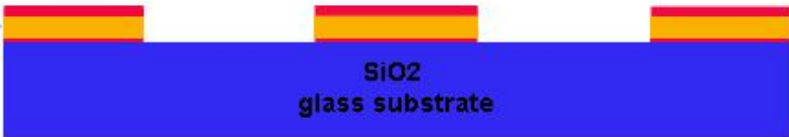
## B Appendix: OSC substrate production

### Process recipe for wafer bottom electrodes (NanoSyd)

1. Clean wafer: Acetone, DI water, spin dry.
2. Deposit adhesion promoter (HMDS).
3. Spin on photoresist (program 2):
  - a. EBS11 spin coater, resist: AZ 5214E, resist thickness = 1.5  $\mu\text{m}$
  - b. Automatic resist dispense
  - c. Spin at 500 rpm for 5 sec (acc. 5000  $\text{rps}^2$ )
  - d. Spin at 4000 rpm for 30 sec (acc. 10000  $\text{rps}^2$ )
4. Prebake: Hot plate, 90°C for 60 seconds.
5. UV exposure: KS Mask aligner, exposure time = 45 sec.
6. Inversion bake: Hot plate, 140°C for 2 minutes.
7. Flood exposure: KS mask aligner, exposure time = 60 sec (no mask).
8. Develop: Developer AZ351B (mix with DI water, ratio 1:4), 60 sec, agitation.
9. Rinse and dry: Rinse in water for 2 min, spin dry.
10. Metal deposition: Cryofox.
11. Lift-off: Ultrasonic in Acetone.

### Process recipe for wafer bottom electrodes illustrations (M. Hausladen)

Related process recipe steps	Section cut glass wafer	
1-2	SiO <sub>2</sub> glass substrate	
3-4	Photoresist SiO <sub>2</sub> glass substrate	
5	mask  Photoresist SiO <sub>2</sub> glass substrate	

6-7	<b>Photoresist</b> <b>SiO<sub>2</sub></b> <b>glass substrate</b> 
8-9	<b>Photoresist</b> <b>SiO<sub>2</sub></b> <b>glass substrate</b> 
10 (layer 1)	<b>Ti = 3nm</b> 
10 (layer 2)	<b>Al = 80nm</b> <b>Ti = 3nm</b> 
10 (layer 3)	<b>Ti = 20nm</b> <b>Al = 80nm</b> <b>Ti = 3nm</b> 
11 (lift off)	<b>Ti = 20nm</b> <b>Al = 80nm</b> <b>Ti = 3nm</b> 

### Recipe for “Cryofox Explorer 600 LT”

The deposition is done with the Cryofox Explorer 600 LT by using electron beam evaporation.

Parameters	Titanium (Ti)	Aluminum (Al)	Titanium (Ti)
Film thickness	20nm	80nm	3nm
Pressure	$3 \cdot 10^{-5}$ mbar	$3 \cdot 10^{-5}$ mbar	$3 \cdot 10^{-5}$ mbar
Deposition rate	2 Å/s	3 Å/s	2 Å/s



## C Appendix: Solution Preparation

All solutions have been produced in the chemistry laboratory at SDU Sønderborg. Due to security reasons gloves, goggles and fume hood were used for each production.

### Recipe for P3HT/PCBM blend

The following is an explanation of the process which was used to produce the P3HT/PCBM blend:

1. Take 200 mg of P3HT and 200 mg of PCBM (Mettler PM460 Delta Range used for weighing)
2. Put both materials in a 15 mL glass vial.
3. Add a magnetic stir bar into the vial.
4. Deposit 10 mL dichlorobenzene with a syringe into the vial.
5. Put on the vial cap and wrap a tape around to lock the cap.
6. Wrap the bottle in aluminum foil to block light from the blend.
7. Place the vial on a magnetic hotplate stirrer which is configured to 65 °C and 600 rpm and let it stir overnight.

#### Materials & suppliers

The P3HT has been bought from “Nano-C, Inc”.

<http://www.nano-c.com/pdf/productguide.pdf> (15.05.2012)

Poly (3-hexylthiophene-2,5-diyl), Catalog number 4002-E, 4002-EE

The supplier for the PCBM is “Rieke Metals, Inc.”

[http://www.riekemetals.com/material\\_science\\_division.html](http://www.riekemetals.com/material_science_division.html) (15.05.2012)

Phenyl C61 butyric Acid Methyl Ester ([60]PCBM) (99.5% purity)

The dichlorobenzene was supplied by “SIGMA-ALDRICH”

<http://www.sigmaaldrich.com/catalog/product/SIAL/240664?lang=en&region=DK> (15.05.2012)

1,2-Dichlorobenzene - anhydrous, 99%

## Recipe for PEDOT blends

The following is an explanation of the process which was used to produce the PEDOT blends:

### PH1000:CPP PEDOT (used during the first 8 weeks of the project)

1. Mix PEDOT:PSS (H.C. Starck CLEVIOS PH-1000) with PEDOT:PSS (H.C. Starck CLEVIOS CPP 105D) at a ratio of 3:1 in 15 mL glass vial.
2. Add 5% dimethyl sulfoxide (DMSO) (corresponding to 0.5 mL DMSO for a 10 ml solution)
3. Add a magnetic stir bar into the vial.
4. Put on the vial cap and wrap a tape around to lock the cap.
5. Wrap the bottle in aluminum foil to block light from the blend.
6. Place the vial on a magnetic stirrer and steer it overnight at room temperature at 300 rpm. (For this project the “RCT basic IKAMAG® safety control” magnetic steerer has been used

### HTL:CPP PEDOT (used the rest of the time during the project)

1. Mix Clevios™ HTL Solar PEDOT with PEDOT:PSS (H.C. Starck CLEVIOS CPP 105D) at a ratio of 1:1 in 15 mL glass vial.
2. Add a magnetic stir bar into the vial.
3. Put on the vial cap and wrap a tape around to lock the cap.
4. Ultrasonicate mixture for 1 hour. (For this project the “Branson Ultrasonic Cleaner, model DHA1000-6E” has been used.)
5. Wrap the bottle in aluminum foil to block light from the blend.

### Material supplier:

Heraeus Conductive Polymers in Leverkusen (Germany)

<http://clevios.com/en/home/clevios-homepage.aspx> (15.05.2012)

- PEDOT:PSS (H.C. Starck CLEVIOS PH-1000)
- PEDOT:PSS (H.C. Starck CLEVIOS CPP 105D)
- Clevios™ HTL Solar PEDOT

Sigma-Aldrich

- Dimethyl sulfoxide (DMSO)

## D Appendix: OSC fabrication and characterization

### Recipe for the fabrication of inverted ITO-free BHJ OSCs

Step	Process
1	Check equipment in glove box (2 tweezers, blue glue stripes, aluminium foil, 2 pipettes, glass wafers & organic solutions). Put needed equipment and material into the small entry chamber on the right side of the glove box.
2	Check pressure on nitrogen gas bottles and turn it on. Turn on the blue valves of the pipes from the nitrogen gas bottles to the glove box, heating plate & spin coater. Check the flow meter of the nitrogen bottle. It should indicate 4 bar.
3	Turn on the power of the vacuum pump of the spin coater. Turn on the valve of the pipes from the vacuum pump to the spin coater. Put blue gloves on and get into the black gloves of the glove box.
4	Spin coater; Enter spin=1000 rpm and time = 45 s.
5	Spin coat substrate with acetone at 1000 rpm for 45 s. Evaporate acetone by putting substrates on hotplate at 90 °C for 120 s.
6	Apply a blue glue stripe. The blue glue stripe should cover about half the length of the electrodes.
7	Add organic solution (P3HT:PCBM) with pipette on to surface of glass wafer and spin coat it at 1000 rpm for 45 s.
8	Turn on the hotplate and bake the glass wafer for 25 minutes 140 °C. Use the clock to time the backing process.
9	Switch off vacuum pump. Close nitrogen valve to spin coater and main chamber.
10	After the baking process, turn on vacuum pump, the valve to the spin coater and main chamber.
11	Apply a blue glue stripe. The blue glue stripe should cover up the bare electrodes and a part of the active layer.
12	Add PEDOT mixture with a pipette on top of the substrate.
13	Bake the glass wafer for 2 minutes at 140 °C. Use the clock to time the backing process. Switch off the hotplate when done.
14	Shake silver paste with the “Ika Vortex Genius 3” and apply it to the OSC

## Optical microscope cell area measurements

First the cells are evaluated with an optical microscope with a 5x-0.1 microscope objective. Digital pictures have been directly taken of the cells surfaces with the optical microscope by using the computer program “PixeLink  $\mu$ Scope”. These digital pictures have a standard resolution of 1600x1200 pixels. The conversion factors for 5x-0.1 microscope objective for a picture with the resolution of 1600x1200 are listed in table 1.

Conversion factor (pixel/mm) for picture with resolution of 1600x1200 for a 5x-0.1 microscope objective
0.635 pixels/ $\mu$ m
635 pixels/mm

Table 1- conversion factors

With Photoshop 11 the picture has been evaluated (see figure 1). Note the color difference of P3HT/PCBM and the PEDOT, which gives a natural border and indicate the length. The opaque rectangular area is the area which has been measured as active solar cell area.

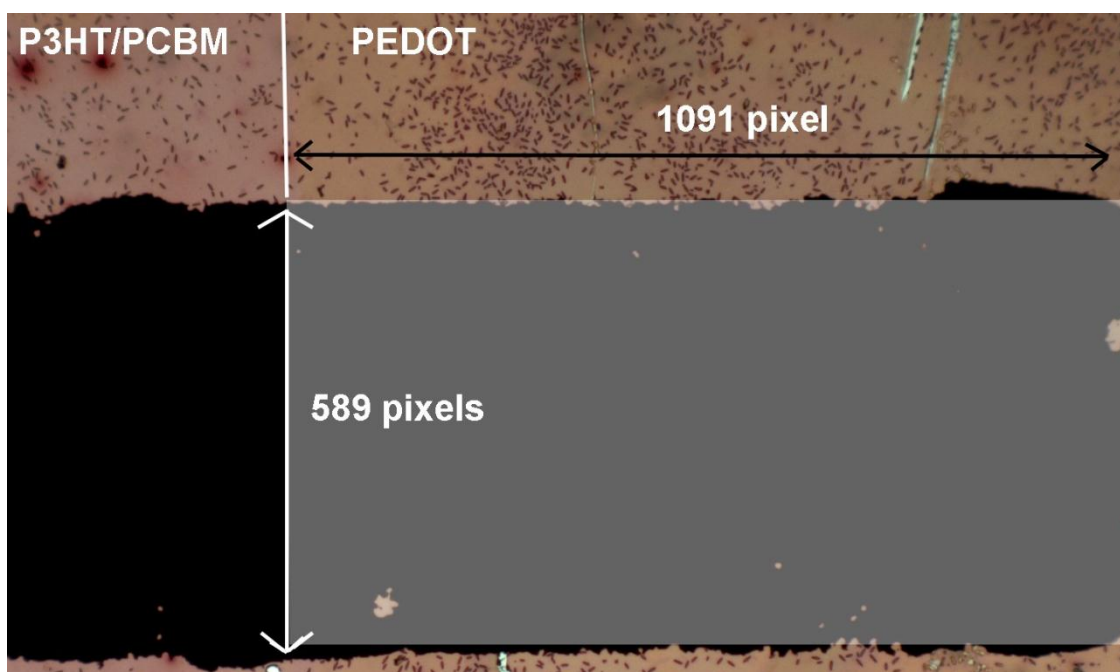


Figure 1 - Sample M2\_cell1 - measurement with Photoshop of active solar cell area

The measurements of cell 1 and cell 2 are displayed in table 2:

	x-length in pixels	y-length in pixels
Cell 1	1091	589
Cell 2	1059	576

Table 2 - pixels of measured object in Photoshop 11

The conversion from the measured pixels to millimeter is listed in table 3 and an example calculation is given by equation 1-1:

$$\text{conversion from pixel to mm} = \frac{\text{length in pixels}}{\text{conversion factor}} = \frac{1091 \text{ pixel}}{635 \frac{\text{pixel}}{\text{mm}}} = 1.72 \text{ mm}$$

	x [mm]	y [mm]	area [mm <sup>2</sup> ] (x*y)	area [cm <sup>2</sup> ]
Cell 1	1.72	0.93	1.59	0.0159
Cell 2	1.67	0.91	1.51	0.0151

Table 3 – conversion from pixel to mm and to cell area

The measurements taken by the vernier are listed in table 4:

	area [mm <sup>2</sup> ]	area [cm <sup>2</sup> ]
Cell 1	1.60	0.016
Cell 2	1.50	0.015

Table 4 - measurements taken by vernier

A comparison of the measurements in table 5 shows a very small difference between them:

	Vernier	Optical microscope	
	area [cm <sup>2</sup> ]		%-difference
Cell 1	0.016	0.0159	0,63%
Cell 2	0.015	0.0151	0,67%

Table 5 – comparison of vernier and optical microscope results

### **Results:**

With the vernier the measurements are mostly influenced by errors due to wrong handling of the vernier or imprecise reading and calibration of the vernier due to eyesight differences from person to person. With the optical microscope the biggest error source is at the computer program where the cell length and width has to be determined.

The two methods result in about the same measurements for the cell area. Looking at the picture 1 almost all the active regions of the cell are covered by the measurements, so one can assume that the computer measurement deliver that fairly accurate measurement of the cell area. The fact that the vernier measurements are very close to the computer measurements, indicates that the vernier is a reliable tool for measuring the cell areas, at least when compared to the computer aided measurements. For the purpose of this project the precision is good and further cell area measurements will be taken with the vernier.

## Voltage sweeps with LabVIEW

This section contains information about the characterization process and the LabVIEW measurement application. Figure 2 shows a screenshot of the custom made LabVIEW application, which was designed by Henrik Hartmann Henrichsen and Jakob Kjelstrup-Hansen. Furthermore table 6 shows a step by step explanation of how the LabVIEW application is configured and how the characterization of the OSC performances is conducted.

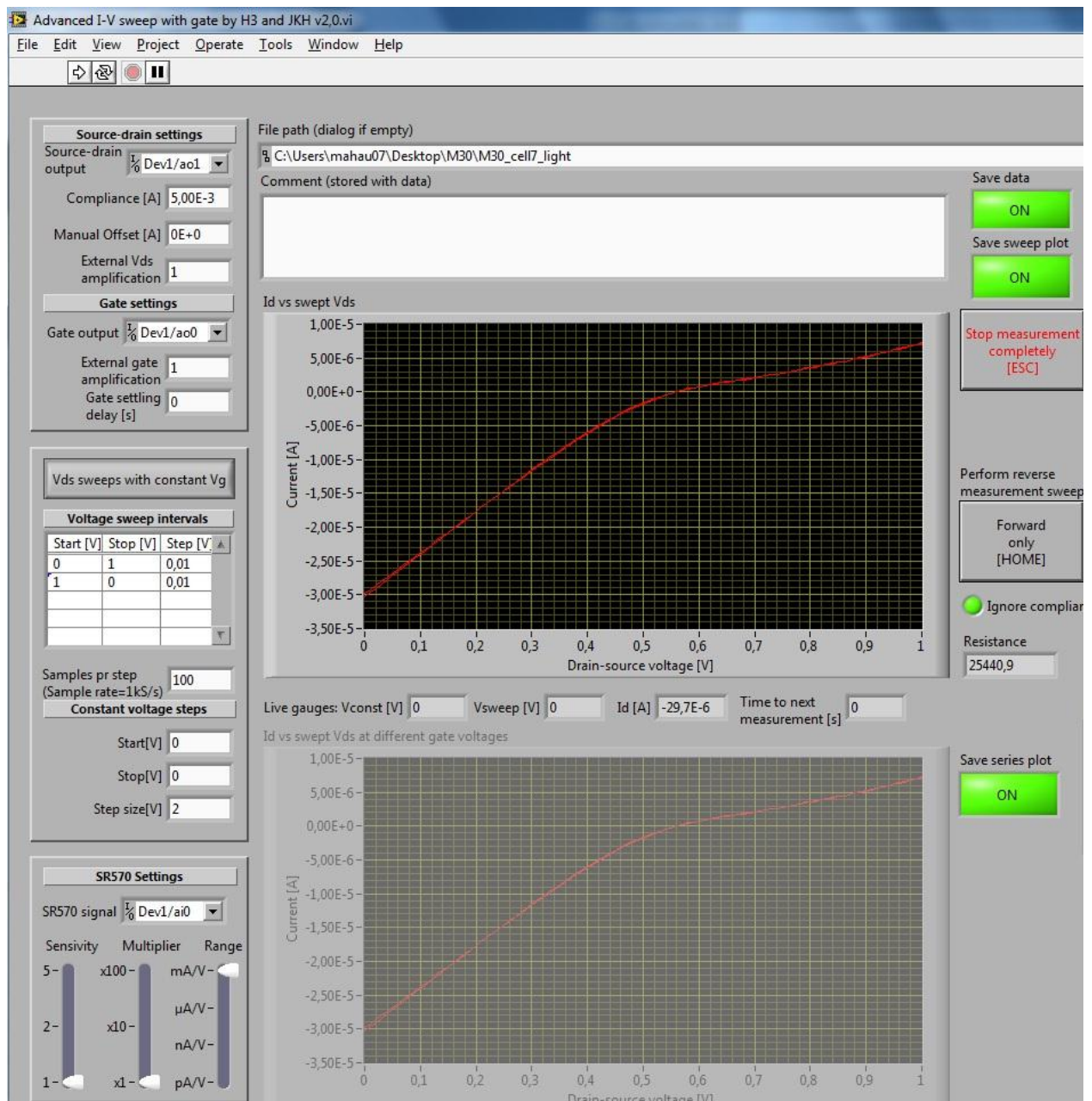


Figure 2 - LabVIEW measurement application (screenshot)



## Measuring IV-curves – step by step procedure

Step	Process
1	Turn on vacuum pump for the electrodes. (Assure that the electrodes stick to the surface (try to move them))
2	Turn on solar simulator power supply and press “lamp start”
3	Measuring the illumination intensity with the reference solar cell Adjust intensity to 1 sun. (1 sun = 100 mW/cm <sup>2</sup> ).
4	Switch the reference solar cell with the black circular platform. This platform has the same height as the reference solar cell.
5	Place your sample on the black circular platform, so it is positioned in the middle of the light cone.
6	Adjust position of electrodes. The probe connected to the DAQ unit should touch the anode (silver-paste) and the probe which is connected to the current amplifier should touch the cathode of the OSC ( Ti-layer).
7	Switch on the current amplifier and adjust the sensitivity to 1 mA/V
8	Configuration of LabView setup Open Labview and run file: ...”sweep with gate by H3 and JKH v.2.0.vi” Change “source-drain-output” to program channel to the one connected to the DAQ card “Dev1/a01” Change “gate output” to “Deo1/a00” Change the sensitivity to “1 mA/V” -> SR570 setting to “1 mA/V” (Dev1/ai0 and multiplier 1x) Change the compliance to 5,00*10 <sup>-3</sup> mA (should be 5x the sensitivity) Voltage sweep intervals; start = 0 V end = 1-1,2 V → end = 1-1,2 V start = 0 V Delete comments in comments window → write comments if necessary Press “Save file” -> “create folder” -> “create file” and press “run“ to perform a measurement
9	When finished with the measurement, press “lamp off” on the power supply. Let the bulb cool down for 5 minutes.
10	Remove electrodes and sample. Turn off amplifier and vacuum pump.

Table 6 – OSC characterization process

## E Appendix: Lifetime measurement non-encapsulated cells

### Measurement standards for OSCs samples

These guidelines purpose are to standardize the measuring process of the I-V characteristics under the solar generator with an AM1.5G spectrum in order to observe the lifetime development of the non-encapsulated and encapsulated OSC's. The intention with the standardized measuring is to create somehow equal conditions for each measurement.

#### Shelf lifetime measurements

- The efficiency of the cell decreases when the sample is illuminated (*see experiment 9.1 & 9.2 p.32*)
  - o To minimize the effects of the measuring process on the cells efficiencies, it is advisable to avoid constant illumination of the OSC's. The procedure will be that the cell is just illuminated for the time it takes to measure it's I-V characteristics. Between each measurement the light from the solar generator is blocked with the light shutter.
  - o In between the measurements the cell is exposed to background illumination. The measured background illumination of the testing area is generally very low compared to the 1 sun illumination of the solar machine, thus this factor can be neglected.<sup>20</sup>

#### General guidelines (both encapsulated and non-encapsulated cells)

- The solar generator and the setup are calibrated, so that the silicon test solar cell is measuring 1 sun.
- Wait about 5 minutes until the solar generator readings are stable.
- The testing solar cell and the organic solar cells both should be aligned in the center of the light cone from the solar generator.
- Each target cells I-V characteristic is measured under no illumination by the solar generator at the beginning of the measurement series in order to verify it's diode characteristics. The important factor is to establish a good contact with the electrodes and the Ti-Al layer of the glass substrate before the cell is illuminated.
- The cells are always measured in the same order.
- A self-designed light shutter only will let light pass onto the cell which is measured. This avoids illumination and degradation of all other cells during the individual cell measurement.
- The cells are stored in a dark environment.

---

<sup>20</sup> 15.03.2012 – 13:00 – semi-cloudy day – 0,020 suns measured with testing solar cell

## Sample M4 and M5 calculations

In table 7 the four device stability parameters  $E_0$ ,  $E_{80}$ ,  $E_S$  and  $E_{S80}$  for sample M4 and M5 are listed.

	Decay from ( $E_0, T_0$ ) to ( $E_{80}, T_{80}$ ) for M4 and M5		Factor between M4 and M5 for decays from $T_0$ to $T_{80}$ for	Decay from ( $E_S, T_S$ ) to ( $E_{S80}, T_{S80}$ ) for M4 and M5			Factor between M4 and M8 for decays from $T_S$ and $T_{S80}$
	$E_0, T_0$	$E_{80}, T_{80}$		$E_S, T_S$	$E_{S80}, T_{S80}$	Difference between $T_S$ and $T_{S80}$	
<b>M4</b> (continuous illumination)	100% @ 0min	80% @ <b>1min 42s</b>	$T_{80,M4}=1\text{min }42\text{s}=102\text{s}$ $T_{80,M5}=1\text{min }=660\text{s}$ <b>Factor=<math>T_{80,M5}/T_{80,M4}=6,47</math></b> <b>M5 is decaying by a factor of 6,5 times slower than M4</b>	60% @ 3min 30s	48% @ 6min	$T_{S,M4}=3\text{min }30\text{s}=210\text{s}$ $T_{S80,M4}=6\text{min }=360\text{s}$ $\Delta T_{M4}=T_{S80,M4}-T_{S,M4}=150\text{s}=\mathbf{2min }30\text{s}$	$\Delta T_{M4}=2\text{min }30\text{s}=150\text{s}$ $\Delta T_{M5}=14\text{min }12\text{s}=852\text{s}$ <b>Factor=<math>\Delta T_{M5}/\Delta T_{M4}=5,68</math></b> <b>M5 is decaying by a factor of 5,7 slower than M4</b>
<b>M5</b> (short illumination)	100% @ 0min	80% @ <b>11min</b>		60% @ 32min 48s	48% @ 47min	$T_{S,M5}=32\text{min }48\text{s}=1968\text{s}$ $T_{S80,M5}=47\text{min }=2820\text{s}$ $\Delta T_{M5}=T_{S80,M5}-T_{S,M5}=852=\mathbf{14min }12\text{s}$	

Table 7 - Stability key parameters ( $E_0, T_0$ ), ( $E_{80}, T_{80}$ ), ( $E_S, T_S$ ) and ( $E_{S80}, T_{S80}$ )

## Sample M4 and M8 calculations

In table 8 the four device stability parameters  $E_0$ ,  $E_{80}$ ,  $E_S$  and  $E_{S80}$  for sample M4 and M8 are listed.

	Decay from ( $E_0, T_0$ ) to ( $E_{80}, T_{80}$ ) for M4 and M8		Relative %-difference for decays from $T_0$ to $T_{80}$ for M4 and M8	Decay from ( $E_S, T_S$ ) to ( $E_{S80}, T_{S80}$ ) for M4 and M8			Relative %-difference for $T_S$ and $T_{S80}$ for M4 and M8
	$E_0, T_0$	$E_{80}, T_{80}$		$E_S, T_S$	$E_{S80}, T_{S80}$	Difference between $T_S$ and $T_{S80}$	
<b>M4</b> (3:1 PH1000: CPP PEDOT)	100% @ 0min	80% @ 1min 42s	$T_{80,M4}=1\text{min }42\text{s}=102\text{s}$ $T_{80,M8}=2\text{min }18\text{s}=138\text{s}$ <b>Factor=<math>T_{80,M8}/T_{80,M4}=1,35</math></b> <b>M8 is decaying by a factor of 1,4 times slower than M4</b>	40% @ 8min 8s	32% @ 11min 6s	$T_{S,M4}=8\text{min }8\text{s}=488\text{s}$ $T_{S80,M4}=11\text{min }6\text{s}=666\text{s}$ $\Delta T_{M4}=T_{S80,M4}-T_{S,M4}=178\text{s}=\mathbf{2min }58\text{s}$	$\Delta T_{M4}=2\text{min }58\text{s}=178\text{s}$ $\Delta T_{M8}=5\text{min }3\text{s}=303\text{s}$ <b>Factor=<math>\Delta T_{M8}/\Delta T_{M4}=1,70</math></b> <b>M5 is decaying by a factor of 1,7 slower than M4</b>
<b>M8</b> (1:1 HTL:CPP PEDOT)	100% @ 0min	80% @ 2min 18s		40% @ 12min 30s	32% @ 17min 33s	$T_{S,M8}=12\text{min }30\text{s}=750\text{s}$ $T_{S80,M8}=17\text{min }33\text{s}=1053\text{s}$ $\Delta T_{M8}=T_{S80,M8}-T_{S,M8}=303\text{s}=\mathbf{5min }3\text{s}$	

Table 8 – Stability key parameters ( $E_0, T_0$ ), ( $E_{80}, T_{80}$ ), ( $E_S, T_S$ ) and ( $E_{S80}, T_{S80}$ )

## F Appendix: Lifetime measurements encapsulated cells

### Initial material and process research for encapsulations

Table 9 lists the results of the initial material and process research which fulfill the key requirements, are available and feasible to process with the equipment and facilities at SDU Sønderborg.

Material	Properties	Processing
<b>Inorganic</b>		
Glass plate	Transparent Very low permeability Not flexible Low cost	Easy to process (BK7 glass wafer cut with dicing saw) Edges seal is a problem (epoxy could be used)
Al <sub>2</sub> O <sub>3</sub> (Aluminum oxide)	Good oxygen barrier (good) Susceptible to corrosion from water. Optical transmission range <sup>21</sup> μm 0.17 - 5.5 (good)	Electron beam evaporation <sup>22</sup> Thermal evaporation  No target material for Cryofox in SDU at the moment  Process with “Edwards Auto 500” is possible, but the deposition process needs to be optimized first
SiNx	Transparent Not flexible Better barrier than performance than SiOx	eBeam, sputter Needs higher processing time than SiOx
SiOx	Transparent Not flexible (brittle) Good WVTR and OTR Acts as UV-filter (like normal window glass)	eBeam, sputter
ZnO	Transparent Good WVTR and OTR	To complex processing – precursors needed (diethylzinc + water) Equipment not available

<sup>21</sup> [http://www.mt-berlin.com/frames\\_cryst/descriptions/sapphire.htm](http://www.mt-berlin.com/frames_cryst/descriptions/sapphire.htm) (15.03.2012)

<sup>22</sup> [http://www.vacengmat.com/downloads/VEM\\_Thin\\_Film\\_Evaporation\\_Guide.pdf](http://www.vacengmat.com/downloads/VEM_Thin_Film_Evaporation_Guide.pdf) (13.03.2012)

Organic		
PDMS (silicon based polymer)	Transparent (good) Flexibly (good) High permeability (bad) Low cost	Can be used as substrate (protective layer) for further depositions  Needs to cure (might increase processing time) Can be applied by spin coating Can be cured in any shape by using molds
PVA (polyvinyl alcohol)	excellent oxygen-barrier high stability upon irradiation Low cost	Can be used for multilayer encapsulations in combination with SiOx <sup>23</sup>  It's hard to work with. Also its brittle (Manuele Schiek, MCI SDU Sønderborg, Ph.D. organic chemistry)
PMMA (Polymethylmethacrylat)	Transparent Good permeability Low cost	Can be spin coated Needs annealing Can be used as a buffer layer
clear UV curable epoxy resin	Transparent Can be used for flexible cells Good barrier properties	Can be spin coated Can be used to seal edges of rigid encapsulations
PET foil	Transparent Can have low permeability if bought from company (e.g. food packaging)	Can be applied directly to the solar cell Lamination processing might be to complex (equipment needed)

Table 9 - Initial material and process research for encapsulations

<sup>23</sup> Julien Gaume - "Photochemical behavior of PVA as an oxygen-barrier polymer for solar cell encapsulation"  
RSC Adv., 2011, Advance Article, DOI: 10.1039/C1RA00350J

## PMMA film thickness

Figure 3 shows the PMMA film thickness (Å) vs. spinning speed (rpm)

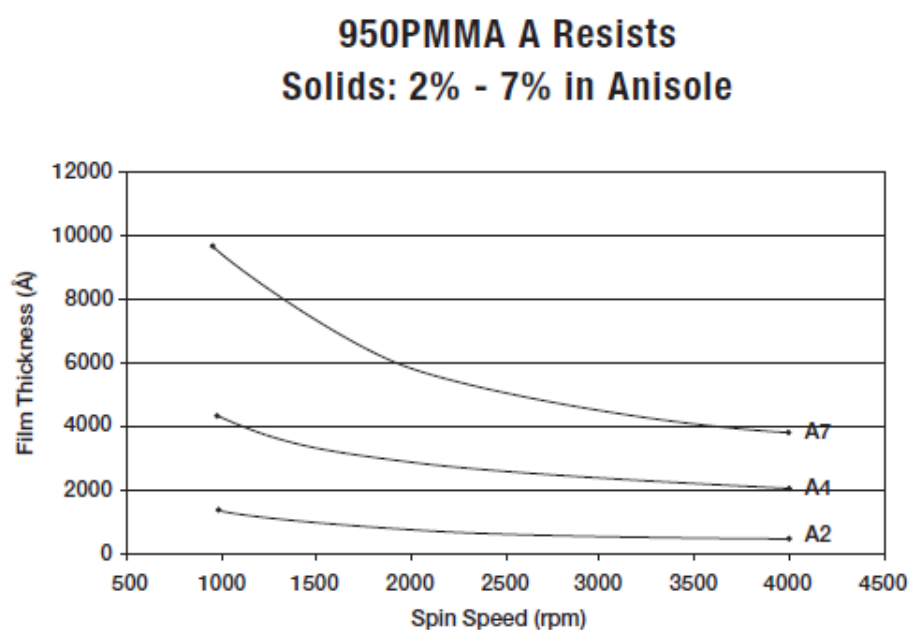


Figure 3 - PMMA datasheet p. 5 - [http://www.microchem.com/pdf/PMMA\\_Data\\_Sheet.pdf](http://www.microchem.com/pdf/PMMA_Data_Sheet.pdf) (27.05.2012)

## Process recipe for PMMA/SiO<sub>x</sub> encapsulation

1. Apply silver paste to cell (close to the electrodes for good conductivity)
2. Cover part of the anode and cathode with blue glue tape
3. Spin on PMMA (program 9)
  - a. *EBS 11 spin coater, PMMA 950 A4, film thickness 420 nm*
  - b. Spin at 500 rpm for 5 sec (ramping 500 rpm/s<sup>2</sup>)
  - c. Spin at 1000 rpm for 30 sec (ramping 500 rpm/s<sup>2</sup>)
  - d. Spin at 0 rpm for 4 sec (ramping 500 rpm/s<sup>2</sup>)
4. Carefully remove tape with tweezers
5. Anneal PMMA @ 90 °C for 5 min
6. SiO<sub>x</sub> deposition: Cryofox using RF sputtering PVD

Parameters	Values
Base pressure	$5 \cdot 10^{-5}$ mbar
Ignition pressure	$1.5 \cdot 10^{-2}$ mbar
Sputter pressure	$3 \cdot 10^{-3}$ mbar
Thickness [nm]	50
Rate [ $\text{\AA}/\text{s}$ ]	0.5
Tooling factor	20

**Table 10 – Cryofox parameters**



## Process recipe for epoxy adhesive encapsulation

1. Apply silver paste to cell (close to the electrodes for good conductivity)
2. Cover part of the anode and cathode with blue glue tape
3. Spin on adhesive
  - a. Laurell *WS-400BZ-6NPP/Lite*, *DELO-KATIOBOND LP VE 110484*, average surface thickness:  $51,4\ \mu\text{m}$
  - b. Spin at 1000 rpm for 45 sec
4. Carefully remove tape with tweezers
5. Cure adhesive with solar generator (light source: 150 Watt Xenon, Ozone Free Arc Lamp)
  - a. Remove AM 1.5 G filter
  - b. Calibrate distance between light source and OSC to about 20 cm.
  - c. Adjust solar generator to 5.5 A
  - d. Curing time under UV-exposure: 2 min
  - e. Curing time after UV-exposure: 20 min